SCUOLA INTERNAZIONALE SUPERIORE DI STUDI AVANZATI
INTERNATIONAL SCHOOL FOR ADVANCED STUDIES

Covalently functionalized carbon nanotubes and their biological applications

Thesis submitted for the degree of Doctor Philosophiae

Candidate
Francesca Maria Toma

Advisors
Prof. Giacinto Scoles
Prof. Maurizio Prato

Coadvisors
Dr. Loredana Casalis
Dr. Tatiana Da Ros
Dr. Marcella Bonchio

October 2009

TABLE OF CONTENTS

Table of contents

ACKNOWLEDGEMENTS

My thanks are due first to two people that represent the best guides for studying science that I could ever have found: Prof. Giacinto Scoles and Prof. Maurizio Prato. They have directed me towards many different collaborations and given me the opportunity to work in an international environment, encouraging me to take an interdisciplinary approach.

I would like to thank Prof. Scoles for his guidance and encouragement, for always making time to offer me advice, to teach and discuss things with me, and above all, for trusting me from the beginning and for giving me innumerable opportunities to learn new things.

Many thanks to Prof. Prato for his invaluable help, knowledge and understanding and for allowing me to experience such a stimulating atmosphere. I would also like to thank him for his gentle and constant presence and for finding the time to see me whenever I asked him.

Special thanks go also to Dr. Tatiana Da Ros, Loredana Casalis and Marcella Bonchio for their enthusiasm, help, useful meetings and invaluable discussions. I have benefited greatly from their precious advice.

Many thanks to all the people I have worked and collaborated with, especially Dr Andrea Sartorel and Mauro Carraro from Padua University, Dr Khuloud Al-Jamal and Prof. Kostas Kostarelos from School of Pharmacy in London, Mr Matteo Iurlo and Prof. Francesco Paolucci from Bologna University. Thanks to Dr. Alberto Bianco for his availability and helpful discussions, Dr. Marco Lazzarino for enabling me to use TASC laborotories and to Glaudio Gamboz for teaching me to use TEM.

Acknowledgements

Thanks also to Prof. Laura Ballerini for electrophysiological studies and especially to Miss Giada Cellot for sharing her neurons with me!

I owe many thanks to all the past and present members of Prof Prato's group and SENILab for the enjoyable experience of working and having good time with them! Thanks to Marian for her cooperation and help. Thanks to Coke for his valuable remarks.

I would like to thank all the people who I have met over this three years, who have enriched me in so many different ways. Thanks to GiokLan for her unlimited kindness and hospitality.

Thank to the SISSA and SBP sector for giving me this precious opportunity.

Special thanks to Carla and Barbara for their company and for making nice my experience in Trieste! Thanks to Denis, Fouzia, Nadja, Joceline, Anu, Tomas, Alessia, Sara S., Fulvio, Pietro, Loredana, Mauro C., Mildred, Chiara, Sara C., Valeria, Niksa, Alan, William and Tatiana for sharing with them unforgettable time.

As always, I want to thank Sara and Marco for their lasting friendship and support, for their constant presence despite the distance.

My really heartfelt thanks to my parents for their support and encouragment through my years of studying, for their extreme love, and to my sister for her useful tips. Thanks to Mauro for his extraordinary patience, for his help and pointers and for lovingly taking care of me!

Many thanks to all of you! I am extremely grateful!

Francesca

ABBREVIATIONS

AFM: atomic force microscopy

[bmim]BF_4: 1-butyl-3-methylimidaziolinium tetrafluoroborate

CNTs: carbon nanotubes

CT: computed tomography

CVD: chemical vapor deposition

DMF: N,N-dimethylformamide

DMSO: dimethylsulfoxide

DOS: density of states

dsRNA: double strand RNA

DTPA: diethylentriaminopentaacetic acid

f-CNTs: functionalized carbon nanotubes

EFM: electrostatic force microscopy

E-EFM: enhanced-electrostatic force microscopy

EPR: enhanced permeability and retention

FET: field effect transistor

FT-CNTs: fluorous-tagged carbon nanotubes

G band: graphite band

G_0: zero-generation

G_1: first-generation

G_2: second-generation

GEF: growth enhancing factors

HiPCO: high pressure CO

[hvim][$(CF_3SO_2)_2N$]: 1-hexadecyl-3-vinylimidazolinium bis(trifluoromethylsulfonyl)imide

Abbreviations

ILs: ionic liquids

MW: microwave

MWCNTs: multi walled carbon nanotubes

o-DCB: ortho-dichlorobenzene

[omim]BF4: 1-methyl-3-octylimidazolinium tetrafluoroborate

PAMAM: polyamidoamine

PSCs: post synaptic currents

RBM: radial breathing mode

RES: reticuloendothelial system

RISC: RNA-induced silencing complex

RNAi: RNA interference

SEM: scanning electron microscopy

siRNA: small interference RNA

SPECT: single photon emission computed tomography

STM: scanning tunneling microscopy

SWCNTs: single walled carbon nanotubes

TEM: transmission electron microscopy

TGA: thermogravimetric analysis

TUNEL: terminal deoxynucleotidyltransferase–mediated nick end labeling

UV-Vis-NIR: Ultraviolet-Visible-Near Infrared

THESIS ABSTRACT

In this thesis covalent functionalization of carbon nanotubes (CNTs) is presented as a powerful tool to allow the use of CNTs for biological applications.

Covalently functionalized CNTs (f-CNTs) have a promising future as drug carrier[1]. In our group, we are currently investigating this opportunity, especially towards multiple functionalization of CNTs to load at once different compounds[2] (drugs, solubilizing agents, imaging payloads). To address this issue, we prepared new CNT derivatives using a dendron moiety with a high number of free amino groups, which could be eventually used to prepare compounds with at least two different payloads.

We have also studied alternative techniques of functionalization, exploiting both thermal heating and microwave (MW) irradiation[3], and succeeding in functionalizing them with a solubilizing agent (i.e. tetra-alkyl ammonium salts) to increase the aqueous solubility of f-CNTs[4].

Taking into account the unique ability of carbon nanotubes to penetrate cell membranes, the positive charges on the derivatized multi-walled CNT (MWCNT) surface make them potentially ideal vectors for small interference (siRNA) delivery. siRNA needs to be translocated into cells because, bearing many negative charges, it cannot cross cell membrane by diffusion. Although viral vectors are widely used, they imply many safety risks and involve inflammatory and immunogenic effects. This is why non-viral vectors are preferable and many cationic derivatives, such as cationic polymers, dendrimers and peptides, are the most quoted candidates to translocate siRNA (and other genetic materials) across cell membrane[5]. Using a fluorescently labeled, non-coding siRNA sequence, we demonstrated that cytoplasmic delivery of the ribonucleic acid is remarkably improved with increasing dendron generation. Furthermore, we demonstrated

also the possibility to translocate toxic-siRNA sequence exploiting this system. These results demonstrate that the new dendron-based derivatives are very promising substrates for application in nanomedicine.

Moreover, we have also investigated the possibility to use CNTs as substrates for neuronal cell growth. We first functionalized CNTs to make them soluble in order to produce CNT-coated glass substrates, and afterwards the functionalizations were burnt to obtain bare CNTs deposited on the glass. CNTs are capable to boost neuronal network activity[6] but the mechanism is still unclear. To address this issue, we produced glass substrates covered with CNTs and studied the morphology and the interactions of the neuronal network. Dual electrophysiological recordings were also performed proving that the connectivity in the neuronal network is improved when CNTs are present.

References

(1) Prato, M.; Kostarelos, K.; Bianco, A. Functionalized carbon nanotubes in drug design and discovery. *Accounts of Chemical Research* **2008**, *41*, 60-68.

(2) Wu, W.; Wieckowski, S.; Pastorin, G.; Benincasa, M.; Klumpp, C.; Briand, J.; Gennaro, R.; Prato, M.; Bianco, A. Targeted delivery of amphotericin B to cells by using functionalized carbon nanotubes. *Angewandte Chemie - International Edition* **2005**, *44*, 6358-6362.

(3) Guryanov I.; Toma F. M.; Montellano López A.; M., C.; Da Ros T.; Angelini G.; D'Aurizio E.; Fontana A.; Prato M.; Bonchio M. Microwave-Assisted Functionalization of Carbon Nanostructures in Ionic Liquids. *Chemistry - A European Journal*.

(4) Herrero, M. A.; Toma, F. M.; Al-Jamal, K. T.; Kostarelos, K.; Bianco, A.; Da Ros, T.; Bano, F.; Casalis, L.; Scoles, G.; Prato, M. Synthesis and Characterization of a Carbon Nanotube−Dendron Series for Efficient siRNA Delivery. *Journal of the American Chemical Society* **2009**, *131*, 9843-9848.

(5) Gao, L.; Nie, L.; Wang, T.; Qin, Y.; Guo, Z.; Yang, D.; Yan, X. Carbon nanotube delivery of the GFP gene into mammalian cells. *Chembiochem* **2006**, *7*, 239-

242.

(6) Lovat, V.; Pantarotto, D.; Lagostena, L.; Cacciari, B.; Grandolfo, M.; Righi, M.; Spalluto, G.; Prato, M.; Ballerini, L. Carbon Nanotube Substrates Boost Neuronal Electrical Signaling. *Nano Letters* **2005**, *5*, 1107-1110.

CHAPTER 1:

GENERAL INTRODUCTION AND AIM OF THE THESIS

1.1 Nanotechnology: Small Can Be Big!

In spite of few extremely visionary sentences about the fact that at the bottom of size scale "an enormous amount (of work) can be done in principle" and "that it would have an enormous number of technical applications" [Feynman in his famous 1959 speech], nobody never talked about "Nanotechnology" before 1974, when this term was introduced by N. Taniguchi[1,2]. Moreover, in the 1980s E. Drexler explored the possibility to build machines manipulating individual atoms[2,3], ending up with a book (the first Nanotechnology book) written in 1986[4]. On the other hand, this obviously does not mean that nanostructures did not exist before that time. They are as old as life itself, since humans soon took advantage of nanosized materials. For example, the first archeological find, the Lycurgus cup (British Museum, London, Figure 1) dated from the 4th century A.D., contains silver and gold nanoparticles[5].

Figure 1. Lycurgus cup, IV A.D., Roman find. A: normal view of the cup; B: view of the cup when illuminated from the inside. It illustrates King Lycurgus' death. © Trustees of the British Museum.

Nanotechnology concerns all structures of nanometer (a billionth of a meter) size, even though also microstructures are often considered as a part of Nanotechnology because, unless they are made of a single kind of atoms, they often contain nanoscale sub-structures.

One of the first implications in this field is the dominant role of the surface. Consider a cube of 1 cm side, the volume is 1 cm^3 and the surface area is 6 cm^2; in contrast, if we subdivide the cubic centimeter into 10^{21} cubes of 1 nm size, the total volume will remain the same (1 cm^3) but the surface area will be $6x10^{21}$ nm^2 (i.e. 6000 m^2), that is more or less equivalent to the surface of a soccer field. It appears clear that small can be really big! The increase of surface area is very useful in many fields as, for example, in drug delivery or catalysis. This is only one of the many features of the nano-range, indeed nanostructures possess many other peculiar properties, originating a wide range of applications in physics, chemistry, engineering, biology and medicine. As a matter of fact several new sub-disciplines have been recently born such as, for example, "nanomedicine" or "nanometrology".

Chapter 1

The discovery and the subsequent applications of CNTs have allowed the development of an entire branch of nanotechnology based on this versatile material[5], the material with which all experiments reported in this thesis have been carried out.

1.2 Carbon Nanotubes[6]

Carbon is the only element of the periodic table that occurs in allotropic forms from 0 dimensions to 3 dimensions, due to its different hybridization capabilities. Hybridization occurs when electronic wave functions of valence electrons can mix with each other and change the occupation of the outer shell s and p orbitals (2s and 2p for the carbon atom). The mixing of a 2s orbital with n= 1, 2, 3 2p electrons is called sp^n hybridization. Fullerene (zero-dimensional), carbon nanotubes (one-dimensional) and graphene (single layer of graphite, two-dimensional) are all made of sp^2 hybridized carbon atoms, whereas diamond (three-dimensional) are sp^3 hybridized; amorphous carbon (three-dimensional) lays in between graphite and diamond with a mixed sp^2 and sp^3 hybridization.

Graphite is a three dimensional layered hexagonal solid lattice of carbon atoms, one single layer of which is a two-dimensions material namely graphene. It is important to introduce graphite because many properties of carbon nanotubes are the direct consequence of graphite properties. To illustrate this point, in Figure 2 we show the unit cell of graphene, where $\overrightarrow{a_1}$ and $\overrightarrow{a_2}$ are unit vectors, in Cartesian coordinates (1).

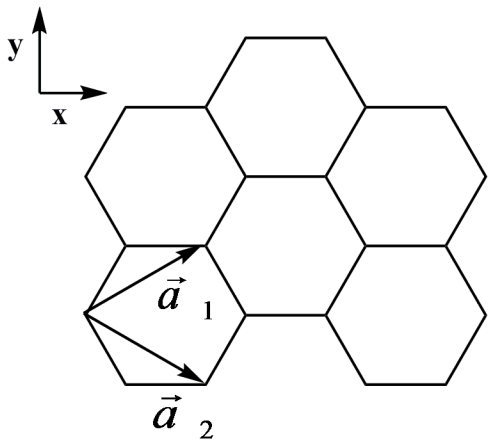

Figure 2. Unit cell of graphite

$$\overrightarrow{a_1} = \left(\frac{\sqrt{3}}{2}\,\mathrm{a}, \quad \frac{\mathrm{a}}{2}\right) \overrightarrow{a_2} = \left(\frac{\sqrt{3}}{2}\,\mathrm{a}, \quad -\frac{\mathrm{a}}{2}\right) (1)$$

Where (a) is the lattice constant of two dimensional graphite (2).

$$a = |\overrightarrow{a_1}| = |\overrightarrow{a_2}| = 1.42 \times \sqrt{3} = 2.46\ \text{Å}\ (2)$$

Carbon Nanotubes were discovered by Iijima in 1991[7], who was awarded in 2008 of the Kavli prize. CNTs can be imagined as a graphene sheet rolled up into a tube, and this is why many of CNTs properties are comparable with those of graphite. Mainly two different types of CNTs can be distinguished: (i) single walled CNTs (SWCNTs) and (ii) multi walled CNTs (MWCNTs). They are generally made of a side wall and two end caps: the sidewall is made of benzene rings and end caps are fullerene-like.

- SWCNTs are composed of a single layer of graphene and their diameter ranges between 0.7 and 1.4 nm depending on the temperature they have been synthesized. In fact, it has been observed that a higher growth temperature gives a larger diameter. This is probably because when the temperature is diminished the probability of generating a pentagonal ring is increased and the generated caps tend to be smaller. At higher temperature, vibrational entropy favors hexagonal rings over pentagonal rings and consequently the diameter is larger. SWCNTs can

be considered as one dimensional object because of their large aspect ratio (i.e. length/diameter = 10^4-10^5). Another essential fact about their structure is related to the six-membered carbon ring orientation in the honeycomb lattice relative to the axis of SWCNTs, that determines a parameter known as chirality ($\overrightarrow{Ch}$, Figure 3).

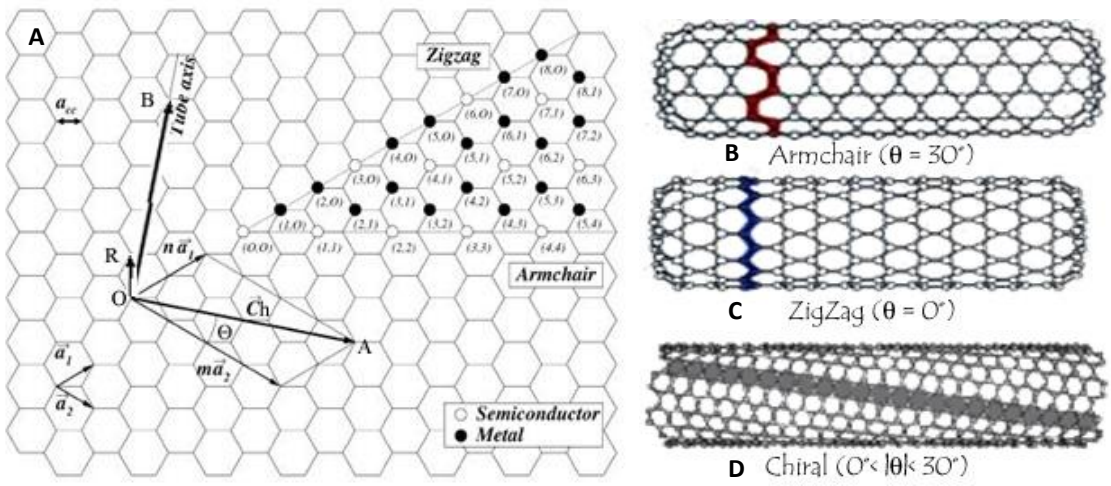

Figure 3. A: unrolled honeycomb lattice of a SWCNT, $\overrightarrow{OA}$, $\overrightarrow{OB}$ and $\overrightarrow{OR}$ are the chiral vector ($\overrightarrow{Ch}$), translational vector ($\vec{T}$) and the symmetry vector ($\vec{R}$)respectively. B, C, D:classification of SWCNTs, armchair, zigzag and chiral respectively. Armchair and zigzag refer to the shape of the cross sectional ring. θ is the chiral angle and denotes the tilt angle of the hexagons with respect to the direction of nanotube axis. Adapted from reference[8].

Fundamentally, the primary classification of SWCNTs is done on the symmetry basis: a SWCNT can be achiral (armchair or zigzag) or chiral, in the latter case the mirror image is not identical to the original structure because the CNT is a spiral.
As reported in Figure 2, also in Figure 3 we can distinguish unit vectors of hexagonal lattice ($\overrightarrow{a_1}$ and $\overrightarrow{a_2}$) that define chirality (3):

$$\overrightarrow{Ch} = n\overrightarrow{a_1} + m\overrightarrow{a_2} \quad (3)$$

n and m are integers and on this basis we can distinguish three different situations: n = m is the case of armchair structure, m = 0 is the case of zigzag structure and all other cases describe chiral nanotube structures. Chirality is important to the defined conductivity: armchair carbon nanotubes are metallic, zigzag and chiral

CNTs are semiconducting. $\overrightarrow{OB}$, which is the translation vector ($\vec{T}$), is parallel to the nanotube axis and normal to $\overrightarrow{Ch}$ (Figure 2). $\vec{T}$ corresponds to the first lattice point of the two-dimension graphene sheet through which this vector passes. We need one more vector to denote SWCNTs structure: this is the symmetry vector ($\vec{R}$), used for generating the coordinates of carbon atom in the nanotube itself.

Transmission electron microscopy (TEM, Appendix A) and above all scanning tunneling microscopy (STM), with results reported also in our group[9] experimentally confirmed this structure (Figure 4).

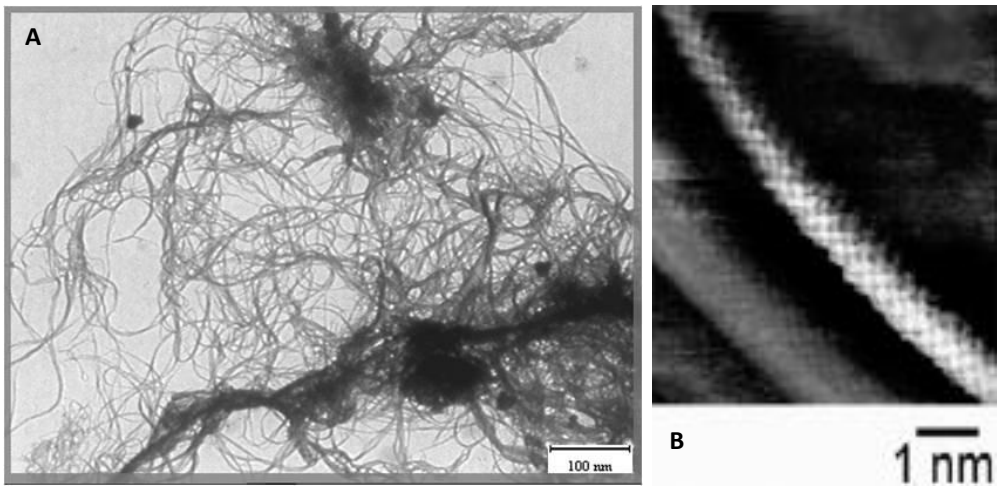

Figure 4. A: TEM image of HiPCO SWCNT (scale bar 100 nm). B: STM image of HiPCO SWCNT[9].

SWCNTs are usually organized into bundles or ropes (see Figure 3A), and it is difficult to proceed in their exfoliation. π- π stacking occurs between the sidewalls and this is why they stack one next to the other. Moreover a hydrophobicity contribution is also expected in determining this entanglement[6]. The order of these intermolecular forces is about 0.5 eV/nm[10].

- MWCNTs are made of many graphene layers and the diameter can be up to 100 nm.

Two main models describe MWCNTs: (i) the Russian doll model or coaxial cylindrically curved model in which many graphene layers are rolled up and arranged in a cylindrical fashion, and (ii) the parchment model in which a single

graphene layer is scrolled as a parchment (Figure 5a and c respectively). A further evolution of the coaxial cylindrically curved model is the coaxial cylindrically poligonized (Figure 5b).

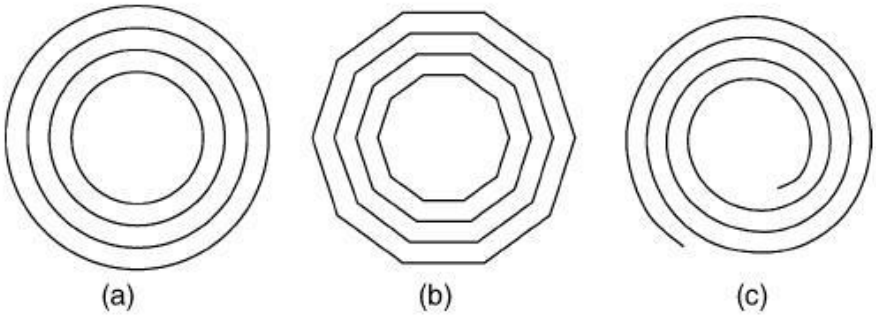

Figure 5. Different models of MWCNTs. (a) coaxial cylindrically curved; (b) coaxial poligonized; (c) scroll graphene sheet[8].

The electronic structure of a MWCNT is considered as the sum of the electronic structures of the constituent nanotubes. Thereby, we state that in the limit of the large nanotube diameter, all the nanotubes properties correspond to those of graphite. The interlayer distance in MWCNT, in fact, is equal to the interlayer distance in graphite (3.35 Å)[6]. These interactions are not sufficient to correlate the chirality of near tubes and MWCNTs are a mix of achiral shells. The result is that the lattice structures of the inner and outer layers are generally incommensurate. Physical properties of MWCNTs have not been explored in detail, because of the difficulty in performing measurements on each single layer. In figure 6, TEM (A) and scanning electron microscopy (SEM) (B) images of MWCNTs are reported. The number of inner shells can be measured with High Resolution TEM.

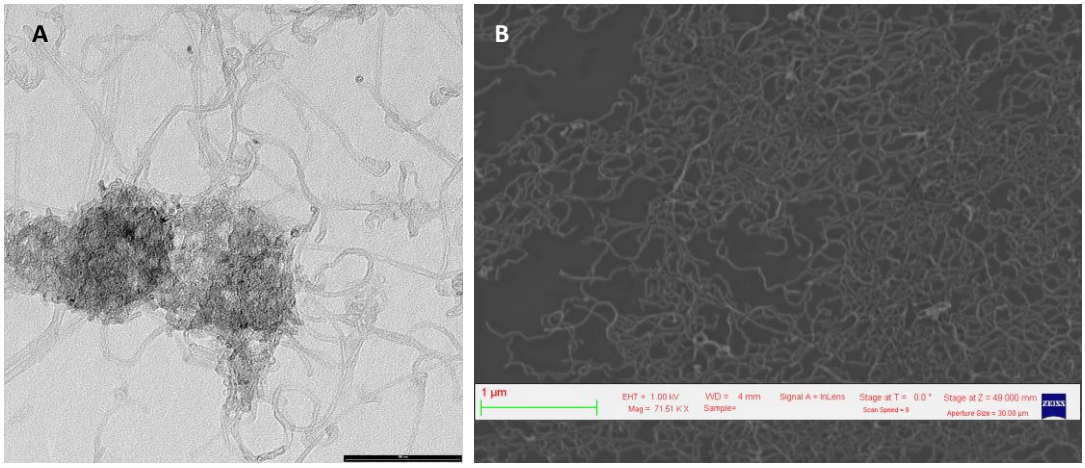

Figure 6. A: TEM image of double walled CNTs (scale bar = 100nm); B: SEM image of MWCNTs (scale bar = 1µm).

1.2.1 Synthesis and Functionalization of CNTs

There are several methods to synthetize CNTs:

- Arc discharge is actually the most common procedure to produce carbon nanostructures. It consists of two electrodes of graphite and a DC voltage is applied between them. The whole system is under pressure control with both a vacuum and a gas line, and MWCNTs are the main product, with fullerenes and amorphous carbon particles as by-products. SWCNTs can be produced as well, varying pressure and temperature conditions. Nanotube are producted at the cathode, while at the anode there is a hole filled with Ni-Co, Co-Y or Ni-Y, a source of metal nanoparticles, catalysts, those consist an impurity of CNTs[11].
- Laser ablation methods were developed by R. E. Smalley (Nobel Laureate in 1996 with R. F. Curl and H. W. Kroto for the discovery of fullerene) at the Rice University. The apparatus consists of a tube, where Ar or He is fluxed, within a furnace. Inside the tube there is a target of graphite mixed with 1% of Co and 1% of Ni, which is vaporized using a pulsed laser and high temperature. Carbon nanostructures are collected in an external trap, while

metal nanoparticles are not trapped inside the cage. Both SWCNTs and MWCNTs can be obtained with this technique[11].

- Chemical Vapor Deposition (CVD) is one of the main interesting synthetic procedures because it employs hydrocarbon decomposition over substrates, where metal nanoparticles have been placed. Ni, Fe or Co, or alloys of these three elements, are used. Impurities due to the pyrolytic graphite are few, but metal nanoparticles are presents, especially at the periphery of CNTs. MWCNTs are grown by decomposition of acetylene. Further, SWCNTs are produced by floating CO with $Fe(CO)_5$ with a disproportionation process, known as "HiPCO" (High Pressure CO)[11].

Beyond the different techniques, it appears immediately clear that CNTs need processing after their synthesis. To address this issue, purification methods and, above all, functionalization approaches are essential to allow manipulation and further application of this material. Usually, metal nanoparticles and amorphous carbon are present as a synthetic residue. In general, CNTs are a fluffy powder difficult to manage, while chemical functionalization contributes to prepare more homogenous and soluble material (Figure 4).

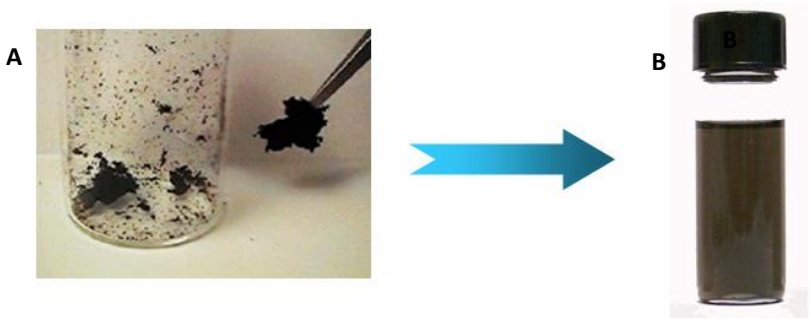

Figure 7. (A) Powder of SWCNTs, (B) DMF solution of f-SWCNTs (via 1,3-dipolar cycloaddition, SWCNTs **9** Chapter 2, Table 2).

Purification concerns acidic treatments that bring to the removal of amorphous particles and metals oxidation. Moreover, aggressive purification procedure can shorten CNTs and produce oxidized nanotubes.

On the other hand, a wide variety of functionalizations have been reported in the literature[10,12,13], the most important of which are summarized in Scheme 1.

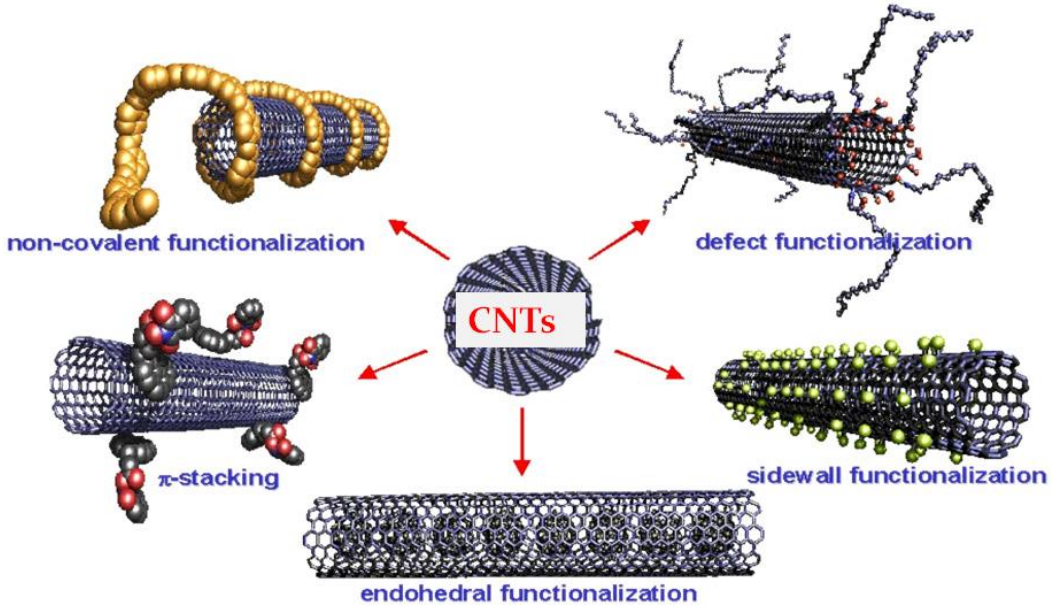

Scheme 1. Most common functionalizations of CNTs are reported. Adapted from reference[12].

We can categorize mainly non-covalent and covalent approaches.

Non-covalent functionalization is based on van der Waals, hydrophobic or π- π interactions (Scheme 1), and it is particularly interesting because it does not perturb the electronic structure of CNTs, and of SWCNTs in particular. This functionalization involves weak forces, and so some applications are prevented. The systems, in fact, are not only difficult to control but also difficult to characterize. The amount of weakly bound molecules is not always calculable; moreover, especially in solution, other interactions can occur and these molecules can be replaced by solvent. Anyway, many examples of non covalent interaction are reported: surfactants are widely used to exfoliate bundles of SWCNTs[14], as well as ionic liquids (discussed in Chapter 2) in order to facilitate CNTs manipulation and further reactions. CNTs wrapping by polymers, including DNA, have been studied[13]; also proteins are able to non convalently interact with CNTs and these are often used for bio-sensor applications[11].

Endohedral is a non convalent functionalization that occurs trapping molecules inside the CNT structure[13].

In covalent functionalization, CNTs are functionalized by not reversible attachment of appendage on the sidewalls and/or on the tips. Also in this case, many different approaches are reported[13]. Briefly, reactions can be performed at the sidewall site (sidewall functionalization) or at the defect sites (defect functionalization), usually localized on the tips. In the first case, fluorination with elemental fluorine at high temperature (400-600°C) has been explored, accomplishing further substitutions with alkyl groups. Furthermore, radical addition via diazonium salt has been proposed by Tour's group. On the other hand, cycloadditions have found wide interests. Besides 1,3-dipolar cycloadditions of azomethine ylides that is described in Chapter 2 and Appendix B, other cycloadditions have been reported, such as carbene [2+1] cycloadditions or Diels-Alder via microwave (MW) irradiation cycloaddition[13]. Side defects functionalization occurs via amidation or esterification reactions of carboxylic residues obtained on CNTs. Moreover, it is feasible that in general caps (i.e. tips when they are not cut) are more reactive than sidewalls because of their mixed pentagonal-hexagonal structure.

f-MWCNTs are not modified in their electronic structure and new properties can be added by means of functionalization. Instead, electronic properties of SWCNTs are perturbed by covalent functionalization and double bonds are irreversibly lost. This may affect conductive property, preventing further CNT applications.

1.2.2 Applications and Properties of CNTs[11]

Mechanical, thermal and conductive properties of carbon nanotubes are outstanding.

For what concerns mechanical properties, the Young modulus, that gives information about the stiffness of material, has been calculated for MWCNT and

SWCNT and, depending on the different type of CNT, it varies from 0.5 up to 1.1 TPa. For comparison, the Young modulus of diamond is 1.2 TPa. Moreover, it has been demonstrated that the breaking strength of a CNT, attached to two AFM tips, is 11-63 GPa for a MWCNT (referred to the outer shell), and 30 GPa (up to 50 GPa) for a SWCNT. These values proved that the mechanical properties of CNTs are very good: in fact, they are related to the cylindrical structure of CNTs that confers structural stability under compression.

Thermal conductivity seems to be higher than for every other material and experiments under ultra high vacuum showed that CNTs are stable at least at 4000 K. In fact, carbon nanotubes benefit of both sp^2 and one-dimensional structure.

Conductive properties are related with the one-dimensional structure of CNTs as well and electrons undergo ballistic conduction. This type of conduction is defined as continuous flow of energy carrying over high distances without stoppers.

Interesting optical properties have been studied in the last few years and many advances in photophysics have been achieved.

The power of CNTs resides on the vast number of applications of this versatile material, which go from electronics to nanomedicine. The final challenge remain in achieving large-scale production and industrial applications of CNTs.

- Carbon nanotubes applications to electronic device fabrication are due to their superlative conductive properties. Transistors, such as field-effect transistors (FETs), have been successfully realized; moreover attempts to develop electromechanical memory devices are under study. CNTs-FETs are used in gas sensing: sensitivity and selectivity of these transistors are improved using f-CNTs, attached to binding ligands. No commercial unit built in this way is available, as far as we know. Instead, thin film of SWCNTs have been incorporated also in transparent transistors for military or industrial electronic systems. Among electronic applications, we can count also CNTs as field emitters. It basically means that CNTs own the peculiar property to emit electrons when an electromagnetic field is applied, because of their peculiar structure (electric field are much stronger

at the tips). While, concerning their thermal properties, aligned CNTs on silicon chips provide high cooling performance for microprocessors.

- Energy applications use both CNTs as electrode material or as conductive filler for the active material. Electronic and electrical properties together with the high surface area are exploited. Energy storage devices such as lithium ion battery and supercapacitors have been investigated, as well as solar cells. In the latter case, silicon-based photovoltaics with solar-energy conversion of 25% and CNTs forming bulk heterojunctions in solar organic cells have been built. Electrodes of CNTs are employed also in electrochemical sensors due to faster electron-transfer kinetics from a number of electroactive-species. These electrodes are often exploited as biosensors for glucose or DNA hybridization.
- Mechanical applications of CNTs are directed to obtain CNTs based composites: NASA is investing large amounts of resources in developing these materials for applications in aerospace.
- There are many examples of biological applications in literature. In this case, CNTs must be water-soluble to avoid cytotoxicity. Thus, functionalization is necessary and covalent functionalization often represents the first choice. CNTs have been exploited for imaging but also as drug vehicles or carriers. This is possible because CNTs are readily internalized by cells and it is possible to introduce a multiple functionalization with different therapeutic agents. As cargo system, they have been developed to carry DNA, proteins or anticancer drugs. However, internalization and excretion and interferences at a systemic level (i.e metabolism) still remain unclear. It seems that different types of functionalization could bring different fate to the CNTs: Dai et al[15] proposed an endocytosis pathway for acid-functionalized SWCNTs, while Bianco et al[16] suggested a passive mechanism in which nanotubes could enter cell like needles. Besides this, it is undeniable that functionalized, water-soluble, CNTs bear an extraordinary affinity to penetrate cells. One of the factors that influences CNT-cell interaction could be also represented by protein adsorption at nanotube surface. Also receptor-mediated mechanism have been proposed[17]. On the other hand, another tricky

question is the destiny of CNTs once inside the cell. Interestingly, Strano and collaborators suggested the first evidence of exocytosis of a SWCNT, reporting that the exocytosis and endocytosis have almost the same rate[18]. At systemic level, it seems that CNTs are excreted by kidneys[19]. We are still pursuing these issues and many different hypothesis and mechanisms, also proposed in this thesis (Chapter 3), concerning functionalizations, drug delivery and cellular uptake and CNTs methabolism are inserting themselves in the ongoing discussions on these subjects.

1.3 CNT toxicity

Toxicity of CNTs represents a hot topic. It relates to the health care of researchers working with this nanomaterial, but it is also an issue concerning all their future applications. In fact, this general anxiety is about more or less all nanomaterial, and nanotoxicology is a new science that verifies the acute and chronic toxicity of all new nanoscale materials. Another problem, to be mentioned, is that nanotechnology and carbon nanotubes have been studied for approximately twenty years and worries about their toxicity seriously arised during the last ten years. This means that results about long-term toxicity are still far to be defined.

Anyway, different studies with as-produced and f-SWCNTs and f-MWCNTs have been performed, sorting out that the toxicity is related to purity and functionalization of CNTs. Wick et al have shown that on lung mesothelic cells (MSTO-211H) cytotoxicity is correlated to the degree of agglomeration. They tested SWCNTs as produced and found that suspended CNTs-bundles are less toxic than asbestos fibers[20]. Nevertheless, it is common opinion that chemically f-CNTs do not exert cytotoxicity[21,22], and, in particular and not surprisingly, that covalent f-CNTs are better than non-covalent functionlized ones, depending on the degree of functionalization[23].

Besides this, a paper appeared on Nature Nanotechnology[24] had an impact in that field that in our opinion has been excessive. These authors reported that

CNTs show asbestos-like pathogeniticity, but their pilot study was developed using long MWCNTs (from 5 to 20 μm). In our study, and in general for biological applications, CNTs are shorter than 1 μm and the average length is usually between 400-600 nm. Moreover, we can add that, for what concerns asbestos, fiber length and diameter are important factors in determining the citotoxicity[25] and it seems that longer fibers are more cytotoxic than shorter ones, even though authors claimed that the debate was still open. To our knowledge, shorter CNTs are also more soluble and then biocompatible.

The toxicological properties of all nanomaterials are not negligible, but a lot of studies are still necessary. From what is reported above, it is clear that covalent functionalization improves the biocompatibility and that the length of CNTs has to be controlled. Indeed, in this thesis, we demonstrate the full biocompatibility of short covalently f-CNTs.

1.4 Aim of the thesis

The uses of CNTs in different fields are really promising and the aim of this work is the preparation of new functionalized CNTs with different applications, focusing our attention on biological purposes.

One of the main limitations of CNTs is the lack of solubility in solvents, especially the biological compatible ones. To overcome this problem, we covalently funtionalize carbon nanotubes using two different approaches. The first one is represented by 1,3-dipolar cycloaddition of azomethine ylides by means of thermal heating, the second one concerns the use of MW irradiation combined with the presence of ionic liquids (ILs) to functionalize CNTs with differently substituted pyrrolidine rings (Chapter 2). On the surface of the derivatives obtained in the thermal conditions we will grow dendron units to increase the water-solubility. Different dendron generations will be prepared to study their solubility, their cellular uptake and their capability to act as siRNA delivery systems (Chapter 3). We will use a RNA sequence able to kill cells, so the effects of the delivery will be

unequivocal. Moreover we will use these compounds to perform preliminary biodistribution studies, necessary to develop the use of CNT for biological applications.

The CNT derivatives will be also explored as substrates for neuronal cultures (Chapter 4). Morphological studies to investigate the interactions between CNTs and cellular membranes will be performed and electrophysiological recordings will be used to characterize the neuronal network.

References

(1) Taniguchi, Norio On the Basic Concept of Nanotechnology. *Proc. ICPE Tokyo* **1974**, *Part II*, 18-23.

(2) Edwards, S. A. *The Nanotech Pioneers: Where Are They Taking Us*; Wiley-VCH, 2006.

(3) Drexler, K. E. Molecular engineering: An approach to the development of general capabilities for molecular manipulation. *Proceedings of the National Academy of Sciences of the United States of America* **1981**, *78*, 5275-5278.

(4) Drexler, E. *Engines of Creation: The Coming Era of Nanotechnology*; Anchor, 1987.

(5) Jr, C. P. P.; Owens, F. J. *Introduction to Nanotechnology*; 1° ed.; Wiley-Interscience, 2003.

(6) Saito, R.; Dresselhaus, G.; Dresselhaus, M. S. *Physical Properties of Carbon Nanotubes*; 1° ed.; World Scientific Publishing Company, **1998**.

(7) Iijima, S. Helical microtubules of graphitic carbon. *Nature* **1991**, *354*, 56-58.

(8) Belin, T.; Epron, F. Characterization methods of carbon nanotubes: A review. *Materials Science and Engineering B: Solid-State Materials for Advanced Technology* **2005**, *119*, 105-118.

(9) Bonifazi, D.; Nacci, C.; Marega, R.; Campidelli, S.; Ceballos, G.; Modesti, S.; Meneghetti, M.; Prato, M. Microscopic and spectroscopic characterization of paintbrush-like single-walled carbon nanotubes. *Nano Letters* **2006**, *6*, 1408-1414.

(10) Singh, P.; Campidelli, S.; Giordani, S.; Bonifazi, D.; Bianco, A.; Prato, M. Organic functionalisation and characterisation of single-walled carbon nanotubes. *Chemical Society Reviews* **2009**, *38*, 2214-2230.

(11) Jorio, A.; Dresselhaus, Gene; Dresselhaus, Mildred S. *Carbon Nanotubes: Advanced Topics in the Synthesis, Structure, Properties and Applications*; 1° ed.; Springer, 2008.

(12) Hirsch, A. Functionalization of single-walled carbon nanotubes. *Angewandte Chemie - International Edition* **2002**, *41*, 1853-1859.

(13) Tasis, D.; Tagmatarchis, N.; Bianco, A.; Prato, M. Chemistry of carbon nanotubes. *Chemical Reviews* **2006**, *106*, 1105-1136.

(14) Vaisman, L.; Wagner, H.; Marom, G. The role of surfactants in dispersion of carbon nanotubes. *Advances in Colloid and Interface Science* **2006**, *128-130*, 37-46.

(15) Kam, N.; Jessop, T.; Wender, P.; Dai, H. Nanotube molecular transporters: Internalization of carbon nanotube-protein conjugates into mammalian cells. *Journal of the American Chemical Society* **2004**, *126*, 6850-6851.

(16) Pantarotto, D.; Singh, R.; McCarthy, D.; Erhardt, M.; Briand, J.; Prato, M.; Kostarelos, K.; Bianco, A. Functionalized carbon nanotubes for plasmid DNA gene delivery. *Angewandte Chemie - International Edition* **2004**, *43*, 5242-5246.

(17) Kam, N.; Liu, Z.; Dai, H. Carbon nanotubes as intracellular transporters for proteins and DNA: An investigation of the uptake mechanism and pathway. *Angewandte Chemie - International Edition* **2006**, *45*, 577-581.

(18) Jin, H.; Heller, D.; Strano, M. Single-particle tracking of endocytosis and exocytosis of single-walled carbon nanotubes in NIH-3T3 cells. *Nano Letters* **2008**, *8*, 1577-1585.

(19) Lacerda, L.; Herrero, M.; Venner, K.; Bianco, A.; Prato, M.; Kostarelos, K. Carbon-nanotube shape and individualization critical for renal excretion. *Small* **2008**, *4*, 1130-1132.

(20) Wick, P.; Manser, P.; Limbach, L.; Dettlaff-Weglikowska, U.; Krumeich, F.; Roth, S.; Stark, W.; Bruinink, A. The degree and kind of agglomeration affect carbon nanotube cytotoxicity. *Toxicology Letters* **2007**, *168*, 121-131.

(21) Smart, S.; Cassady, A.; Lu, G.; Martin, D. The biocompatibility of carbon nanotubes. *Carbon* **2006**, *44*, 1034-1047.

(22) Dumortier, H.; Lacotte, S.; Pastorin, G.; Marega, R.; Wu, W.; Bonifazi, D.; Briand, J.; Prato, M.; Muller, S.; Bianco, A. Functionalized carbon nanotubes are non-cytotoxic and preserve the functionality of primary immune cells. *Nano Letters* **2006**, *6*, 1522-1528.

(23) Sayes, C.; Liang, F.; Hudson, J.; Mendez, J.; Guo, W.; Beach, J.; Moore, V.; Doyle, C.; West, J.; Billups, W.; Ausman, K.; Colvin, V. Functionalization density dependence of single-walled carbon nanotubes cytotoxicity in vitro. *Toxicology Letters* **2006**, *161*, 135-142.

(24) Poland, C.; Duffin, R.; Kinloch, I.; Maynard, A.; Wallace, W.; Seaton, A.; Stone, V.; Brown, S.; MacNee, W.; Donaldson, K. Carbon nanotubes introduced into the abdominal cavity of mice show asbestos-like pathogenicity in a pilot study. *Nature Nanotechnology* **2008**, *3*, 423-428.

(25) Goodglick, L.; Kane, A. Cytotoxicity of long and short crocidolite asbestos fibers in vitro and in vivo. *Cancer Research* **1990**, *50*, 5153-5163.

CHAPTER 2:

COVALENT FUNCTIONALIZATION OF CARBON NANOTUBES

2.1 Synthesis and Physicochemical characterization of a Carbon Nanotube–Dendron Series[1]

By means of widely used thermal reactions we succeeded in the synthesis of a new series of polyamidoamine (PAMAM) dendron-functionalized MWCNT derivatives, characterized by the presence of numerous tetra-alkyl ammonium salts at the periphery of the dendron.

The polyamidoamine (PAMAM) dendrons attached onto MWCNTs[1] enhance their aqueous solubility due to the presence of many polar groups. A stepwise synthetic process was followed to achieve growth of the dendron on the MWCNTs

[1] The work reported in the first part of this chapter has been published in: *Journal of American Chemical Society*, **2009**, 131 (28), pp 9843-9848. "Synthesis and characterization of a carbon nanotube-dendron series for efficient siRNA delivery" by Herrero M.A., Toma F.M., Al-Jamal K.T., Kostarelos K., Bianco A., Da Ros T., Bano F., Casalis L., Scoles G., Prato M.

up to the second-generation. Pristine MWCNTs, initially functionalized using 1,3-dipolar cycloaddition of azomethine ylides, were further modified by combining a double additions of methyl acrylate, including a complete addition of the amino groups, with ethylene diamine addition, leading to an exhaustive amidation of the ester functionalities (Scheme 1). The second generation dendron bears the highest number of peripheral primary amino groups (4 amino groups per dendron moiety), which eventually undergo a process of alkylation using an epoxy derivative[2]. The same alkylation was also performed for zero, first and second-generation (G_0, G_1 and G_2 respectively).

In detail, functionalization of MWCNTs using the 1,3-dipolar cycloaddition of azomethine ylides was used to introduce the pyrrolidine moiety at the external surface and the tips of MWCNTs **1** (Scheme 1). First-generation (G_1) and second-generation (G_2) dendron-MWCNT **4** and **7** were synthesized by repeating twice the two-step reaction using methyl acrylate and ethylene diamine. We proceeded in alkylation of the (G_0) dendron-MWCNT **1**, (G_1) dendron-MWCNT **4** and (G_2) dendron-MWCNT **7** with a glycidyl trimethylammonium chloride epoxy derivative to generate polycationic dendron-MWCNT **2, 5** and **8**, respectively (Scheme 1)[2]. The Kaiser test allowed quantification of the amino groups for the different generations of dendrons before alkylation[3]. The test gave negative results for the alkylated conjugates (**2**, **5** and **8**), consistent with complete conversion of the primary amino groups. The amount of primary amino groups on MWCNT **1** was measured by the Kaiser test as 481 μmol/g. Subsequent Kaiser tests gave amine loadings of 718 μmol/g and 1097 μmol/g for the first and second generation, respectively.

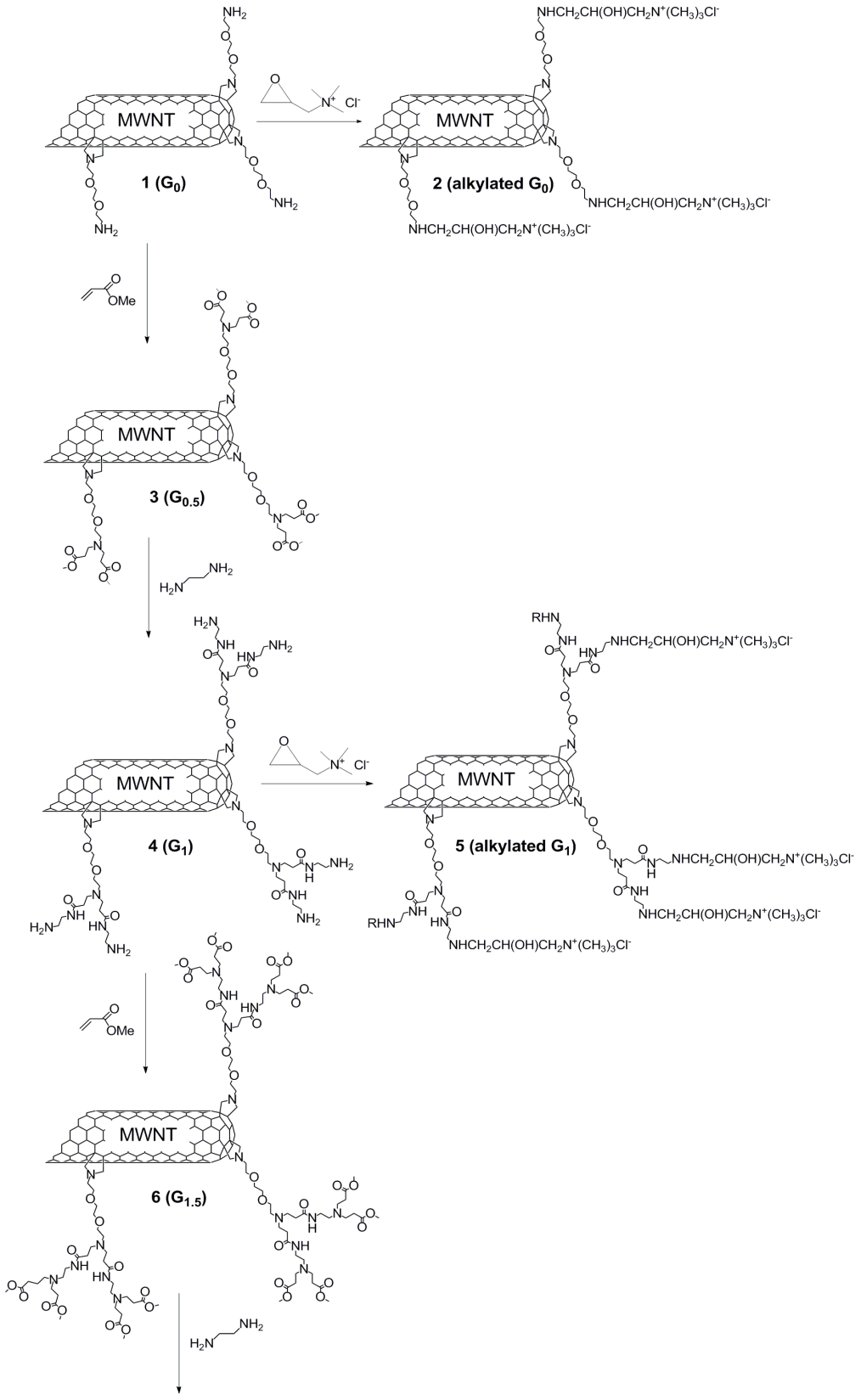
MWNT
1 (G0)
2 (alkylated G0)
3 (G0.5)
4 (G1)
5 (alkylated G1)
6 (G1.5)

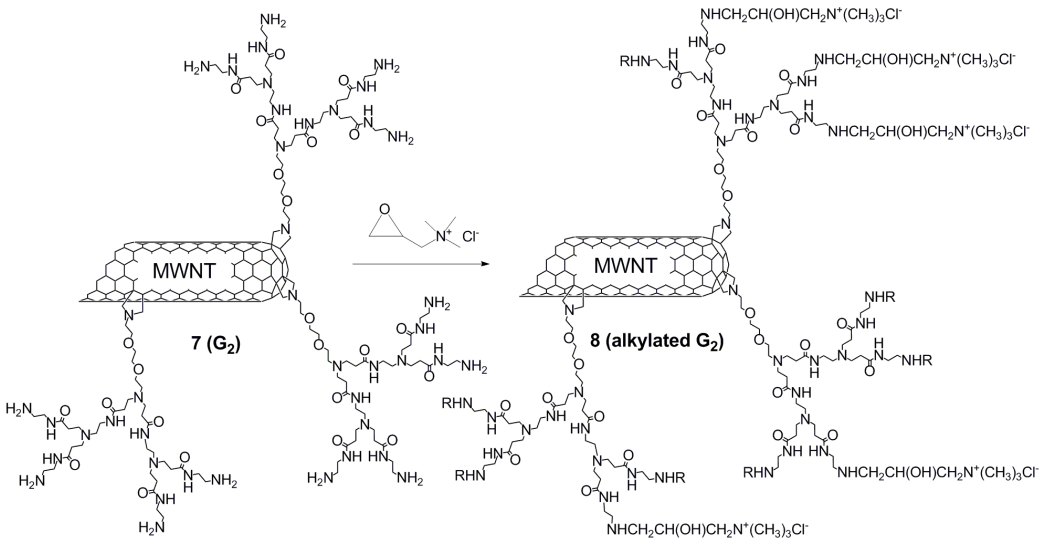

Scheme 1. Reaction conditions for the synthesis of G_2 PAMAM dendron-MWCNTs and consequent alkylation of primary amino groups with glycidyl trimethylammonium chloride. MeOH, 40 °C, 48 h. R = -$CH_2CH(OH)CH_2N(CH_3)_3^+Cl^-$.

The different CNT conjugates were fully characterized by standard techniques, as thermogravimetric analysis (TGA), TEM, and both atomic force microscopy (AFM) and enhanced electrostatic force microscopy (E-EFM).

The solubility of the charged dendron-MWCNTs was assessed in water. The insets of Figure 1 display the differences in the dispersibility of the conjugates. A clear increase in solubility was observed going from MWCNT **1** to the higher alkylated dendron generations. The aqueous solution of compound **8** was stable for at least four weeks at room temperature without formation of any precipitate and the solubility obtained was up to 3 mg/mL.

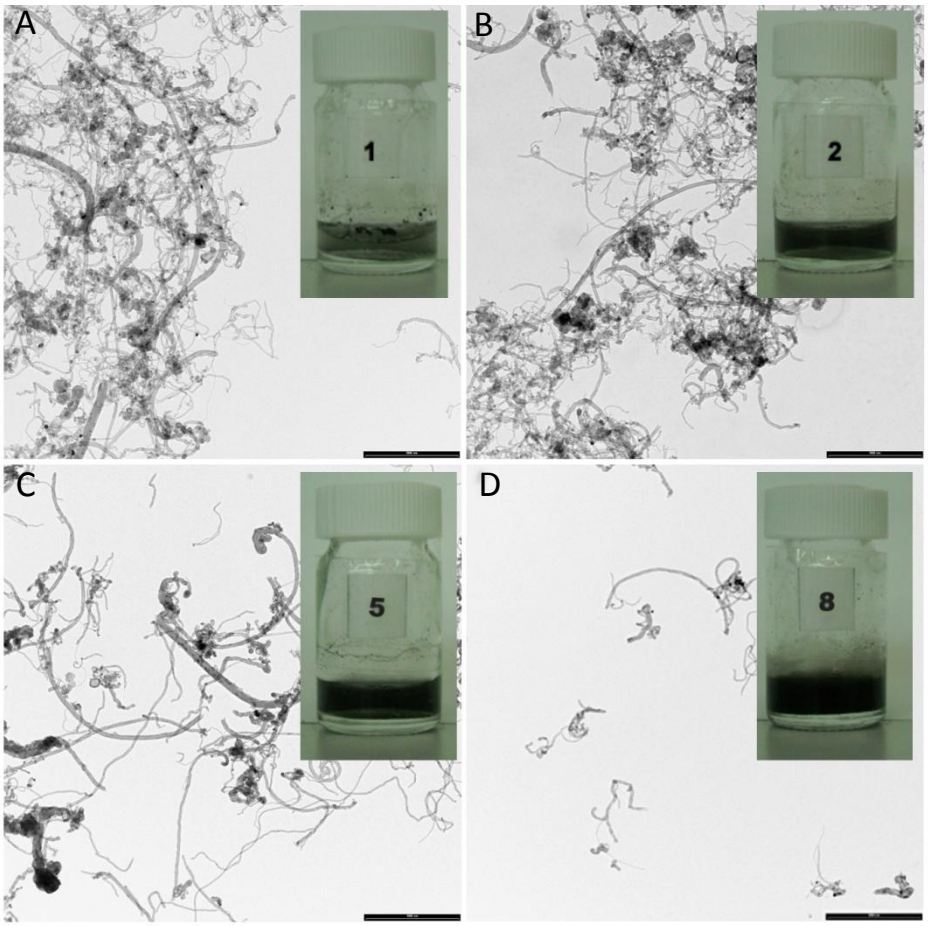

Figure 1. TEM image of (A) MWCNT **1**; (B) alkylated (G_0) dendron-MWCNT **2**; (C) alkylated (G_1) dendron-MWCNT **5;** (D) alkylated (G_2) dendron-MWCNT **8**. Scale bar is 1 μm. Inset: MWCNT **1**, alkylated (G_0) dedron-MWCNT **2**, alkylated (G_1) dendron-MWCNT **5**, and alkylated (G_2) dendron-MWCNT **8** (all solubilized at 1 mg/mL of H_2O).

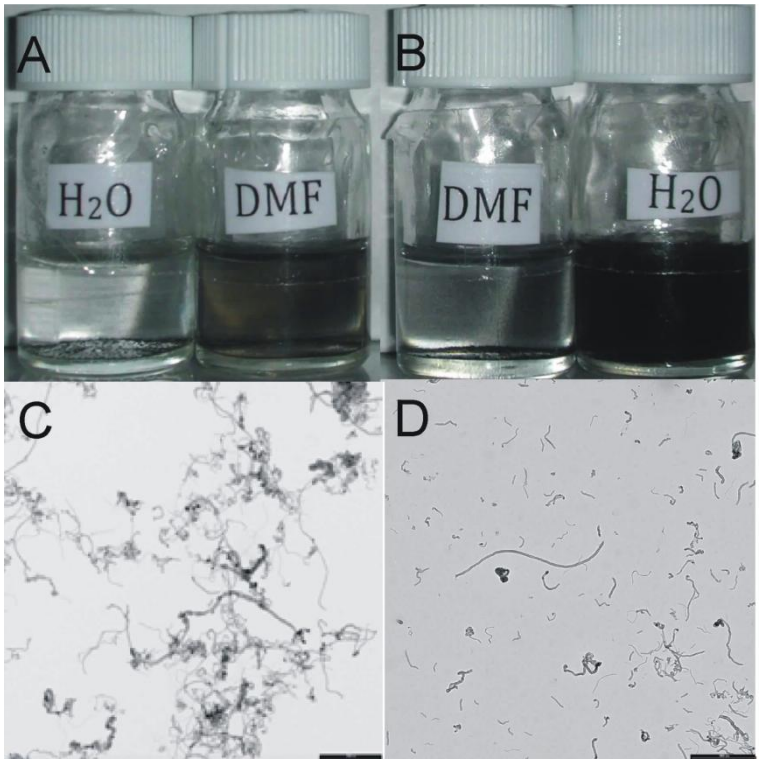

Figure 2. A) (G_2) dendron-MWCNT **7** (0.3 mg) in 3 mL of DMF and H_2O, respectively; B) alkylated (G_2) dendron-MWCNT **8** (0.3 mg) in 3 mL of DMF and H_2O, respectively. C) TEM image of (G_1) dendron-MWCNT **4** (dissolved in water), and D) TEM image of alkylated (G_2) dendron-MWCNT **8** (dissolved in water). Scale bar is 1 μm.

Moreover, the water solubility of conjugate **8** was tenfold higher than conjugate **7** with solubility of 3 mg/mL and 0.1 mg/mL, respectively. Figure 2A shows that dendron-MWCNT **7** disperses better in dimethyl formammide (DMF), with relatively low solubility in water. Alkylated conjugate **8**, on the other hand, exhibits reversed behavior, with enhanced solubility in water (Figure 2B). TEM images confirm the presence of MWCNTs, showing morphological differences for the different dendron generations in water, including a remarkable increase in the degree of dispersibility (Figure 2C and 2D).

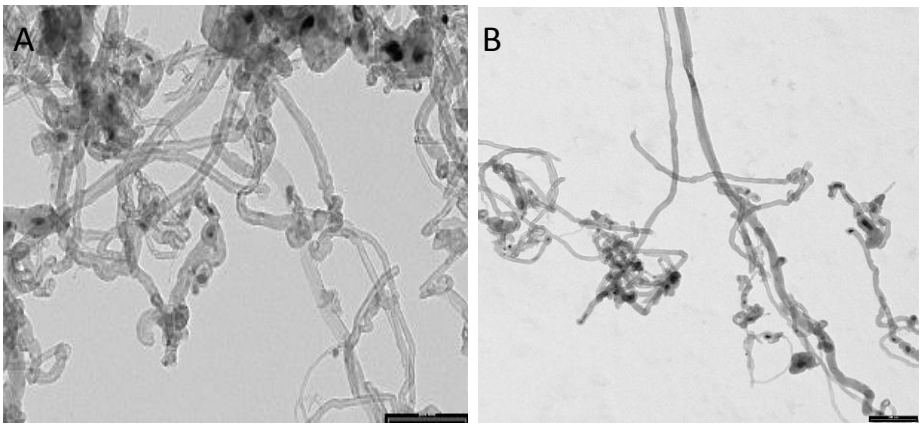

Figure 3. TEM image of (A) Boc-amino protected MWCNTs **1**, and (B) MWCNT **6**. Scale bar: 200 nm**.**

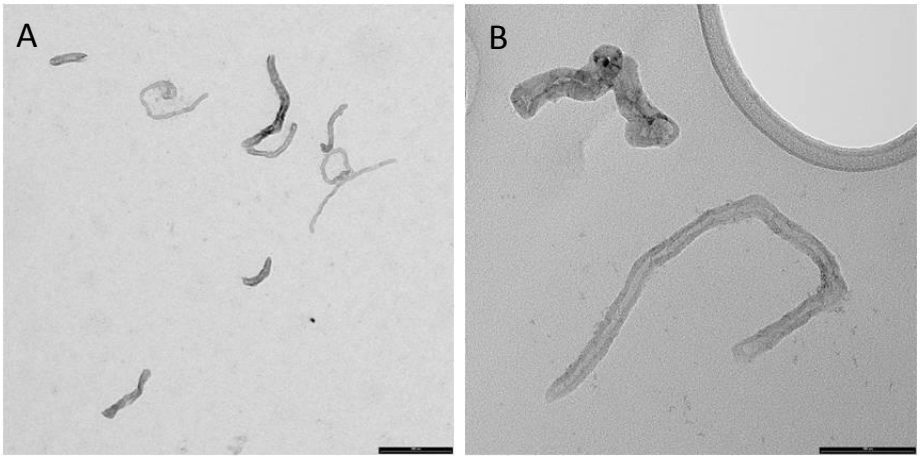

Figure 4. TEM images of dendron-MWCNT **6**. Scale bar: 200 nm (A) and 100 nm (B).

The f-MWCNTs were structurally studied by TEM (Figure 1-4). The images confirm the presence of MWCNTs, showing morphological differences for the different dendron generations in water, including a remarkable increase in the degree of dispersibility.

In addition to TEM, alkylated (G_2) dendron-MWCNT **8** was characterized by AFM, performed by depositing a sample of the aqueous dispersion on a mica surface. A progressive increase in the diameter of the nanotubes as the dendritic structure grew was observed. The AFM images show in the sample both individualized and small bundles of MWCNTs. The 3D view of cropped section of Boc-amino protected MWCNT **1** and dendron-MWCNT **8** from a 1.2 × 1.2 μm^2 AFM topographic image along their line profiles are shown in Figure 5A and 5B,

respectively. As can be seen, there is a clear increase in diameter of the MWCNT conjugates with the increasing of dendron generations. To evaluate the average profile, the diameter of pristine MWCNTs, Boc-amino protected MWCNT **1** and dendron-MWCNT **8** was measured, giving values that range from 21-25 nm for Boc-amino protected MWCNT **1** and up to 36-40 nm for MWCNT **8**, respectively (Figure 5C).

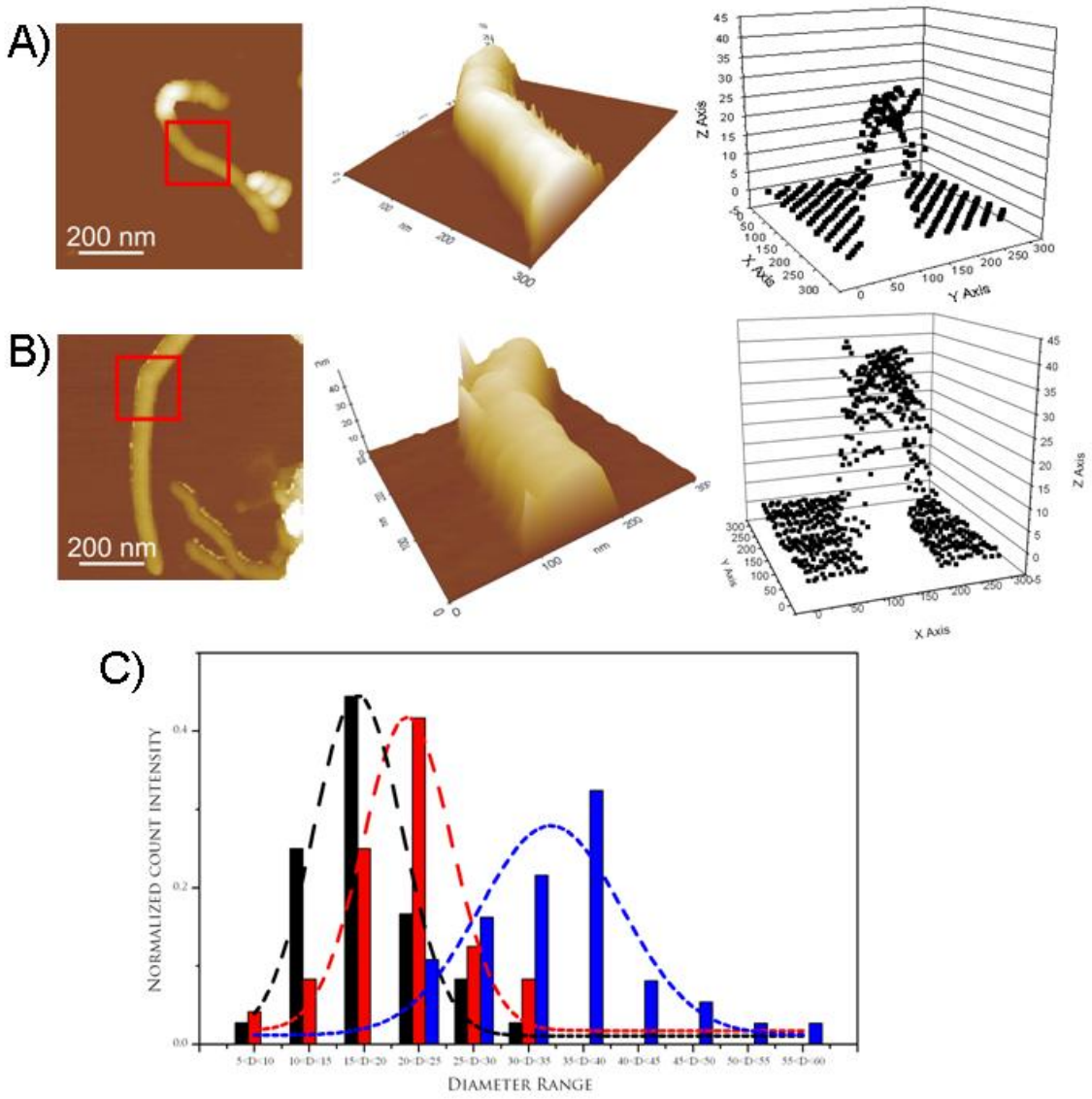

Figure 5. 1.2 × 1.2 μm^2 AFM topographic images of (A) MWCNTs after 1,3-dipolar cycloaddition reaction (Boc-amino protected MWCNT **1**), and (B) the alkylated (G_2) dendron-MWCNTs **8** along their 3D view of

cropped segments [red square box in part (A) and (B) and line profiles (right plots)]. (C) Diameter distribution of pristine MWCNTs (black), MWCNT after 1,3-dipolar cycloaddition reaction (Boc-amino protected MWCNT **1**) (red), and alkylated (G_2) dendron-MWCNT **8** (blue). The three curves represent the Gaussian fit of the data.

The weight loss for the highly functionalized conjugates, calculated from the thermogravimetric curves at 450°C, was directly correlated to the increase of mass around the CNTs, introduced at each step. The mass attributed to functionalities increased from 12.5% in the first-generation **4** to 18 % in the second-generation dendron-MWCNT **7**. The final derivative **8** showed a 28% mass loss (Figure 6). The number of the functional groups for the final dendron-MWCNT **8** calculated from the TGA curve corresponds to 237 μmol/g, resulting in 948 μmol/g of amine groups for the precursor MWCNT **7**. This value was in good agreement with the value found using the Kaiser test (1097 μmol/g).

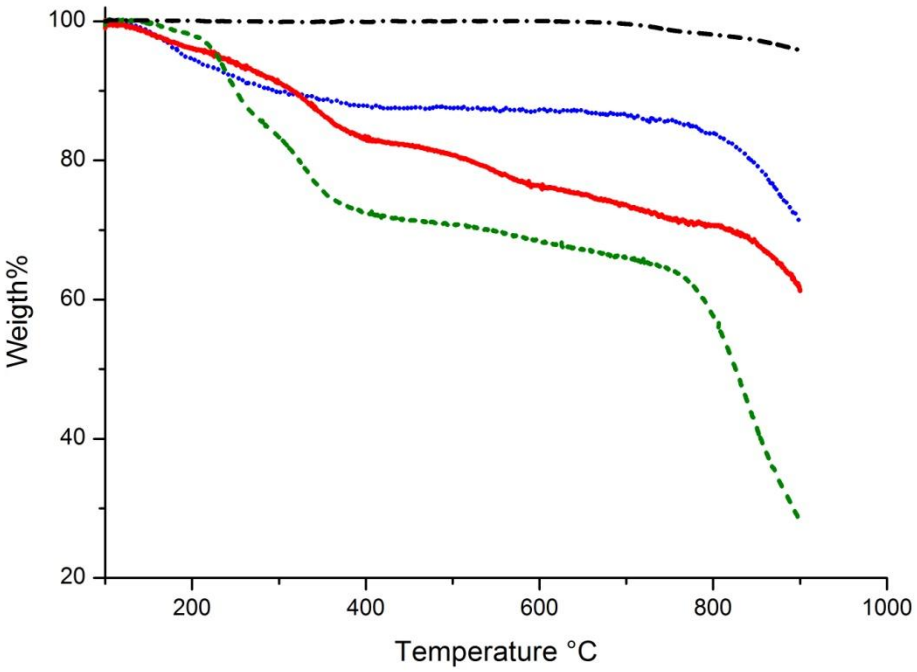

Figure 6. TGA curves of pristine MWCNTs (black dash dot line), G_1 dendron-MWCNT **4** (blue dot line), G_2 dendron-MWCNTs **7** (red solid line) and alkylated G_2 dendron-MWCNT **8** (green dash line). All the experiments were performed under N_2 atmosphere.

In order to assess the presence of functionalized groups on the MWCNT surface, we investigated the electrostatic properties of dendron-functionalized MWCNTs deposited on a silicon substrate. By means of E-EFM we studied the localization of positive charges due to the quaternary salt of the moieties.

We investigated, at different applied biases, two different samples: pristine MWCNTs and MWCNTs **8**, each of them deposited as methanolic solutions on a silicon oxide surface.

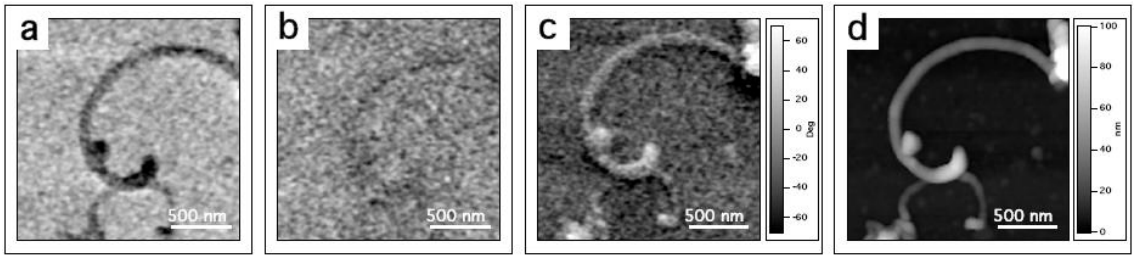

Figure 7. E-EFM phase images respectively at a) -3V, b) 0V and c) 3V, of pristine MWCNTs; d: topography of pristine MWCNTs.

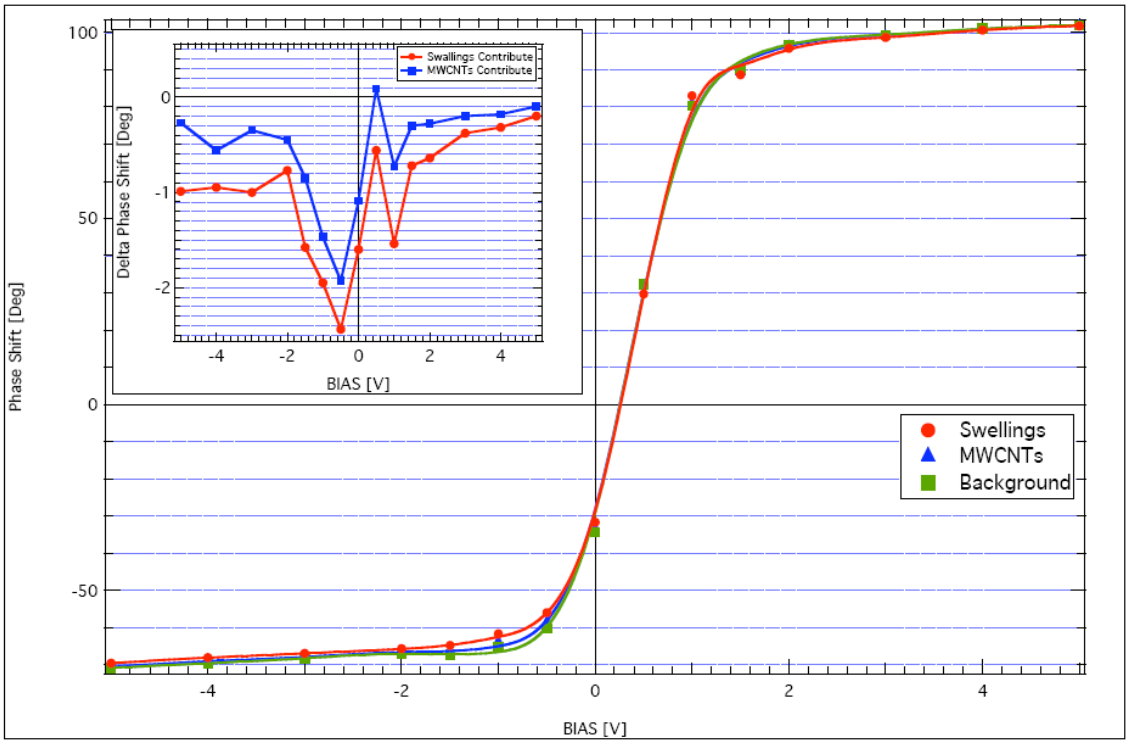

Figure 8. Phase shift versus bias plot of: background (green square symbol), nanotube body (blue triangular symbol) and "sweelings" (red circular symbol) for pristine MWCNTs on silicon oxide. The phase-shift is related to the different regimes: repulsive for negative phase shift, and attractive for positive phase shifts.

We reported the topography, the simultaneosly acquired phase images and corresponding plots of pristine MWCNTs. Herein, we noticed that some swellings, as impurities, appeared also in the case of not-functionalized nanotubes. Noteworthy, impurities have a different phase shift with respect to the functionalizations of MWCNTs. In fact, we plotted E-EFM phase signals for three different areas for unmodified MWCNTs:silicon oxide background, nanotubes and "swellings". The phase shift versus applied probe bias is shown in Figure 7a, b and c. We can assert that the total charge on the surface is negative and this is proved by graph trend in Figure 7 (repulsion for negative biases, attraction in case of positive voltages). This general behavior may be explained by the presence of negative terminations distributed on the silicon oxide surface. The behavior of the

swellings, in this case, does not have any difference compared to that one of the nanotubes.

We proceeded in the analysis of MWCNT **8**. In the topographic image shown in Figure 9D, we can distinguish three different areas: a homogeneous substrate (i), the nanotubes, uniformly dispersed on the substrate (ii), and some "decorations" (iii) that appear along the nanotubes in the case of dendron f-MWCNTs.

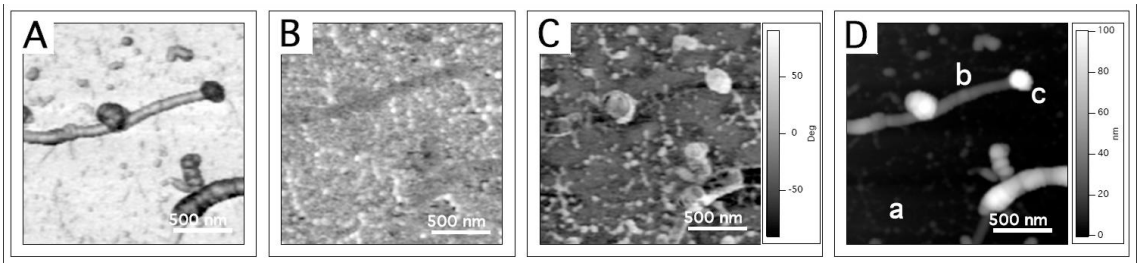

Figure 9. E-EFM phase images respectively at A) -3V, B) 0V and C) 3V, of derivative dendron f-MWCNTs **8**; D) topographic image (a,b and c are respectively the background, the nanotube body and the decorations).

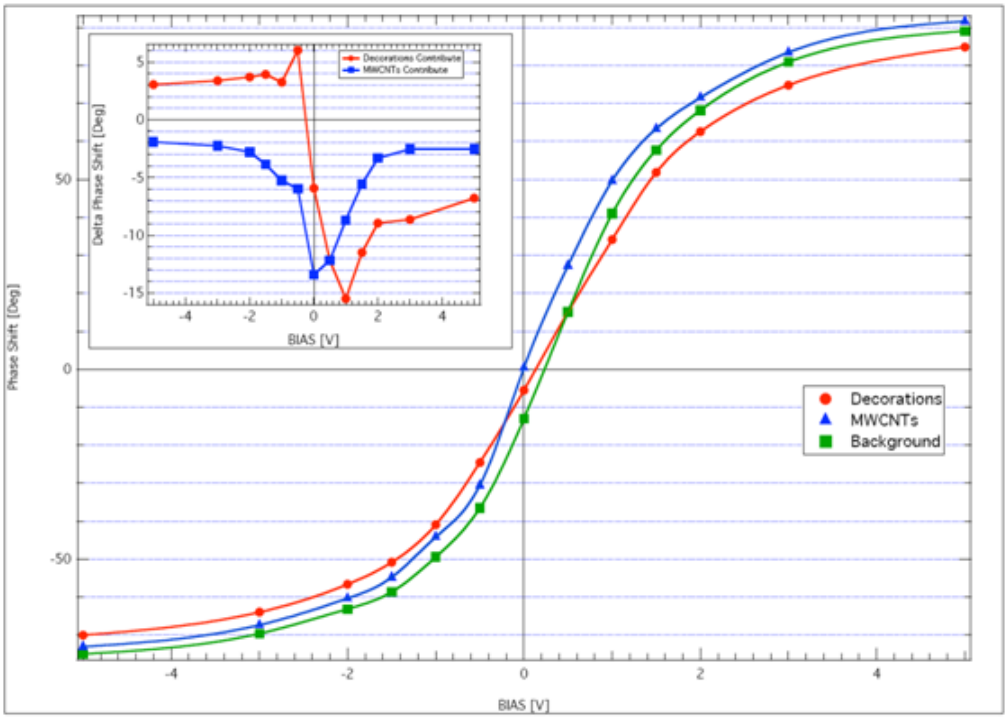

Figure 10. Phase shift versus bias plot of : background (green), nanotube body (blue) and "decorations" (red) for f-MWCNTs on silicon oxide. The phase-shift is related to the different regimes: repulsive for negative phase shift, and attractive for positive phase shifts.

These "decorations" behave differently from the nanotube body in the phase-shift electrostatic images. To investigate the electrostatic nature of such areas, we plotted E-EFM phase signals for each of the previously described areas (silicon oxide background, nanotubes and "decorations") as a function of different values of the applied DC voltage. Results are shown in Figure 10. It is evident from the figure that the "decorations" are in general less attracted by the tip, with respect to the substrate, at positive bias, and less repulsed at negative bias. This is compatible with a positive or, at least, less negative than the substrate charge distribution localized at the "decorations". More in general, although the presence of positive charges on MWCNTs, we can assert that the total charge felt by the tip on the sample (i.e. background + MWCNT+ decorations) is negative, as proved by the trends of the graphs in Figure 10 (repulsion for negative biases, attraction in case of positive voltages). This general behavior can be explained, as before, by the presence of negative terminations distributed along the whole silicon oxide surface. To better evidence the different contribution of the MWCNTs body and of the "decorations" to the electrostatic measurements, we have subtracted from the two curves the background phase signal and the nanotube phase signal (that contains also the background contribution) respectively. The results are shown in the inset of graph Figure 10. We can immediately see that the "decorations" behave differently from the nanotube bodies: the "decorations" trace has a central symmetry (with respect to the axis origin), compatible with a localized positive charge, while the nanotube body is symmetric with respect to the y-axis, compatible with the behavior of a dipole. The comparison of these data to the one reported for pristine MWCNTs (Figure 8), clearly shows that "swellings" behaves differently form "decorations" and are more like the CNT body.

A possible explanation for this response is the easy polarizability of carbon nanotubes due to electron mobility. The asymmetry of the polarization is reasonably due to the silicon oxide negative charges below the MWCNTs that reduce the dipole for negative tip voltages.

We can confirm that the nanotubes behave as non-symmetric dipoles, due to the influence of the underneath silicon oxide surface, while we can discriminate the presence of positive charges localized at the functionalization sites.

We are currently investigating the electrostatic behavior of SWCNTs with the same functionalizations, in order to better understand this type of interactions.

2.2 Microwave-Assisted Functionalization of Carbon Nanotubes in Ionic Liquids[2]

In this section, an innovative strategy for the functionalization of carbon nanotubes is presented, designed by the combined use of ILs and microwave irradiation (Appendix B).

Building on the fullerene experience, a wide variety of reactions have been carried out for the covalent functionalization of CNTs. At variance with the fullerene analogues, CNTs require harsh temperature and/or pressure conditions, with a large use of organic solvents and long reaction times. Therefore, microwave (MW) assisted and solvent-free protocols have been developed to accelerate reactions and produce f-CNTs efficiently. A recent achievement has been the double functionalization of SWCNTs with azomethine ylides and arene radical additions, both promoted by MW[6,7]. In this perspective, the optimization of CNTs functionalization methods should also address the replacement of hazardous VOCs with alternative reaction media. To this end, ILs have been used successfully for a

[2] The work reported in the second part of this chapter is a part of a paper recently accepted for publication in *Chemistry – A European Journal*. "Microwave-Assisted Functionalization of Carbon Nanostructures in Ionic Liquids" by Ivan Guryanov I., Toma F.M., Montellano López A., Carraro M., Da Ros T., Angelini G., D'Aurizio E., Fontana A., Maggini M., Prato M., Bonchio M.

variety of organic transformations at room temperature[8]. Recognized advantages of ILs are their tuneable composition, polar character, non-volatility, thermal resistance, complementarity with water or other green media and liquid electrolyte behavior. In addition, IL phases are instrumental for fast and selective MW-heating by ionic conduction mechanism, with negligible vapour pressure and safer set-up conditions[9,10]. Aggregation phenomena, driven by the low solubility of CNTs in polar environment, are expected to affect the reactivity behavior in IL media. Noteworthy, it has been recently demonstrated that SWCNTs, upon grinding with ILs, form highly viscous gels termed "bucky gels" with extraordinary mechanical properties, and thermal[11], electrochemical[12,13] and rheological properties[14] have been investigated by several authors. The gelation refers to mixtures in which an exfoliation process of the nanotube bundles is induced by the tendency of ILs to adsorbe around the SWCNT surface. The use of bucky gels as reaction media has been investigated for the addition of diazonium ions to the SWCNT surface[15]. Exfoliation of the SWCNT ropes by the IL environment accelerates the reaction which occurs in minutes at room temperature.

We investigated the effect of MW irradiation and ILs on the 1,3-dipolar cycloaddition of azomethine ylides to SWCNTs by screening the reaction protocol together with the IL medium composition, the concentration factor, the applied MW power and the simultaneous cooling of the system. This latter turned out to be crucial for directly dosing high levels of MW power to the reaction without over-heating[16,17]. Our results include: (i) the evaluation of the cycloaddition kinetics and selectivity in both *o*-DCB and IL containing media; (ii) optimization of the synthetic protocol towards multi-substitution on the CNTs surface; (iii) extension of the optimized protocol to fluorous-tagged aldehydes. Under MW-assisted reaction in IL phases, fluorous-tagged CNTs (FT-CNTs) could be readily isolated. Preliminary investigations showed a remarkable solubility of FT-CNTs in fluorous phases, with potential application in catalysis, material science and membrane-based technology[18].

The combined use of MW-activation and ILs provides a new strategy for the functionalization of purified, non-oxidized SWCNTs by 1,3-dipolar cycloaddition. We explored the use of the so-called "bucky gels", as reaction media, when exposed to reagents and to MW irradiation. We have tested three different ILs, namely 1-butyl-3-methylimidaziolinium tetrafluoroborate ([bmim]BF_4), 1-methyl-3-octylimidazolinium tetrafluoroborate ([omim]BF_4) and 1-hexadecyl-3-vinylimidazolinium bis(trifluoromethylsulfonyl)imide ([hvim][$(CF_3SO_2)_2N$]) (Scheme 2) to evaluate the influence of the length of the alkyl chain (4, 8 or 16 carbon atoms, respectively) and of the presence of an additional π bond (in the case of [hvim][$(CF_3SO_2)_2N$]) on the SWCNT exfoliation ability and cycloaddition promotion.

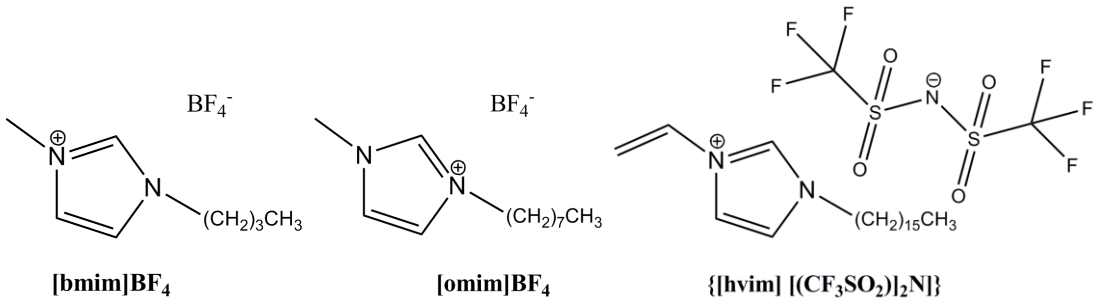

Scheme 2. Molecular formulas of [bmim]BF_4, [omim]BF_4 and [hvim]$CF_3SO_2)_2N$]

The exfoliation ability has been investigated, in collaboration with University of Chieti, through rheological measurements at 25 and 60°C in order to study the changes in stability, consistency and degree of the IL coating on the SWCNTs by varying the IL nature and the temperature. Indeed, the affinity of ILs for the SWCNT surface is fundamental for the formation of the gels as pure ILs do not possess any elastic component. Rheological measurements in the dynamic mode at a constant shear stress indicate a viscoelastic gel-like behaviour for the investigated IL-SWCNT mixtures with the measured storage moduli (elastic, *G*') dominating the loss moduli (viscous, *G*") by one order of magnitude and exhibiting little frequency dependence over the range of angular frequencies tested.

This piece of evidence highlights the existence of weak interactions within the gel[11]. On the other hand, they point to a large number of weak physical cross-links among the SWCNT bundles mediated by ILs. As a matter of fact cation-π interactions, and also weaker π-π interactions between alkylimidazolium cations and the sp^2-carbon framework of SWCNTs, may orient and trigger clustering of the surrounding imidazolium ions and consequently interconnect neighbouring SWCNTs. In addition, an increase in the temperature (from 25 to 60°C) provokes a decrease of the viscosity and also a further reduction of the endured shear stress. As far as the comparison of the investigated gel is concerned, the trend of the complex viscosity η**, of the elastic modulus and of the steady shear viscosity η follow approximately the order [hvim][$(CF_3SO_2)_2N$] > [omim]BF_4 ≥ [bmim]BF_4. The higher the values of *G'* and *G"*, the greater the number of interactions and/or the stronger the interactions within the gel[19]. This evidence points to the fact that, besides the prevailing cation-π interactions as already highlighted elsewhere[11], Van der Waals interactions between ILs and SWCNTs surface, due to the presence of the alkyl chains on the imidazolyl group, do affect the viscosity of the final gels. Nevertheless, additional π-π interactions cannot be excluded in the case of [hvim][$(CF_3SO_2)_2N$].

Table 1. Rheological characterization of the IL-SWCNT gels.

IL[a]	*G'*/Pa[b] at 25°C (at 60°C)	*G"*/Pa[b] at 25°C (at 60°C)	η**/cP[b,c] at 25°C (at 60°C)	τ_y/Pa at 25°C (at 60°C)	η/cP[d] at 25°C (at 60°C)
[bmim]BF_4	550 (300)	55 (50)	$8.9\cdot10^5$ ($4.3\cdot10^5$)	12 (5)	5000 (1000)
[omim]BF_4	800 (200)	80 (50)	$13\cdot10^5$ ($3.6\cdot10^5$)	25 (4)	7200 (1800)
[hvim][$(CF_3SO_2)_2N$]	(2500)	(400)	($43\cdot10^5$)	(9)	(2400)

[a] Pure [bmim]BF_4, [omim]BF_4 and [hvim]][$(CF_3SO_2)_2N$] have a viscosity of 80 cP at 25°C and 70 cP at 60°C, 240 cP at 25°C and 200 cP at 60°C and 200 cP at 60°C, respectively. [b] Shear stress (τ) 1.0 Pa satisfying the linear viscoelasticity; angular frequency (ω) varied from 0.1 to 10 Hz. [c] Calculated at the frequency of 0.1 Hz. [d] Calculated at γ 10 s^{-1}.

The gel phase provides the CNTs with a uniform coating of IL film, which favors exfoliation and assists the covalent modification of the carbon surface (Scheme 3)[20,21]. In this scenario, the pseudo-supported IL layer acts as a sort of extracting medium to: (i) solubilize and transfer the starting reagents, (ii) promote the *in-situ* formation of active intermediates, (iii) stabilize uphill pathways and transition states.

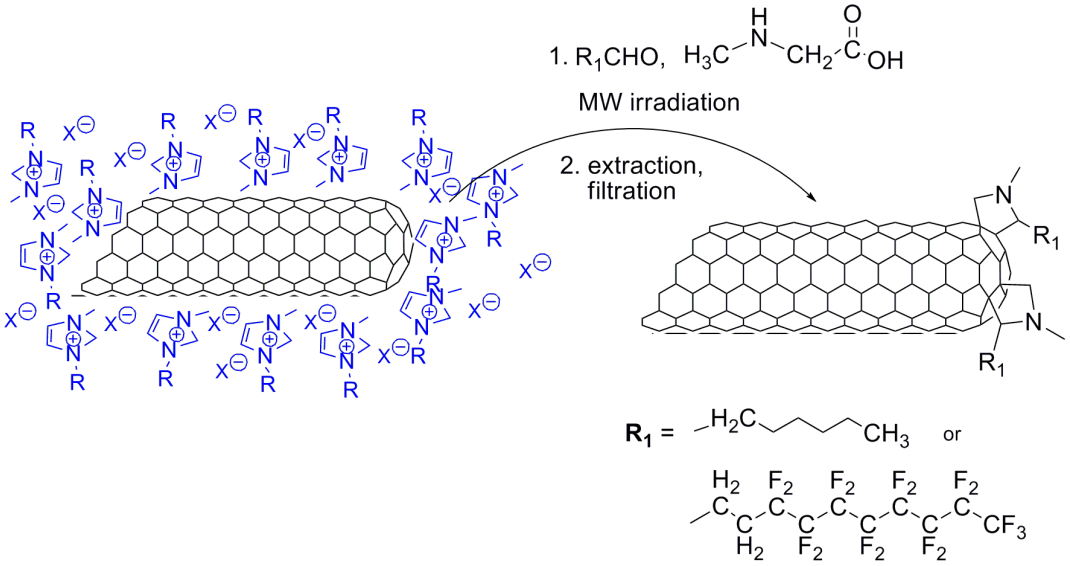

Scheme 3. Azomethine ylide cycloadditions to IL-containing bucky gels under MW irradiation

Furthermore, the IL matrix sets forward a molecular heater array, under MW irradiation, to foster a flash and highly efficient thermal activation for endothermal processes. With this aim, we have investigated the 1,3 dipolar addition of azomethine ylides to SWCNTs in IL-structured gels (Table 2). In the first instance, the degree of CNT functionalization (i.e. the number of attached functions per carbon atom of the nanotube) has been established by TGA that enables us to evaluate the total mass loss as derived from the functional groups covalently attached to the CNT surface, after subtraction of the pristine SWCNT contribution. The f-SWCNTs have been further characterized with a variety of techniques, including Raman, UV-Vis-NIR spectroscopies and TEM. The MW-assisted protocol has been compared with the conventional synthesis in either

molecular solvent (DMF) or [bmim]BF_4 performed for 5 days at 120 °C (entries **9** and **10** in Table 2). The loss of weight were calculated with respect to the starting material (SWCNTs CNI®).

Table 2. MW-assisted azomethine ylide cycloaddition to SWCNTs in IL.

entry[a]	Aldehyde	Solvent/T[b]	TGA wt loss %[c]	N[e]
9[e]	CH_3-$(CH_2)_5$CHO	DMF, 120°C	7	1/164
10[e]	CH_3-$(CH_2)_5$CHO	[bmim]BF_4, 120°C	7	1/156
11[f]	CH_3-$(CH_2)_5$CHO	[bmim]BF_4, MW	9	1/120
12[f]	CH_3-$(CH_2)_5$CHO	[omim]BF_4, MW	6	1/191
13[f]	CH_3-$(CH_2)_5$CHO	[hvmim][$(CF_3SO_2)_2$N], MW	0	0
14[f],[g]	CH_3-$(CH_2)_5$CHO	[bmim]BF_4/*o*-DCB, MW	16	1/60
15[f],[h]	C_8F_{17}-$(CH_2)_2$CHO	[bmim]BF_4, MW	14	1/239
16[f],[i]	C_8F_{17}-$(CH_2)_2$CHO	[bmim]BF_4, MW	16	1/211
17[h],[l]	C_8F_{17}-$(CH_2)_2$CHO	[bmim]BF_4, MW	27	1/108

[a] In all reactions: SWCNT Carbon Nanotechnologies Incorporated, 5-10 mg, sarcosine 1.0 mmol, aldehyde 2.0 mmol. [b] Solvent or IL gel and conditions with conventional heating (°C) or MW irradiation under magnetic stirring and simultaneous cooling by compressed air (MW). [c] % Weight loss determined by thermogravimetric analysis [d] SWCNT functionalization coverage per carbon atom. [e] Sarcosine 0.2 mmol, aldehyde 0.2 mmol, 5 day reaction. [f] 20 W, T_{bulk}=120 °C, 1h. [g] [omim]BF_4/*o*-DCB=1/3. [h] aldehyde 0.2 mmol, sarcosine 0.2 mmol. [i] Aldehyde 0.5 mmol, sarcosine 0.5 mmol. [l] 50 W, T_{bulk}=140 °C, 1h.

Noteworthy, MW irradiation, for 1h, at 20 W is instrumental for good to excellent functionalization of SWCNTs, yielding group coverage up to 1/60. This result represents one step forward in the chemistry of CNTs, as far as product yields and reaction time are concerned[6,7]. Moreover, under the conditions adopted, the bucky gels respond properly to MW absorption, with a well-behaved and reproducible temperature/pressure raise profile, so that the scaling-up of the synthesis is feasible with a controlled and safer reaction set-up. It is known that pristine SWCNTs, under solvent-free MW irradiation, undergo intense heat release in conjunction with uncontrolled spark emission and ignition phenomena. In a dense/viscous solvent environment, such highly effective MW absorption is

prevented, but also the flash MW-induced thermal activation is suppressed[6,7]. In this light, the bucky gel matrix does represent a powerful alternative, as the IL medium shields the strong SWCNT response while providing a safer source of instant heating, by virtue of its fully ionic character.

Data in Table 2 allow to address the impact of the IL nature and of *o*-DCB as co-solvent on the reaction efficiency. In particular, an increased performance is registered in low viscosity bucky gels. Indeed, the functionalization coverage decreases in the order [bmim]BF_4> [omim]BF_4> [hvim]$(CF_3SO_2)_2N$ (entries **11**-**13** in Table 2), thus ranking the IL in the reverse order with respect to the viscosity determination discussed previously. The different ability of the investigated bucky gels to function as solvent for the dipolar cycloaddition probably stems from the different mesoscopic structure of the gels formed. Indeed, many gels contain domains whose microviscosity is close to that of the neat liquid component (the IL in this case)[22], leading to relatively short translational diffusion coefficients despite a very high macroscopic viscosity. Indeed, in the present cases, the measured G' and G'' moduli clearly highlight increased interactions within the gel on increasing the length of the alkyl chain, with [hvim][$(CF_3SO_2)_2N$] being the IL characterized by the greatest number of interactions and/or the strongest interactions. Therefore, in the latter case, the mobility of one or more reactants might be particularly reduced, e.g. by selective entrapment in the gel network, to an extent adversely affecting the reaction rate.

TEM characterization of entries **9**, **12** and **13** in Table 2 (Figure 11) clearly prove the exfoliation effect of ILs with respect to entry **9**, improving dispersibility independently from the degree of functionalization.

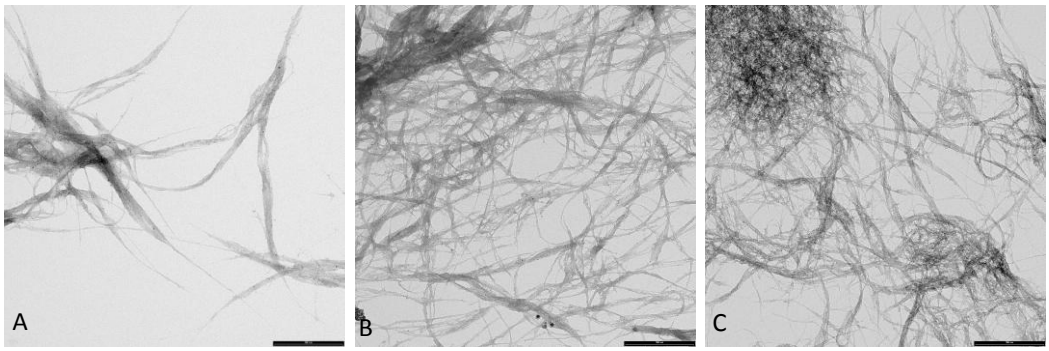

Figure 11. TEM images of f-SWCNTs, obtained as described in Table 2 and dispersed in DMF (1 mg/mL): A) entry **9;** B) entry **12;** C) entry **13**. TEM bar: 500 nm.

TGA and UltraViolet-Visible-NearInfraRed (UV-Vis-NIR) graphics for entries **10**, **12** and **13** are reported in Figure 12.

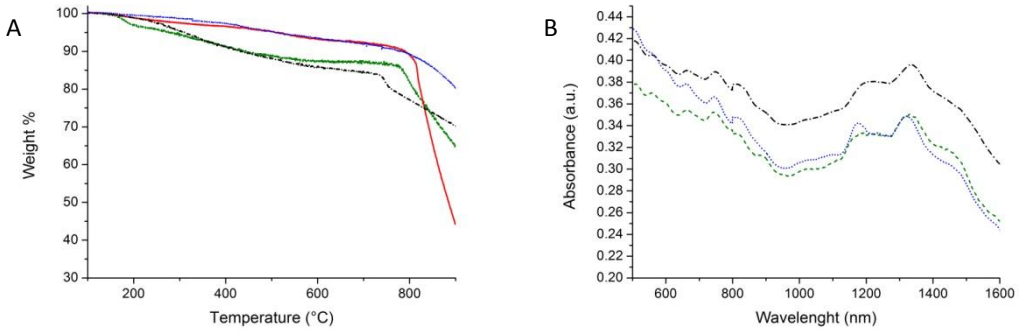

Figure 12. A) TGA curves of SWCNTs CNI® (red solid line) and f-SWCNTs, obtained as described in Table 2: entries **10** (black dash dot line), **12** (green dash line), **13** (blue dot line). B) UV-NIR spectra of f-SWCNTs, obtained as described in Table 2: entries **10** (black dash dot line), **12** (green dash line), **13** (blue dot line).

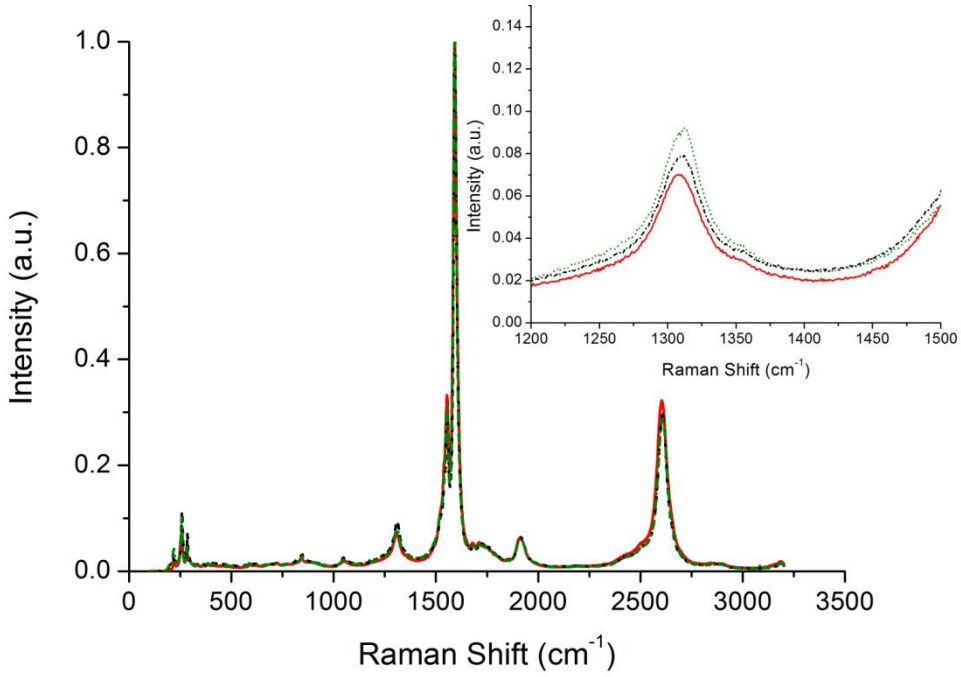

Figure 13. Time evolution of Raman spectra collected for pristine SWCNT and for functionalized samples under MW-irradaiation: SWCNTs CNI® (red solid line), entry **11** table 2 (black dash dot line), entry **14** table 2 (green dash line). In the inlet, it is visible the increase of the Disorder (D) band: higher is the functionalization degree, higher is the D band in Raman spectrum.

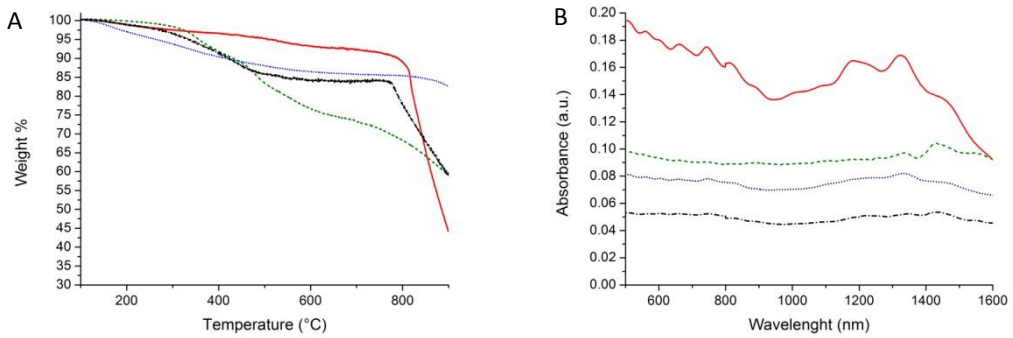

Figure 14. A) TGA curves of SWCNTs CNI® (red solid line) and of f-SWCNTs, obtained as described in Table 2: entries **9** (blue dot line), **11** (black dash dot line), **14** (green dash line). B) UV-NIR spectra in DMF of SWCNTs CNI® (red solid line), entry **9** Table 2 (blue dot line), entry **11** Table 2 (black dash dot line), entry **14** Table 2 (green dash line).

The addition of *o*-DCB as a co-solvent brings about a substantial improvement of the SWCNT functionalization yield (entry **14** in Table 2). This result is unequivocally confirmed by the time-evolution of the Raman spectra, collected with excitation at 632.8 nm, of the SWCNTs treated by MW irradiation under the reaction conditions (Figure 13). The comparison with the Raman features of the starting material, showing a small disorder mode at 1314 cm^{-1}, points to a gradual increase of the D-band corresponding to the functionalization progress. Inspection of the radial breathing mode (RBM) spectral region (<400 cm^{-1}) provides direct evidence that the applied MW-assisted protocol is not affecting the overall distribution of the nanotube types. As a further remark, the partial loss of the characteristic interband transitions between van Hove singularities of SWCNTs is also consistent with the occurrence of their functionalization (Figure 14).

TEM images indicate that the nanotube bundles are well-dispersible in polar organic solvents, like DMF (Figure 15).

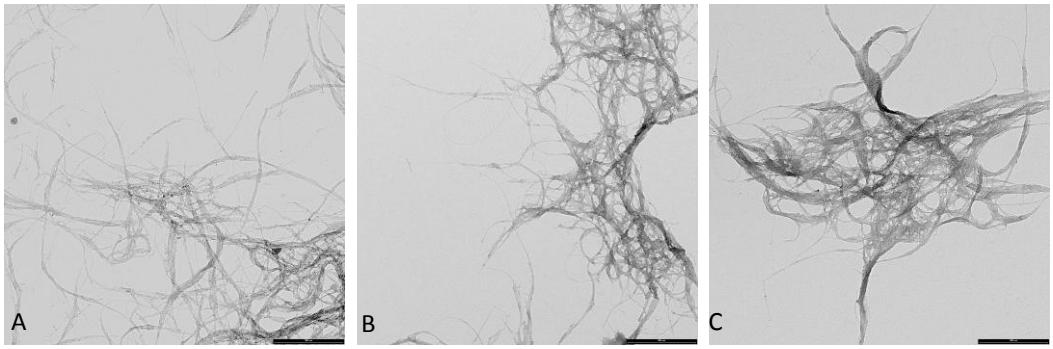

Figure 15. TEM images of: A) derivative **10**, B) derivative **11** and C) derivative **14**, obtained as reported in Table 2. TEM bar: 500 nm. Samples were dispersed in DMF.

The rational explanation for the enhanced efficiency observed with the molecular co-solvent is likely twofold, and not only related to solubilization/diffusion effects, but also due to the parallel inhibition of the competitive retro-cycloaddition process. Indeed, pyrrolidine cycloreversion has been demonstrated also in the case of covalently modified SWCNTs, under thermal and catalytic conditions[4].

The MW-assisted protocol has been applied to the introduction of fluorous-tagged pyrrolidine moieties onto the SWCNT surface (entries **15**-**17** in Table 2). Interestingly a 1/108 functional coverage is obtained by using a lower excess of the fluorous-tagged aldehyde, at an applied MW power of 50W. The resulting material features an unprecedented affinity for fluorinated phases. Solutions up to 1 mg in 1 ml of solvent, remain stable for weeks, without showing appreciable material precipitation (Figure 16). TGA data and TEM images provide converging evidence of the expected functionalization (Figure 17 and Figure 18).

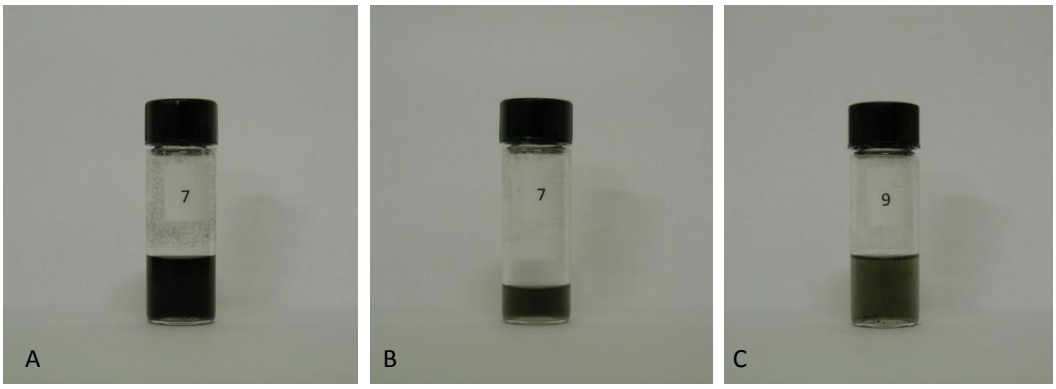

Figure 16. Pictures of vials containing FT-CNTs in hexafluoro-isopropanol, obtained as described in Table 2: a) entry **15**: suspension with 0.5 mg/mL; b) entry **15**: suspension with 0.1 mg/mL; c) entry **17**: solution with 0.5 mg/mL.

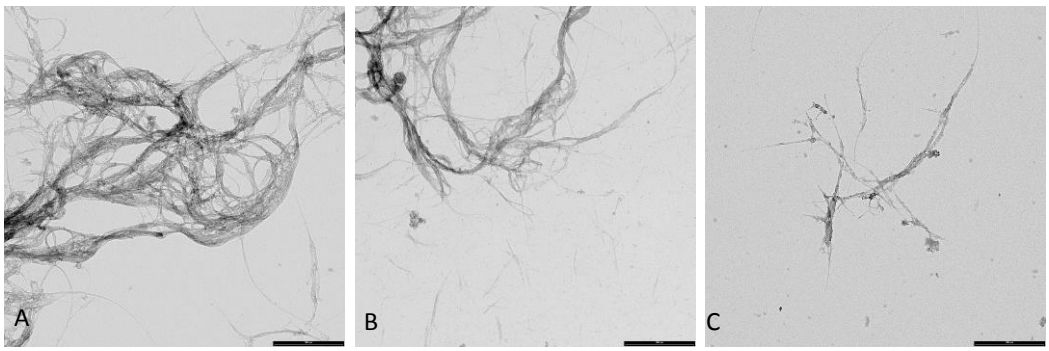

Figure 17. TEM images of FT-CNTs, obtained as described in Table 2 and dissolved (1 mg/mL) in hexafluoro isopropanol: A) entry **15**; B) entry **16**; C) entry **17**. TEM bar: 500 nm.

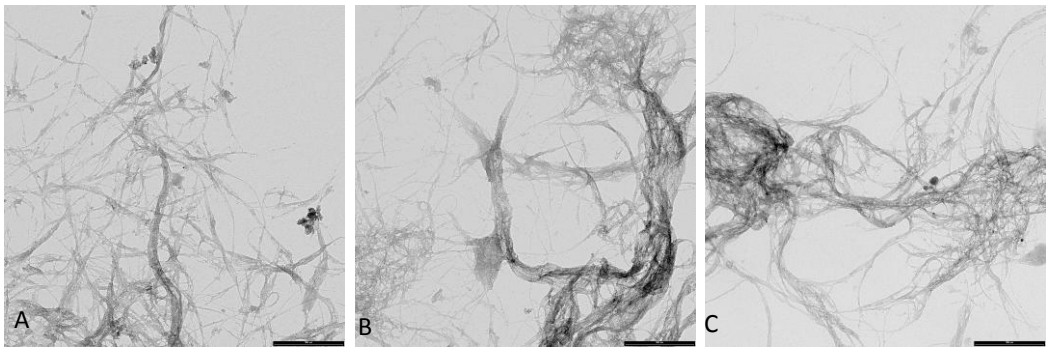

Figure 18. TEM images of FT-CNTs, obtained as described in Table 2 and dissolved (1 mg/mL) in DMF: A) entry **15**; B) entry **16**; C) entry **17**. TEM bar: 500 nm.

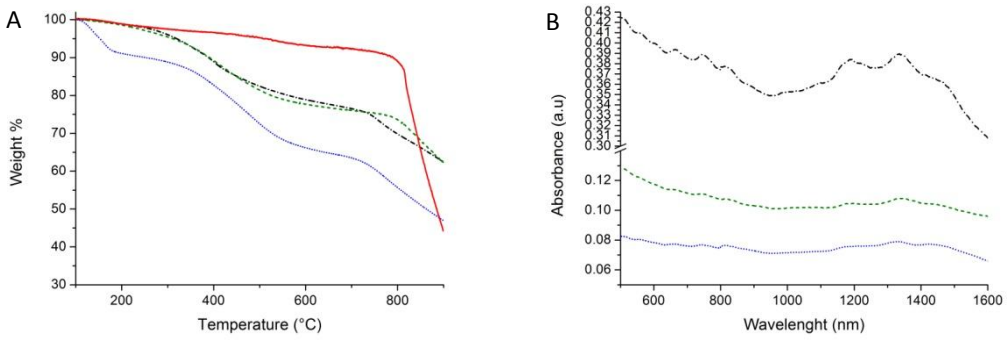

Figure 19. A) TGA curves of SWCNT CNI® (red solid line) and of f-SWCNTs, obtained as described in Table 2: entries **15** (black dash dot line), **16** (green dash line), **17** (blue dot line). B) UV-NIR spectra of FT-CNTs, obtained as described in Table 6: entries **15** (black dash dot line), **16** (greendash line), **17** (blue dot line).

TGA and UV-NIR spectra of entries **15**, **16** and **17** (Table 2) are reported in Figure 19. Thus, the loss of van Hove singularities, especially for entries **8** and **9** is consistent with the proposed degree of functionalization.

The reported results[23] have paved the way for more complex syntheses to be performed under MW irradiation.

References:

(1) Campidelli, S.; Sooambar, C.; Diz, E.; Ehli, C.; Guldi, D.; Prato, M. Dendrimer-functionalized single-wall carbon nanotubes: Synthesis, characterization, and

photoinduced electron transfer. *Journal of the American Chemical Society* **2006**, *128*, 12544-12552.

(2) Oh, S.; Kim, Y.; Ye, H.; Crooks, R. M. Synthesis, Characterization, and Surface Immobilization of Metal Nanoparticles Encapsulated within Bifunctionalized Dendrimers. *Langmuir* **2003**, *19*, 10420-10425.

(3) Sarin, V.; Kent, S.; Tam, J.; Merrifield, R. Quantitative monitoring of solid-phase peptide synthesis by the ninhydrin reaction. *Analytical Biochemistry* **1981**, *117*, 147-157.

(4) Langa, F.; De La Cruz, P. Microwave irradiation: An important tool to functionalize fullerenes and carbon nanotubes. *Combinatorial Chemistry and High Throughput Screening* **2007**, *10*, 766-782.

(5) Loupy, A. *Microwaves in Organic Synthesis*; 2° ed.; Wiley-VCH, 2006.

(6) Brunetti, F.; Herrero, M.; Muñoz, J.; Díaz-Ortiz, A.; Alfonsi, J.; Meneghetti, M.; Prato, M.; Vázquez, E. Microwave-induced multiple functionalization of carbon nanotubes. *Journal of the American Chemical Society* **2008**, *130*, 8094-8100.

(7) Brunetti, F.; Herrero, M.; Muñoz, J.; Giordani, S.; Díaz-Ortiz, A.; Filippone, S.; Ruaro, G.; Meneghetti, M.; Prato, M.; Vázquez, E. Reversible microwave-assisted cycloaddition of aziridines to carbon nanotubes. *Journal of the American Chemical Society* **2007**, *129*, 14580-14581.

(8) Martins, M.; Frizzo, C.; Moreira, D.; Zanatta, N.; Bonacorso, H. Ionic liquids in heterocyclic synthesis. *Chemical Reviews* **2008**, *108*, 2015-2050.

(9) Leadbeater, N.; Torenius, H.; Tye, H. Microwave-promoted organic synthesis using ionic liquids: A mini review. *Combinatorial Chemistry and High Throughput Screening* **2004**, *7*, 511-528.

(10) Habermann, J.; Ponzi, S.; Ley, S. Organic chemistry in ionic liquids using non-thermal energy-transfer processes. *Mini-Reviews in Organic Chemistry* **2005**, *2*, 125-137.

(11) Fukushima, T.; Kosaka, A.; Ishimura, Y.; Yamamoto, T.; Takigawa, T.; Ishii, N.; Aida, T. Molecular ordering of organic molten salts triggered by single-walled carbon nanotubes. *Science* **2003**, *300*, 2072-2074.

(12) Fukushima, T.; Asaka, K.; Kosaka, A.; Aida, T. Fully plastic actuator through layer-by-layer casting with ionic-liquid-based bucky gel. *Angewandte Chemie - International Edition* **2005**, *44*, 2410-2413.

(13) Takeuchi, I.; Asaka, K.; Kiyohara, K.; Sugino, T.; Terasawa, N.; Mukai, K.; Fukushima, T.; Aida, T. Electromechanical behavior of fully plastic actuators based on bucky gel containing various internal ionic liquids. *Electrochimica Acta* **2009**, *54*, 1762-1768.

(14) Kim, H.; Choi, J.; Lim, S.; Choi, H.; Kim, H. Preparation and nanoscopic internal structure of single-walled carbon nanotube-ionic liquid gel. *Synthetic Metals* **2005**, *154*, 189-192.

(15) Price, B.; Hudson, J.; Tour, J. Green chemical functionalization of single-walled carbon nanotubes in ionic liquids. *Journal of the American Chemical Society* **2005**, *127*, 14867-14870.

(16) Berardi, S.; Bonchio, M.; Carraro, M.; Conte, V.; Sartorel, A.; Scorrano, G. Fast catalytic epoxidation with H2O2 and [γ-SiW10O36(PhPO)2]4- in ionic liquids under microwave irradiation. *Journal of Organic Chemistry* **2007**, *72*, 8954-8957.

(17) Carraro, M.; Sandei, L.; Sartorel, A.; Scorrano, G.; Bonchio, M. Hybrid polyoxotungstates as second-generation POM-based catalysts for microwave-assisted H2O2 activation. *Organic Letters* **2006**, *8*, 3671-3674.

(18) Tasis, D.; Tagmatarchis, N.; Bianco, A.; Prato, M. Chemistry of carbon nanotubes. *Chemical Reviews* **2006**, *106*, 1105-1136.

(19) Kim, J.; Kim, D.; Kim, S. Effect of modified carbon nanotube on physical properties of thermotropic liquid crystal polyester nanocomposites. *European Polymer Journal* **2009**, *45*, 316-324.

(20) Tu, W.; Lei, J.; Ju, H. Functionalization of carbon nanotubes with water-insoluble porphyrin in ionic liquid: Direct electrochemistry and highly sensitive amperometric biosensing for trichloroacetic acid. *Chemistry - A European Journal* **2009**, *15*, 779-784.

(21) Wu, B.; Hu, D.; Kuang, Y.; Liu, B.; Zhang, X.; Chen, J. Functionalization of carbon nanotubes by an ionic-liquid polymer: Dispersion of Pt and PtRu nanoparticles on carbon nanotubes and their electrocatalytic oxidation of methanol. *Angewandte Chemie - International Edition* **2009**, *48*, 4751-4754.

(22) Skrzypczak, A.; Neta, P. Diffusion-controlled electron-transfer reactions in ionic liquids. *Journal of Physical Chemistry A* **2003**, *107*, 7800-7803.

(23) Guryanov I.; Toma F. M.; Montellano López A.; Carraro, M.; Da Ros T.; Angelini G.; D'Aurizio E.; Fontana A.; Prato M.; Bonchio M. Microwave-Assisted Functionalization of Carbon Nanostructures in Ionic Liquids. *Chemistry - A European Journal*.

CHAPTER 3:

MWCNT DENDRON SERIES FOR EFFICIENT siRNA DELIVERY

Biological studies reported in this chapter were done in collaboration with Dr. Khuloud T. Al-Jamal and Prof. Kostas Kostarelos from the Nanomedicine Laboratory, Centre for Drug Delivery Research, The School of Pharmacy, University of London; and Dr Alberto Bianco from CNRS, Institut de Biologie Moléculaire et Cellulaire, Immunologie et Chimie Thérapeutiques, Strasbourg, France.

3.1 Drug delivery in cancer nanotechnology: siRNA

After cardiovascular pathologies, cancer is one of the most important diseases and affects a large portion of the western world. The etiology of this disease, which is comprehensive of a numbers of different typologies, is related to genetic instability and/or multiple DNA alterations. One of the main problems is to selectively distinguish between healthy and tumor cells, and in this respect compared to current approaches in cancer treatment, nanotechnology's recent

achievements are promising major breakthrough in patient care. As the U.S. National Cancer Institute states[1], nanotechnology offers the unprecedented opportunity to study and interact with normal and cancer cells in real time, at molecular and cellular scales, and during the earliest stages of the cancer process. Nanoscale molecular structures are similar in size to large biomolecules and, under the right conditions, they can easily enter cells or pass the blood vessels.

The biomedical nanotechnology approach (namely nanomedicine) can be really useful in cancer therapy at three different stages of the tumoral process: early detection, imaging and therapeutic treatment of tumors[2]. For instance, delivery system gives us the possibility to target therapeutic or contrast agents directly to the desired organ or tissue using nanovectors. They tipically consist of a core decorated on the surface with targeting molecules and/or solubilising agents, and bearing inside therapeutic agent or imaging payloads. They, in fact, are engineered to release the loaded units after reaching the target, carring out their activity only or mainly there, strongly decreasing the side effects. The recognition units can generally be molecules, which are recognized by receptors expressed (or in a favorable case over-expressed) on the surface of cells in tumor tissues. The targeting can take place by an active recognition, due to the presence of a special unit (active targeting), but can also happen passively, by natural cellular uptake being, in this case, strictly related to enhanced permeability and retention effect (EPR). EPR concern tumor angiogenesis, where blood vessels bear numerous and larger fenestration in cancerous than in normal tissues, due to the demands of a rapid growth. The endothelium of cancer blood vessels is, in fact, characterized by the presence of few perycytes and smooth muscle cells and this causes the shape of fenestrations[2]. Moreover, usually in tumor tissue there is a lack of lymphatic vessels and these two characteristics, with the consequent cell expression of receptors for growth factors and cell adhesion, allow the use of multiple targeting strategies that underwent extravasation and protracted lodging[3]. In this scenario,

reticuloendothelial system (RES), as a part of the immune system and consisting mostly in macrophages and monocytes localized in lymph nodes, spleen and Kupffer cells, plays a determinant role because, tuning their size, nanovectors can target or can escape its cells.

The approval of Abraxane™ by FDA has been the major success for cancer nanotechnology in the last years. It consists of paclitaxel coupled to albumin as delivery agent. This formulation has been successfully adopted in the therapy of metastatic breast cancer[4]. Generally, the advantages of using nanovectors are the possibility to overcome poor solubility of some drugs, to protect them from metabolic and immune system attacks, to alter the biodistribution by tuning the nanovector size (exploiting the EPR effect), and to control the release profile by coupling with enzyme sensitive linkers.

Pharmacokinetics and pharmacodynamics are also important parameters in studying this new carriers, and *in vivo* biodistribution studies represent one of the necessary steps in the development of vectors.

RNA interference mechanism is crucial to study gene functions and to defeat many diseases as genetic diseases, HIV, influenza or cancer. siRNA consits of a double stranded RNA that leads to the degradation of the complementary endogenous mRNA and it is responsible for knocking down specific genes related to illness[5]. RNA interference (RNAi) mechanism was discovered by Jorgensen in 1990[6] and the related theory was improved by Mello in 1998[5]: they proved that dsRNA injected in *C. Elegans* was able to knock down genes. RNAi is based on DICER, RNAse III able to cut the dsRNA in small nucleotides, i.e. small interference RNAs (siRNAs). siRNA has a length of about 20-25 ribonucleotides with two nucleotides overhanging at 3' end. This peculiarity enables the siRNA to interact with the RNA-induced silencing complex (RISC) inducing gene silencing and cleavage of mRNA. The strand incorporated in the RISC is a guide that activates the enzymatic complex to selectively degrade the complementary mRNA. The use of siRNA is quite new and it was introduced in 2002 by T. Tuschl[7], and it constitutes an improvement with respect to dsRNA, which

induces an immunogenic response, while the siRNA does not activate this response.

Even though siRNA could bypass the cellular defense mechnism because of its length, it needs to be delivered inside cells because it bears many negative charges and it is not able to cross cell membrane by diffusion. Viral vectors are widely used but they imply many risks in safety and involve inflammatory and immunogenic effects. This is why non-viral vectors are preferable and many cationic derivatives (such as cationic polymers, dendrimers or peptides) are the most quoted candidates to translocate siRNA across cell membrane. Moreover, the main part of the existing carriers has been developed to deliver DNA into the nucleus and they usually undergo to normal endocytosis and subsequent endolysosomal processing[8].

The first attempt of gene silencing using carbon nanotubes was reported by Dai et al[9] in 2005. They f-SWCNTs using non-covalent approach with phospholipidic-polyethilenglycole chains and attached DNA or siRNA by disulfur bond showing the translocation of these complexes inside the cells. Afterwards, Zhang et al[10] gave the first proof of silencing the expression of transcriptase, using a positively charged SWCNT derivative. At the same time, also our group started working on this subject reporting that plasmid DNA can be delivered to induce recombinant expression of genes[11]. More recently, we demonstrated the ability of MWCNTs **10** to deliver siRNA into human tumor human xenograft model *in vivo*[12].

3.2 CNTs and Dendrimers as drug carriers

We have previously discussed about citotoxicity and the possible biological applications of CNTs (Chapter 1) together with their ability to enter cells[13] and their biocompatibility once functionalized[14,15]. More in detail, carbon nanotubes own an high aspect ratio, and the large surface area can be exploited to load different compounds at once. This represents a powerful outcome to escape

multi-drug resistance effects that are often developed by tumor cells[16]. Few examples have been reported in our group by Pastorin et al[17,18], presenting the double functionalization of CNTs with Methotrexate and a fluoresceine probe. So, we decided to couple the advantages of using CNTs with those of using dendrimers. These are also promising cargo for drug delivery because they bear a lot of functionalities where drugs or solubilizing agents can be attached. Nevertheless, the biocompatibility constitutes one of the main concern and many studies have been done[19]. Toxicity depends on three different factors: i) internal core, ii) dendrimer generation, and iii) surface charge. In detail, at high doses only generations higher than G7 show remarkable toxicity and immunogenicity[20]. Noteworthy, PAMAM has been extensively studied for biological application and two commercial derivatives (Polyfect® and Superfect®) are available as gene transfecting agent. It seems, indeed, that amino terminating PAMAM condenses DNA, and protects it when it is circulating in blood stream[21].

Moreover, Fischer et al studied the cytotoxicity of polycation reporting a rank in toxicity of amine, i.e. primary amine > secondary amine > tertiary amine[22].

Herein, we used positively charged MWCNT derivatives with a second generation PAMAM dendron to complex a siRNA toxic sequence and deliver it to transfect mammalian cells.

3.3 MWCNTs dendron series for an efficient siRNA delivery[1]

The alkylated dendron-MWCNT adducts, reported in Chapter 2 (MWCNTs **2**, MWCNTs **5** and MWCNTs **8**), were complexed with a non-coding siRNA sequence and the complexes were successfully used to transfect mammalian

[1] Part of the work reported in this chapter has been published in: *Journal of American Chemical Society*, **2009**, 131 (28), pp 9843-9848. "Synthesis and characterization of a carbon nanotube-dendron series for efficient siRNA delivery" by Herrero M.A., Toma F.M., Al-Jamal K.T., Kostarelos K., Bianco A., Da Ros T., Bano F., Casalis L., Scoles G., Prato M. One more manuscript is currently in preparation.

cells. We have discovered that the cytoplasmatic delivery of siRNA remarkably increases with the dendron generation (from G_0 to G_2) if compared to the ammonium f-MWCNT precursors (MWCNTs **1**). In this study we used a different batch of CNTs, with a different degree of functionalization if compared to that one reported in Chaper 2. The whole dendron series were prepared starting from the same batch of CNT (MWCNTs **1**), to achieve comparable results in degree of functionalization. Figure 1 and Table 1 reported respectively the TGA analyses and the degree of functionalization of the dendron, calculated by TGA and Kaiser Test.

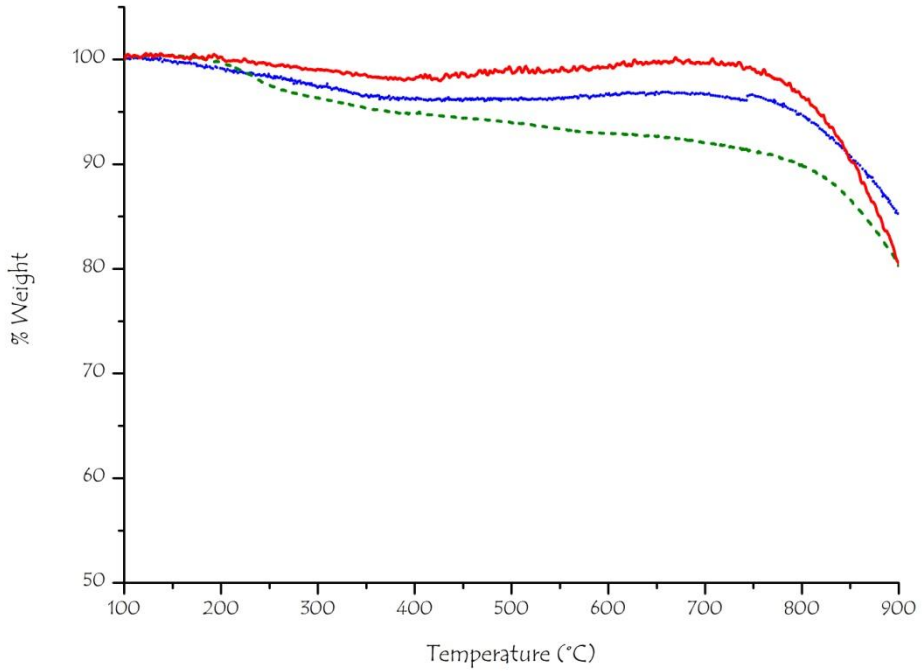

Figure 1. TGA curves of alkylated (G_0) dendron MWCNTs **2** (red solid line), alkylated (G_1) dendron-MWCNT **5** (blue dot line), alkylated (G_2) dendron-MWCNT **8** (green dash line). All the experiments were performed under N_2 atmosphere.

Table 1. The weight percentage was calculated at 450°C.

	%Weight	Funct/C[a]	mmol/g[b]	mmol/g[c]
Alkylated (G_0) dendron MWCNT **2**	98.6	1915	0.0429	0.072
Alkylated (G_1) dendron MWCNT **5**	96.2	1476	0.0543	0.111
Alkylated (G_2) dendron MWCNT **8**	94.4	2049	0.0384	0.212

(a) Number of functional groups per each carbon atom and (b) mmol/g calculatied by means of TGA analysis; (c) Kaiser test's results.

The data reported in Table 1 show a good correlation between the generations of the alkylated dendrons.

3.3.1 (G_2)dendron-MWCNT:siRNA complexation

As previously shown[23], cationic carbon nanotubes are able to efficiently condense nucleic acids and to deliver them into mammalian cells. Complexation between the polycationic alkylated (G_2) dendron-MWCNT **8** and siRNA was observed by agarose gel electrophoresis (Figure 2A).

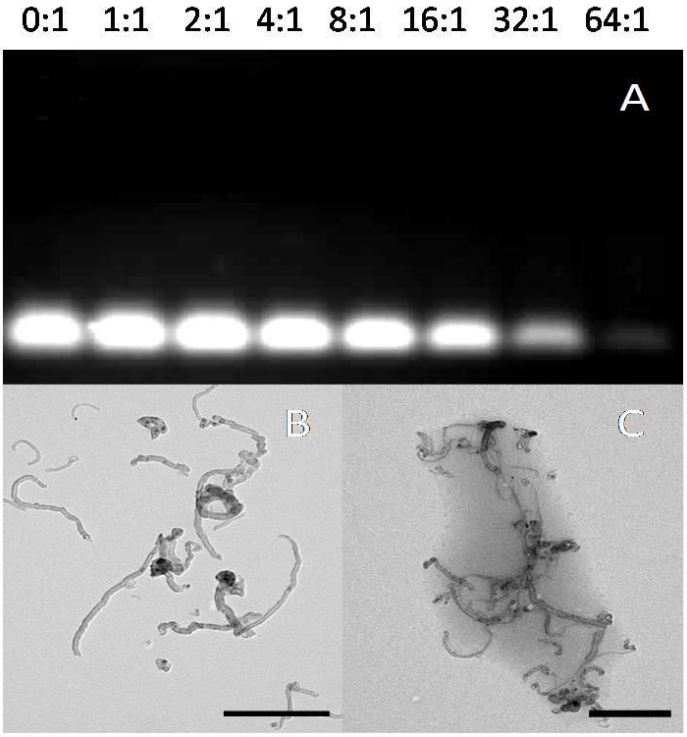

Figure 2. (A) Electrophoretic motility of MWCNT **8** (reconstituted at 1.0 mg/ml in 10% dextrose) complexed with siRNA. Various mass ratios of the MWCNT **8** were complexed to a fixed 0.5 μg siRNA; (B) TEM images of MWCNT **8** alone or (C) complexed to siRNA at 1:16 (MWCNT:siRNA) mass ratio . The scale bar is 500 nm.

The amount of free siRNA migrating into the gel was reduced by increasing the alkylated (G_2) dendron-MWCNT:siRNA mass ratio to almost no free siRNA for 64:1 mass ratio, as evidenced by the reduction of the ethidium bromide fluorescence intensity in the last two lanes. These results are consistent with previous studies performed in our group[12]. The interactions between the siRNA duplex and the alkylated (G_2) dendron-MWCNT **8** were also shown using TEM. In this case mass ratios lower than 64:1 were used. Figures 2B and 2C show the association of siRNA around the MWCNTs, which are highly dispersed. The complexation is evident by the formation of highly electron dense areas (darker in TEM) around the alkylated (G_2) dendron-MWCNT **8** and clustering of the nanotubes presumably due to bridging by the negative siRNA.

3.3.2 Effect of the different generation alkylated dendron-MWCNT:siRNA cellular uptake

To establish if the complexation of different generation alkylated dendron-MWCNTs with siRNA had any effect on the cellular uptake of siRNA, human cervical carcinoma (HeLa) cells were incubated with the dendron-MWCNT complexed with a non-coding siRNA sequence. In order to observe whether the siRNA was internalized in cells, it was fluorescently labelled at the 3′-end with ATTO 655 emitting at 690 nm. The complexes were prepared using a dendron-MWCNT:siRNA mass ratio 16:1 as previously optimized[12], and cellular uptake was observed using confocal microscopy under identical optical conditions. Very interestingly, all cells remained intact with no signs of toxicity after incubation with the complexes (see Appendix B for details).

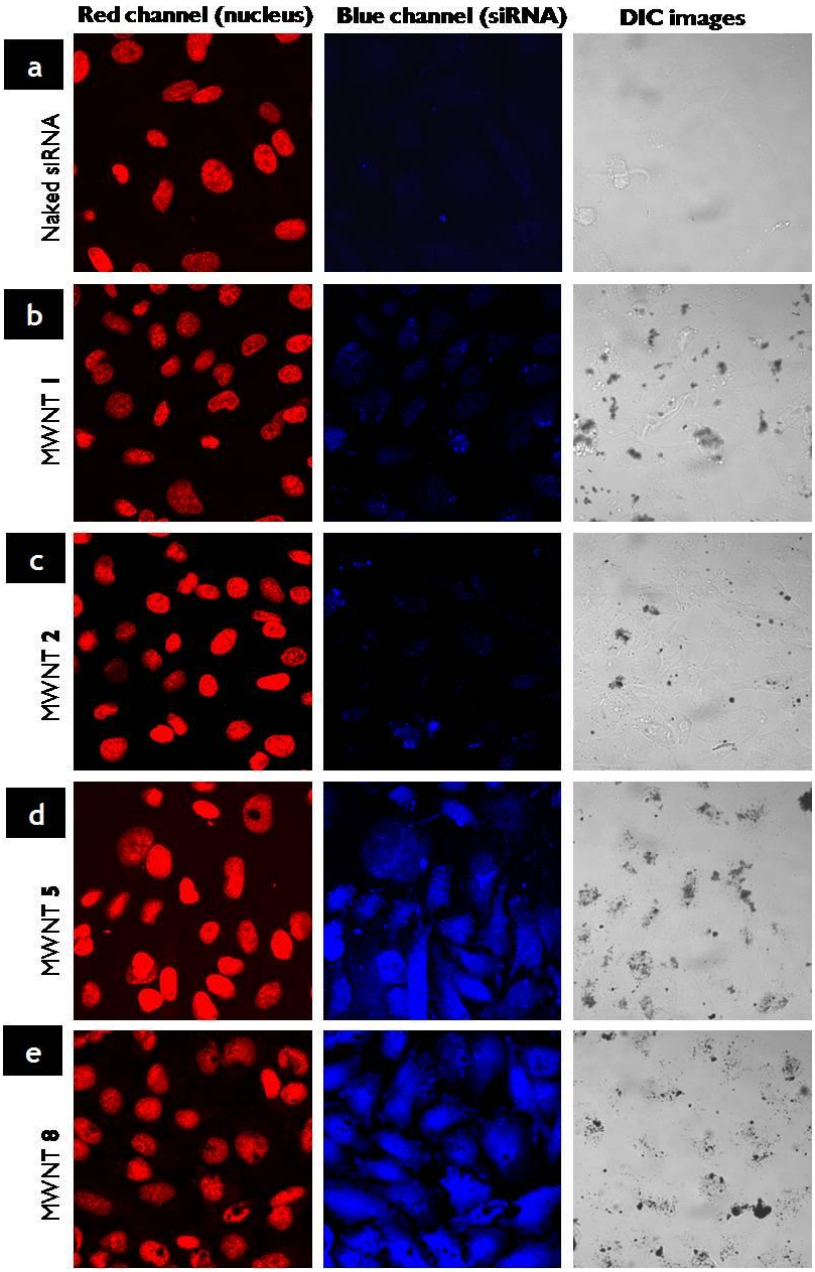

Figure 3. Confocal microscopy and differential interference contrast (DIC) images of HeLa cells obtained after 24 hr incubation with (a) ATTO 655-labeled siRNA alone, ATTO 655-labeled siRNA complexed to (b) MWCNT **1**, (c) alkylated (G_0) dendron-MWCNT **2**, (d) alkylated (G_1) dendron-MWCNT **5** and (e) alkylated (G_2) dendron-MWCNT **8** at 16:1 mass ratio and 80 nM siRNA concentration (equivalent to 16 µg/ml dendron-MWCNT). Cells were incubated with the complexes for 4 hrs in serum-free media after which serum-containing media was added to make the final concentration of serum to 10%. Nuclei were

counterstained with propidium iodide. Images show an increase in the intracellular uptake of siRNA as shown by the increase in the blue fluorescence (siRNA) in the following order e > d> c >b. siRNA alone gave almost no detectable fluorescence in the cells (a).

Figure 3 shows that dendron-MWCNTs with increased degree of branching and alkylated dendron generations exhibited more effective intracellular siRNA delivery than MWCNT **1**, while almost no uptake of siRNA alone was observed (Figure 3a)**.** The fluorescent signal from ATTO 655-labelled siRNA was found diffused throughout the cytoplasm of cells treated with the dendron-MWCNT:siRNA complexes, without any indication of localization in intracellular vesicles (usually evidenced by highly fluorescent pockets within the cell). The morphology of the cells did not seem to be affected by the dendron-MWCNT, indicating that the uptake of siRNA was not a result of cellular damage, but presumably due to the translocation of the dendron-MWCNT through the plasma membrane. Confocal microscopy studies at early time points (4 hrs) after incubation of the f-MWCNT:siRNA complexes indicated fluorescence signals of lower intensity compared to the 24hr data shown here. At both time points the fluorescent signal from the siRNA-ATTO655 was observed throughout the whole cell volume without localization in the nucleus or other cellular compartment. However, the cellular internalization of the siRNA was always nanotube-dependent. In order to have a better understanding of the mechanism by which dendron and ammonium f-MWCNT:siRNA complexes enter into cells, systematic cell trafficking studies of these complexes are warranted and are currently under investigation in our laboratories. This data show that higher dendron generations grown on the MWCNT surface could lead to more efficient cytoplasmic delivery of siRNA, indicating that such constructs can potentially reach higher highly effective levels of gene silencing. Therefore, using a siRNA sequence that can be cytotoxic to cells only when delivered efficiently, we have shown that internalization of the alkyalted (G_2) dendron-MWCNT:siTOX complexes could lead to biologically active delivery of the siRNA, and gene silencing evidenced by extensive apoptosis and cell death.

Thus, we chose MWCNTs **8** for the further studies.

3.3.3 Alkylated (G_2) dendron-MWCNT:siRNA delivery and silencing with a cytotoxic sequence

The cytotoxicity of alkylated (G_2) dendron-MWCNT **8** alone was first evaluated using human lung epithelial cell cultures (A549) incubated with different doses (2.5-10 μg/ml) for 24 h. The cytotoxicity was evaluated after incubation (24h) and at 72 h by flow-cytometry using the Annexin V/Propidium iodide (PI) assay (Figure 4).

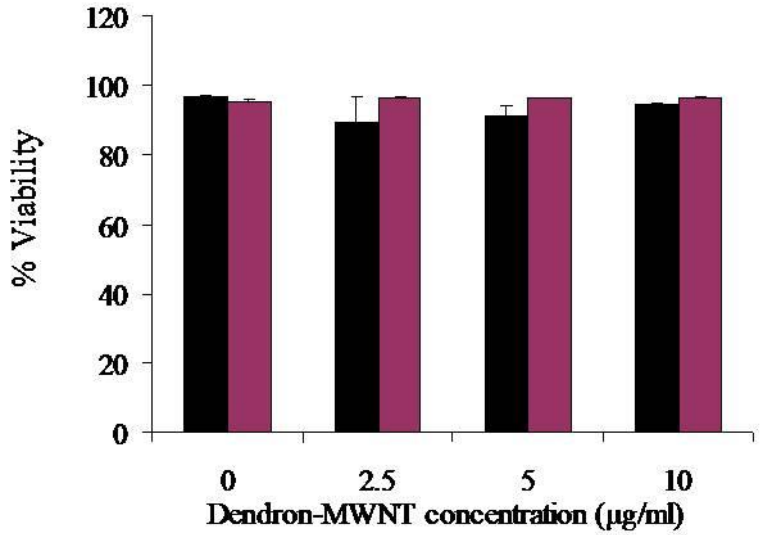

Figure 4. Cytotoxicity assays performed on A549 monolayers incubated with media containing 0, 2.5, 5 and 10 μg/ml of dendron-MWCNT **8**. Cells were washed and re-incubated with complete media and assayed for death after 24 (black bars) and 72 h (magenta bars) by Annexin V/propidium iodide assay using flow cytometry.

No sign of toxicity was observed up to 10 μg/ml after 24 h or 72 h. Similar results were also obtained by two independent toxicity assays (LDH and MTT; Figure 5) altogether indicating that the dendron-MWCNT is innocuous at concentrations up to 40 μg/ml to A549 cells.

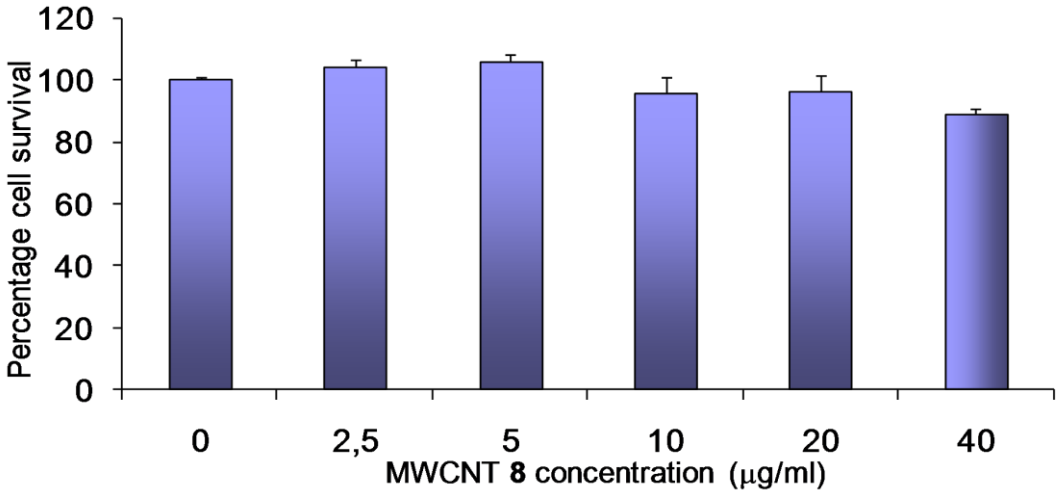

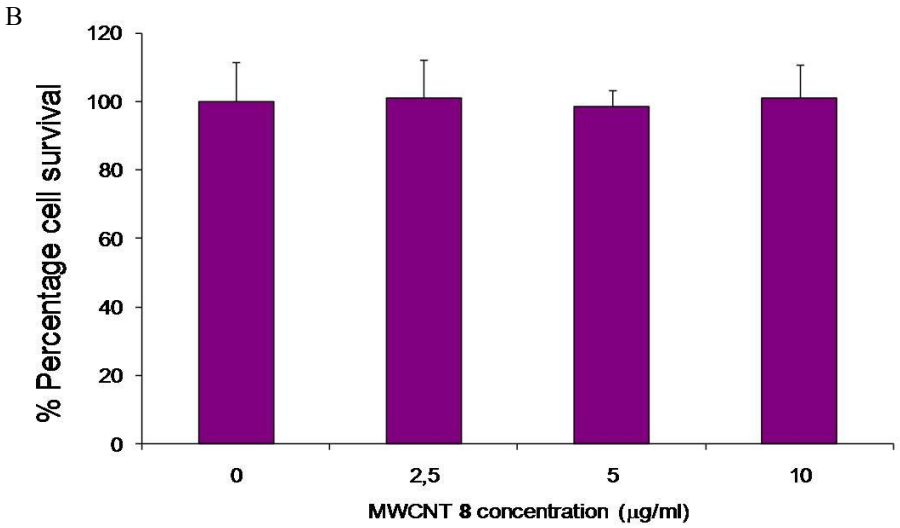

Figure 5. (A) LDH test performed on A549 monolayers incubated with media containing 0, 2.5, 5 and 10 μg/ml of dendron-MWCNT **8**. (B) MTT test performed on A549 monolayers incubated with media containing 0, 2.5, 5, 10, 20 and 40 μg/ml of dendron-MWCNT **8**.

Annexin V/PI test highlight the presence of apoptotic cells: viable cells are both Annexin V and PI negative, whereas cells in early apoptosis are only Annexin V permeable, and apoptotic cells are permeable to both Annexin V and PI. MTT (a

tretrazole derivative) test is an enzymatic test to evaluate the activity of mitochondria. Viable cells are able to convert MTT to a purple colored molecule. Finally, LDH (lactate dehydrogenase) assay measures the quantity of NADH oxidized as a function of cell membrane permeability.

3.2.4 Alkylated (G_2) dendron-MWCNT:siRNA delivery and silencing with the use of a cytotoxic sequence

To assess if the dendron-MWCNT:siRNA complexes can be considered a real alternative to non-viral vector systems for the efficient delivery of siRNA, a commercial apoptosis-inducing siRNA sequence (siTOX®) was selected. Effective delivery of siTOX in cells leads to a cytotoxic response and cell death[24]. HeLa cells were incubated with free siTOX (80 nM) or complexed with the alkyalted (G_2) dendron-MWCNT **8** at 1:16 mass ratio (equivalent to 16 μg/ml dendron-MWCNT **8**) for 24 h and transfection was assessed after 48 h using the terminal deoxynucleotidyltransferase–mediated nick end labeling (TUNEL) reaction. Apoptotic cells were green stained because of incorporation of fluorescein-12-dUTP at 3'-OH using the Terminal Deoxynucleotidyl Transferase onto the ends of nicked DNA, while propidium iodide counterstained the nuclei in red (Figure 6). Only few apoptotic cells can be seen in cultures treated with the dendron-MWCNT **8** alone (Figure 6B), in agreement with the cytotoxicity results obtained from Annexin V/PI assay or with siRNA alone (Figure 6C). The majority of cells treated with dendron-MWCNT:siTOX were stained in green with a concomitant reduction in the total number of nuclei, indicating extensive cell death (Figure 6D). Fewer cells were seen in the alkylated (G_2) dendron-MWCNT:siTOX treated panel because cell death leads to detachment of cells before or during TUNEL assay processing. Overall, these data indicate that dendron-MWCNT **8** was able to condense, intracellularly translocate and successfully deliver biologically active siRNA sequences.

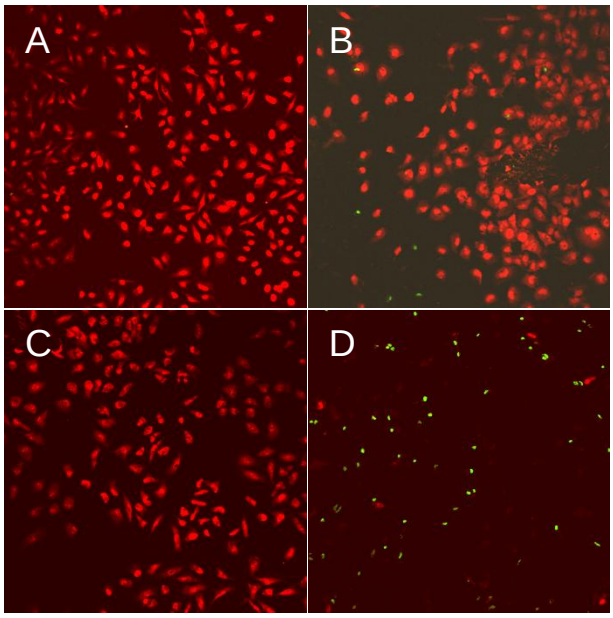

Figure 6. Confocal microscopy images of HeLa cells obtained 48 h after transfection with alkyalted (G_2) dendron-MWCNT **8**:siTOX (16:1 mass ratio) using the TUNEL assay. Untreated cells (A) or cells treated with dendron-MWCNT **8** (B) or siTOX alone (80 nM) (C) exhibited no sign of apoptosis, while cells treated with siTOX (D) complexed with the alkyalted (G_2) dendron-MWCNT **8** show evident signs of apoptosis (green) and cell death (fewer cells).

3.2.5 In vivo biodistributional study of dendron-MWCNT derivative

In our group, the evaluation of biodistribution of MWCNTs **1** linked to [^{111}In]DTPA (diethylentriaminopentaacetic acid) was already reported and urinary excretion was proved[25]. It is well known that the main excretion way for drugs is the renal one, in fact an average of 650 mL/min of plasma are filtrated by renal glomeruli. In this process the molecular weight is predominant, and drugs up to 60kDa can pass through renal capillaries. Substances, which do not undergo renal excretion because of their weight, are eliminated by the liver. Beside molecular weight, other factors govern the elimination process, like pH or liposolubility of xenobiotics. Nevertheless, the nanoparticles elimination process can be more complicated and Choi et al studied the renal clearance of quantum dots, discovering that it is related to the hydrodynamic diameter as well as to molecular weight[26]. Preclinical studies are essential for clinical

applications and we reported the in vivo biodistribution of DTPA-MWCNT **7** (Scheme 1) complexed with ^{111}In. In detail, diethylene triamine pentaacetic anhydride was added to a Dimethylsulfoxide (DMSO)/DMF solution of MWCNT **7** (Kaiser Test of 1097 μmol/g, Chapter 2). Thus, the product was complexed with $^{111}InCl_3$, a γ-emitting radionuclide, to obtain [^{111}In]DTPA-MWCNTs **7**.

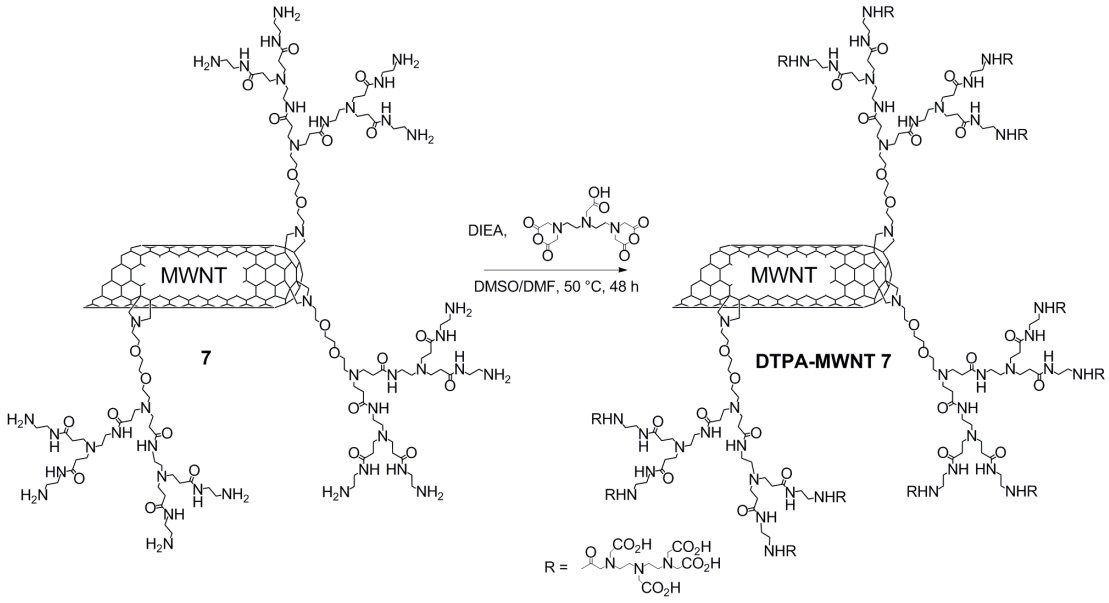

Scheme 1. DTPA-MWCNT **7** synthesis.

TEM image of DTPA-MWCNT **7** is reported in Figure 7, showing that no significant change occurred after the reaction.

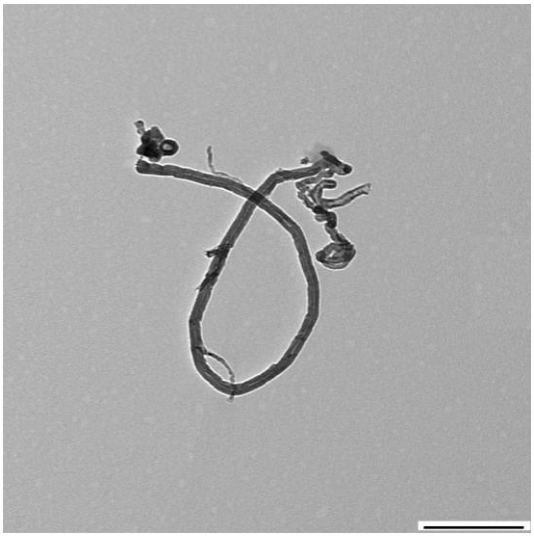

Figure 7. TEM image of DTPA-MWCNTs **7** (Scale bar 100 nm).

50 μg of [^{111}In]DTPA-MWCNT **7** were administrated by tail vein injection to Balb/C mice and after 24h the Single Photon Emission Computed Tomography (SPECT) was performed to visualize the systemic distribution of MWCNT derivative. SPECT allows few days biodistribution imaging and 3D projections can be software reconstructed by different sagittal section images (Figure 8a).

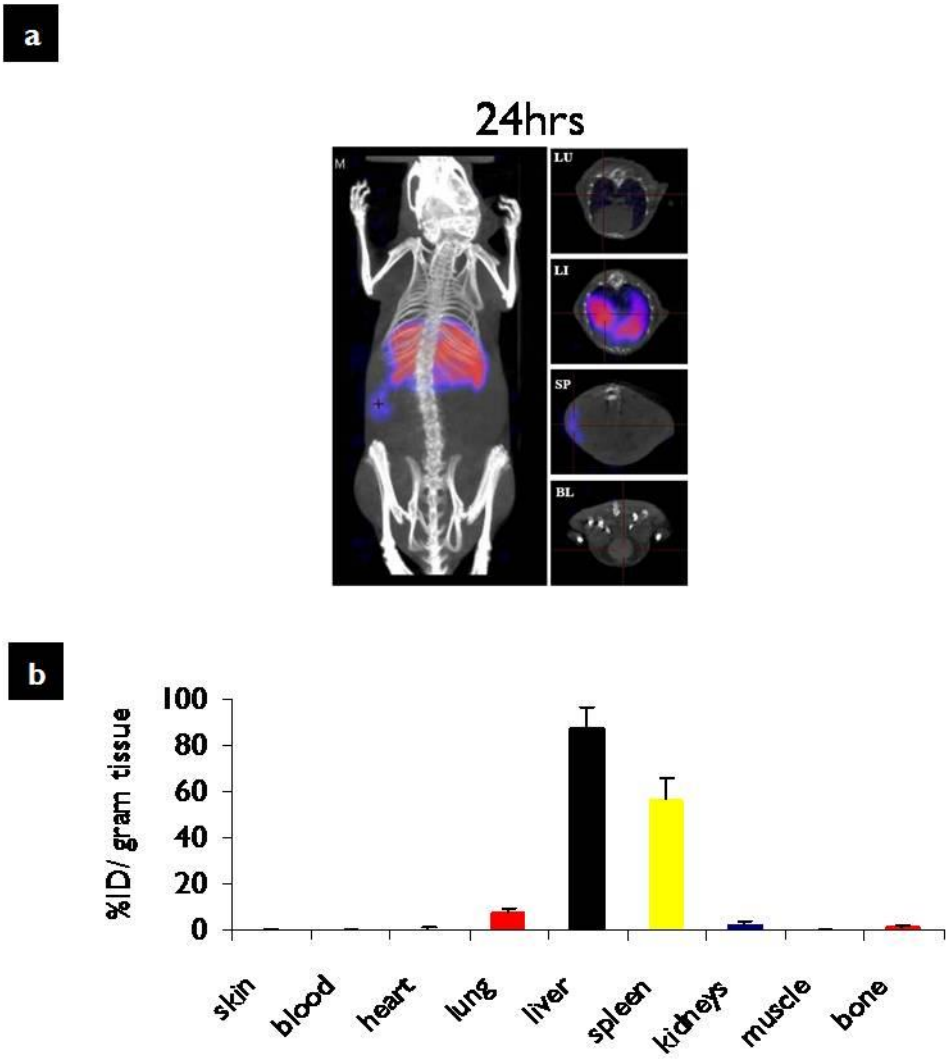

Figure 8. *In vivo* biodistribution of [^{111}In]DTPA-dendron-MWCNT in Balb/C mice after single dose administration via tail vein shown after 24hrs by **(a)** SPECT/CT , or **(b)** gamma counting expressed as percentage injected dose (%ID) per gram tissue 24hrs. Data were expressed as means ± SD (n=3-4).

In Figure 8b, biodistribution analysis is reported, highlighting that the majority of the MWCNT **7** are concentrated in liver and spleen. Spleen is responsible for mechanical filtration of blood and this is probably the reason why MWCNTs are accumulated in it, but to clarify this point further studies are necessary, and we are now functionalizing MWCNTs **8** with fluorescent probe to study more in detail and to achieve a detailed understanding of the fate of our derivatives. Finally, the

balance between the excretion and retention of CNTs should be thoroughly studied, particularly following multiple administrations, in order to better understand the accumulation of f-CNTs inside the body with respect to their rate of excretion.

References:

(1) Exploring Nanotechnology in Cancer.

(2) Cuenca, A.; Jiang, H.; Hochwald, S.; Delano, M.; Cance, W.; Grobmyer, S. Emerging implications of nanotechnology on cancer diagnostics and therapeutics. *Cancer* **2006**, *107*, 459-466.

(3) Ferrari, M. Cancer nanotechnology: opportunities and challenges. *Nat Rev Cancer* **2005**, *5*, 161-171.

(4) Nie, S.; Xing, Y.; Kim, G.; Simons, J. *Nanotechnology applications in cancer*; 2007; Vol. 9, pagg. 257-288.

(5) Fire, A.; Xu, S.; Montgomery, M.; Kostas, S.; Driver, S.; Mello, C. Potent and specific genetic interference by double-stranded RNA in caenorhabditis elegans. *Nature* **1998**, *391*, 806-811.

(6) Napoli, C.; Lemieux, C.; Jorgensen, R. Introduction of a chimeric chalcone synthase gene into petunia results in reversible co-suppression of homologous genes in trans. *Plant Cell* **1990**, *2*, 279-289.

(7) Martinez, J.; Patkaniowska, A.; Urlaub, H.; Lührmann, R.; Tuschl, T. Single-stranded antisense siRNAs guide target RNA cleavage in RNAi. *Cell* **2002**, *110*, 563-574.

(8) Gao, K.; Huang, L. Nonviral methods for siRNA delivery. *Mol. Pharm* **2009**, *6*, 651-658.

(9) Kam, N.; Liu, Z.; Dai, H. Functionalization of carbon nanotubes via cleavable disulfide bonds for efficient intracellular delivery of siRNA and potent gene silencing. *Journal of the American Chemical Society* **2005**, *127*, 12492-12493.

(10) Zhang, Z.; Yang, X.; Zhang, Y.; Zeng, B.; Wang, S.; Zhu, T.; Roden, R. B. S.; Chen, Y.; Yang, R. Delivery of telomerase reverse transcriptase small interfering RNA in complex with positively charged single-walled carbon nanotubes suppresses tumor growth. *Clin. Cancer Res* **2006**, *12*, 4933-4939.

(11) Singh, R.; Pantarotto, D.; McCarthy, D.; Chaloin, O.; Hoebeke, J.; Partidos, C.; Briand, J.; Prato, M.; Bianco, A.; Kostarelos, K. Binding and condensation of plasmid DNA onto functionalized carbon nanotubes: Toward the construction of nanotube-based gene delivery vectors. *Journal of the American Chemical Society* **2005**, *127*, 4388-4396.

(12) Podesta, J. E.; Al-Jamal, K. T.; Herrero, M. A.; Tian, B.; Ali-Boucetta, H.; Hegde, V.; Bianco, A.; Prato, M.; Kostarelos, K. Antitumor activity and prolonged survival by carbon-nanotube-mediated therapeutic siRNA silencing in a human lung xenograft model. *Small* **2009**, *5*, 1176-1185.

(13) Pantarotto, D.; Singh, R.; McCarthy, D.; Erhardt, M.; Briand, J.; Prato, M.; Kostarelos, K.; Bianco, A. Functionalized carbon nanotubes for plasmid DNA gene delivery. *Angewandte Chemie - International Edition* **2004**, *43*, 5242-5246.

(14) Smart, S.; Cassady, A.; Lu, G.; Martin, D. The biocompatibility of carbon nanotubes. *Carbon* **2006**, *44*, 1034-1047.

(15) Dumortier, H.; Lacotte, S.; Pastorin, G.; Marega, R.; Wu, W.; Bonifazi, D.; Briand, J.; Prato, M.; Muller, S.; Bianco, A. Functionalized carbon nanotubes are non-cytotoxic and preserve the functionality of primary immune cells. *Nano Letters* **2006**, *6*, 1522-1528.

(16) Singh, R.; Lillard Jr., J. Nanoparticle-based targeted drug delivery. *Experimental and Molecular Pathology* **2009**, *86*, 215-223.

(17) Pastorin, G.; Wu, W.; Wieckowski, S.; Briand, J.; Kostarelos, K.; Prato, M.; Bianco, A. Double functionalisation of carbon nanotubes for multimodal drug delivery. *Chemical Communications* **2006**, 1182-1184.

(18) Prato, M.; Kostarelos, K.; Bianco, A. Functionalized carbon nanotubes in drug design and discovery. *Accounts of Chemical Research* **2008**, *41*, 60-68.

(19) Svenson, S. Dendrimers as versatile platform in drug delivery applications. *European Journal of Pharmaceutics and Biopharmaceutics* **2009**, *71*, 445-462.

(20) Roberts, J. C.; Bhalgat, M. K.; Zera, R. T. Preliminary biological evaluation of polyamidoamine (PAMAM) dendrimers. *Journal of Biomedical Materials Research* **1996**, *30*, 53-65.

(21) Yellepeddi, V.; Kumar, A.; Palakurthi, S. Surface modified poly(amido) amine dendrimers as diverse nanomolecules for biomedical applications. *Expert Opinion on Drug Delivery* **2009**, *6*, 835-850.

(22) Fischer, D.; Li, Y.; Ahlemeyer, B.; Krieglstein, J.; Kissel, T. In vitro cytotoxicity testing of polycations: Influence of polymer structure on cell viability and hemolysis. *Biomaterials* **2003**, *24*, 1121-1131.

(23) Lu, Q.; Moore, J.; Huang, G.; Mount, A.; Rao, A.; Larcom, L.; Ke, P. RNA polymer translocation with single-walled carbon nanotubes. *Nano Letters* **2004**, *4*, 2473-2477.

(24) Oh, J.; Razfar, A.; Delgado, I.; Reed, R.; Malkina, A.; Boctor, B.; Slamon, D. 3p21.3 tumor suppressor gene H37/Luca15/RBM5 inhibits growth of human lung cancer cells through cell cycle arrest and apoptosis. *Cancer Research* **2006**, *66*, 3419-3427.

(25) Lacerda, L.; Soundararajan, A.; Singh, R.; Pastorin, G.; Al-Jamal, K.; Turton, J.; Frederik, P.; Herrero, M.; Li, S.; Bao, A.; Emfietzoglou, D.; Mather, S.; Phillips, W.; Prato, M.; Bianco, A.; Goins, B.; Kostarelos, K. Cover Picture: Dynamic Imaging of Functionalized Multi-Walled Carbon Nanotube Systemic Circulation and Urinary Excretion (Adv. Mater. 2/2008). *Advanced Materials* **2008**, *20*, NA.

(26) Soo Choi, H.; Liu, W.; Misra, P.; Tanaka, E.; Zimmer, J. P.; Itty Ipe, B.; Bawendi, M. G.; Frangioni, J. V. Renal clearance of quantum dots. *Nat Biotech* **2007**, *25*, 1165-1170.

CHAPTER 4:

CNT SUBSTRATES FOR NEURONAL CULTURES: A MORPHOLOGICAL STUDY

Electrophysiological studies reported in this chapter were done in collaboration with Miss Giada Cellot and Prof. Laura Ballerini neurophysiologists from the Life Science Department, B.R.A.I.N., University of Trieste.

4.1 Introduction: a new standard for substrate preparation[1]

As it has been already mentioned, CNTs have extraordinary conductive properties (Chapter 1) and their potential role in repairing injured nerves in the brain and spinal cord has recently been shown by Ballerini, Prato and collaborators[1] and has recently captured wide interest, as shown by its citation record of approximately 100 citations in 4 years. This research field has thrieved because of the biocompatibility of functionalized CNTs and especially because their highly electrically connected structure when used as surface supported substrates. CNTs coated glasses, indeed, are well established substrates for cell cultures as they are known to promote cell attachment, differentiation, growth and long term

[1] The data reported in this chapter have not been pusblished yet.

survival comparably with those obtained using other growth enhancing factors (GEF) to coat glass (like poly-ornithine, poly-lysine or matrigel). Moreover a promising application in this field is related to the chemical functionalization of CNTs: the common factors used to pre-treat glass substrates are in fact positively charged, and it has been shown that neuronal growth and development are enhanced on this kind of scaffold[2].

In this thesis we continue the effort started in our group by Lovat et al in 2005[1] and later by Cellot et al[3], testing the impact of CNT substrates on neuronal network activity by means of dual electrophysiological recordings. We performed both electrophysiological measurements, and morphological studies of hippocampal neuronal cultures grown over carbon nanotube substrates to investigate the interactions between CNTs and neurons. In Lovat et al[1] the occurrence frequency of spontaneous postsynaptic currents (PSCs) was monitored, as a parameter to assess the network efficacy and the functional synapses formation of neuron growth on CNT substrates. PSCs are induced in postsynaptic neurons by neurotransmitters released by presynaptic neuron immediately after the action potential. Neurons grown on CNTs displayed on average a six-fold increase in the frequency of PSCs with respect to control (bare glass substrate). The authors[1] proved also that this boosting of network activity was not related to a higher number of surviving neurons and in general neurons deposited on CNTs did not exhibit any difference in "basal electrophysiological properties" with respect to control.

The procedure to prepare CNTs-coated substrates follows mainly the previous work of Lovat et al[1]. In addition, we decided to standardize it and to produce a common protocol that could allow us to vary other parameters, such as CNT density, length or type of functionalization and making correlations with the biological response. 1,3 dipolar cycloaddition (Chapter 2) is needed to increase the solubility of CNTs, facilitating dissolution in DMF and improving the homogeneity upon the glass substrates. Attempts to prepare substrates with as-produced, impure, MWCNTs were already reported[1], without any result: metal nanoparticles

are present in this case as a residue of CNTs synthesis, and represent a risk for neuronal survival

MWCNTs **9**, reported in scheme 1, were synthesized (as already reported in Chapter 2, Table 2) and were characterized by means of TGA under air to assess the metal content (Figure 2).

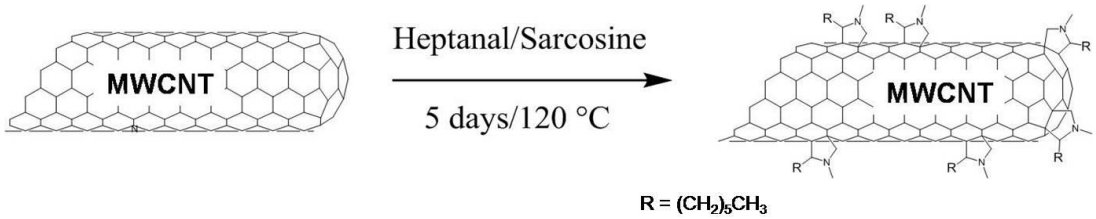

Scheme 1. 1,3-dipolar cycloaddition, thermal condition on MWCNTs

The metal content was found to be about 3.9 % and it did not perturb cell viability.

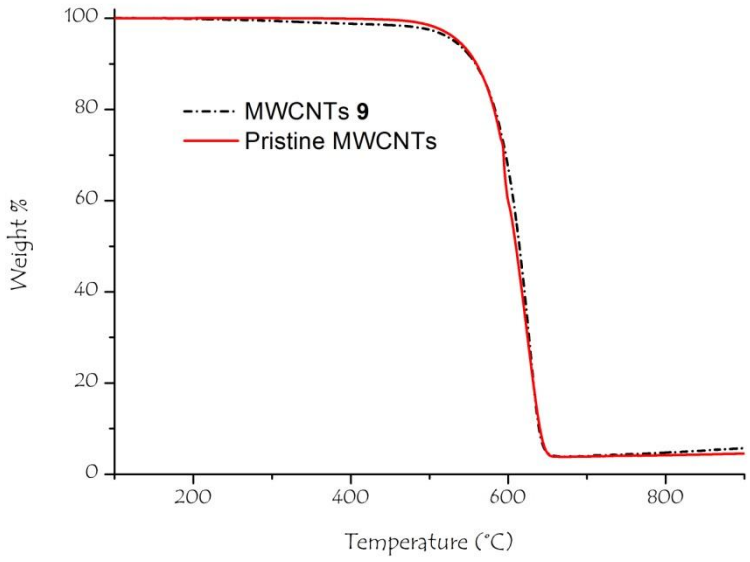

Figure 1. TGA under air atmosphere of Pristine MWCNTs (red solid line) and MWCNTs **9** (black dash dot line)

These nanotubes were characterized also with TEM and their average length was calculated (Figure 2). The dispersion ranges (graph in Figure 2) from less than 200 nm to 1250 nm (n=91), the calculated average value being 480 nm (± 250 nm).

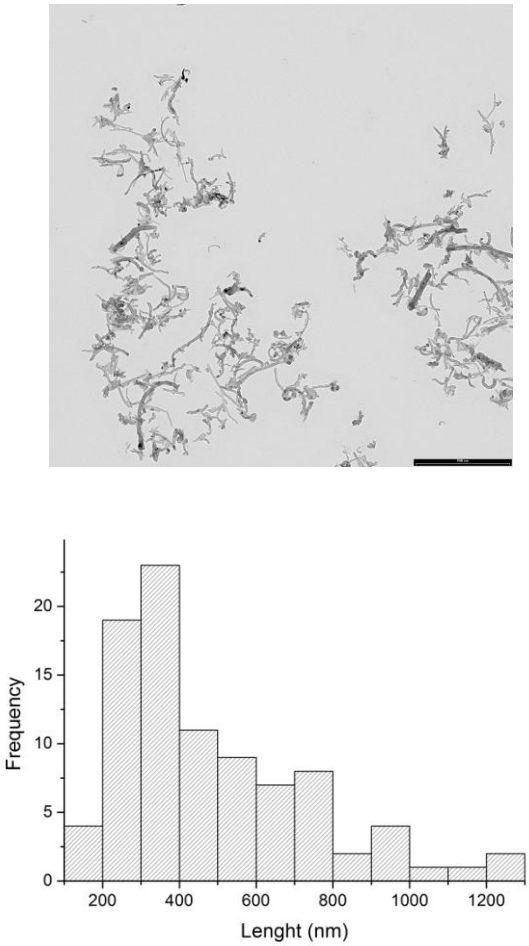

Figure 2. TEM image of MWCNTs **9** (scale bar 1 micron). Distribution of MWCNTs **9** diameters.

Our first attempt was to produce a protocol to improve reproducibility and, above all, to avoid possible cause of neuronal toxicity. After other tests, 5 mL of a water solution (0.04 mg/mL) of MWCNTs **9** were evaporated over 3 glass substrates that were deposited in a crystallizer (crystallizer surface area = 1809 mm^2). The solution was slowly dried out leaving an average density of CNTs per glass substrate of $1.1x10^{-4}$ mg/mm^2, calculated as quantity of MWCNTs in the 5 mL of solution (0.2 mg) divided by the surface area of the crystallizer. The substrates were then placed in oven at 350 °C under nitrogen atmosphere in order to remove the organic functionalization. The main drawback of this method is that the substrate becomes inhomogeneous in coverage, and there are too many "areas" that do not allow patch clamping measurements. Neuronal cultures were,

nevertheless, produced from dissociated hippocampal neurons obtained from brains of newborn rats, and leaving the cells growing on MWCNT modified substrates for 8 days, then glasses were fixed with glutaraldehyde and coated with about 10 nm of Ni, for SEM imaging (Appendix A). Although neurons showed high affinity for the substrates, the biological response was smaller than previously reported[1,3] and this was enough to discard this substrate preparation protocol.

To improve the substrate preparation, we optimized the concentration conditions, choosing to deposit 2 mL by depositing 10 times 0.2 mL of a solution of MWCNTs **9**, at 0.01 mg/mL. The density of the MWCNT film over the glass (glass surface area = 288 mm^2) was about $7x10^{-5}$ mg/mm^2, calculated as an average of the quantity of MWCNTs divided by the surface area of the glass. Then, we treated the substrates for 20 minutes in oven under N_2 atmosphere (Scheme 2), to remove the functionalization.

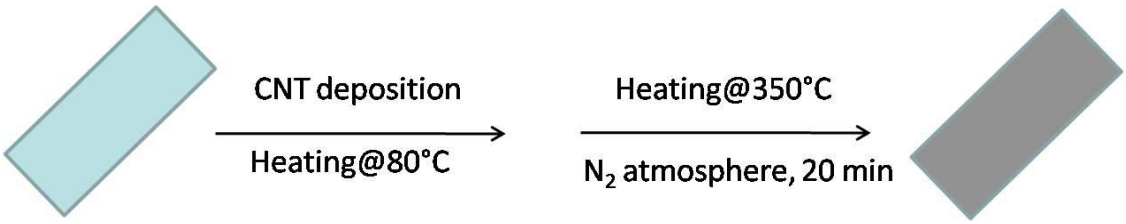

Scheme 2. Schematic representation of MWCNTs depostition over glass substrates and subsequently defunctionalization.

SEM characterization of these substrates was then performed, as shown in Figure 4 A and B, and their enlargements in Figure 4 C and D.

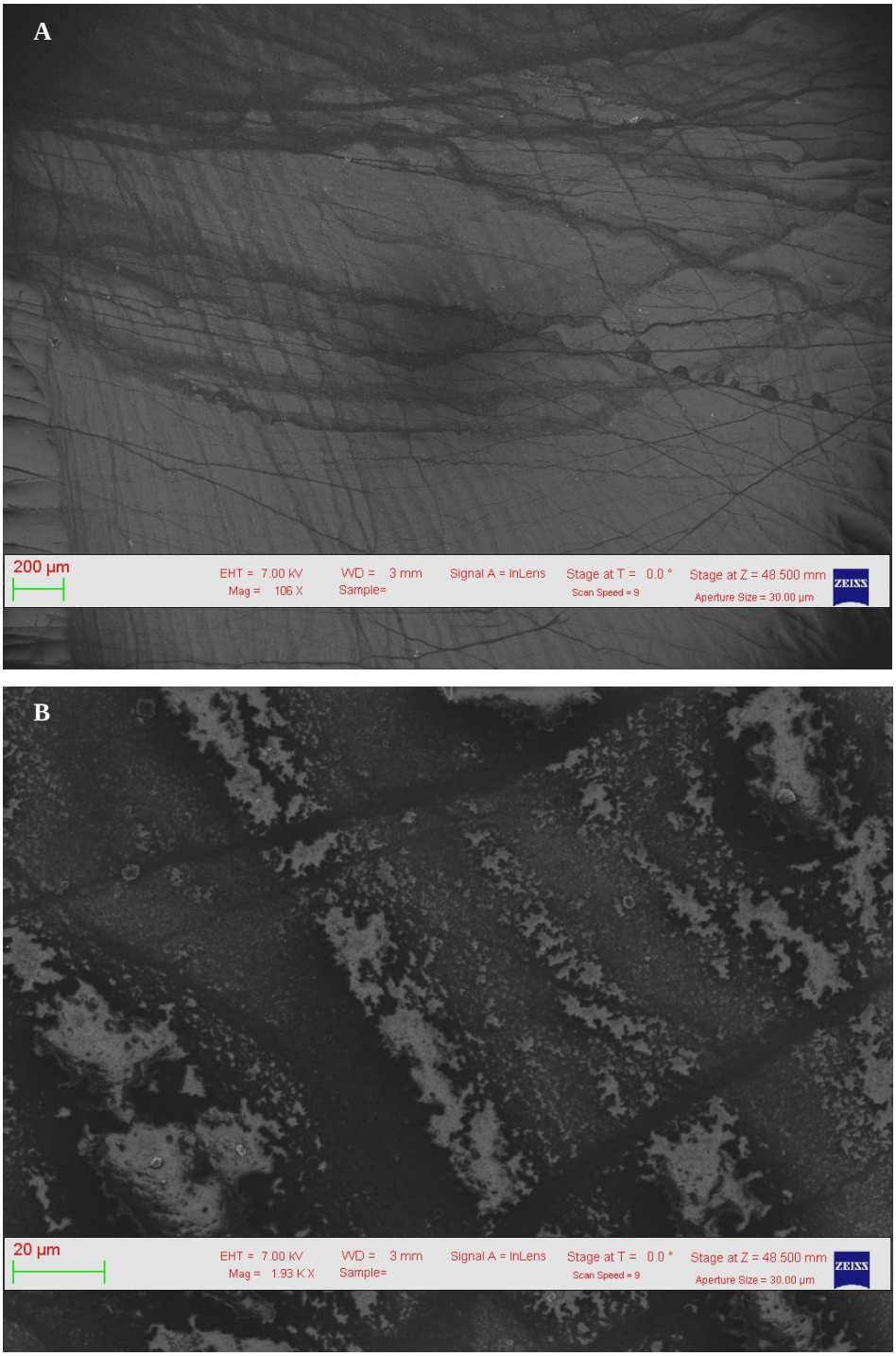
A
200 µm
EHT = 7.00 kV
Mag = 106 X
WD = 3 mm
Sample=
Signal A = InLens
Stage at T = 0.0 °
Scan Speed = 9
Stage at Z = 48.500 mm
Aperture Size = 30.00 µm
ZEISS
B
20 µm
EHT = 7.00 kV
Mag = 1.93 K X
WD = 3 mm
Sample=
Signal A = InLens
Stage at T = 0.0 °
Scan Speed = 9
Stage at Z = 48.500 mm
Aperture Size = 30.00 µm
ZEISS

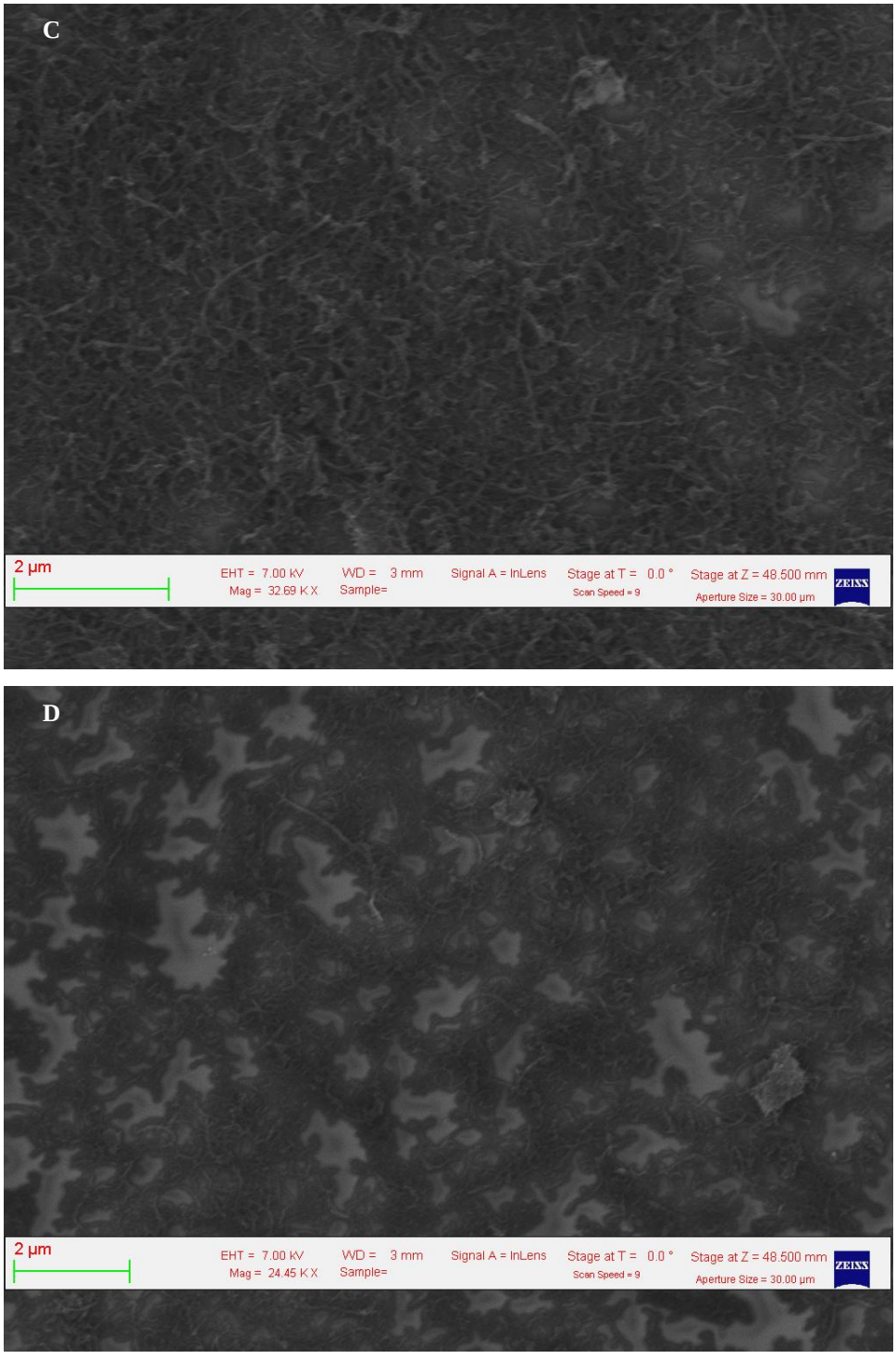

Figure 4. SEM images of DMF solution MWCNTs **9** coated substrates (scale bar A 200 µm; B 20 µm; C, D 2 µm).

From Figure 4, it is visible that these substrates are homogenous in the MWCNT content. On these substrates, the electrophysiological results obtained by Cellot et al[3] were reproduced.

By means of single-cell electrophysiology, Cellot et al[3] demonstrated that direct interaction of CNTs with the neuronal membrane affects each cell activity. They discovered that carbon nanotubes increase the probability of generating a depolarization in membrane potential after a series of action potentials induced by injections of current pulses into the soma of the cell. Such a phenomenon, which is calcium mediated, is a mark of an increased ability of neurons in integrating back-propagating action potentials in the distal compartments of dendrites and, in simpler terms, makes the neurons more excitable. A schematic representation of a neuron is presented in Figure 5.

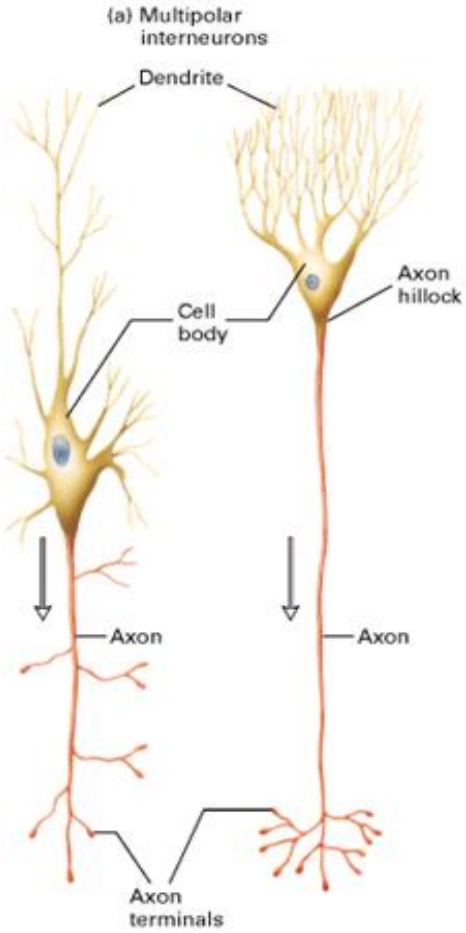

Figure 5. Schematic representation of central nervous system neurons[4].

The mechanism underlying this phenomenon has not been totally clarified yet, but the authors proposed the hypothesis that nanotubes, thanks to both the characteristic nanostructure and the good conductive properties, provide an electrical short-cut between adjacent regions of soma and dendrites, that favors the back-propagation of action potentials. Such an idea was also supported by TEM images, showing the existence of several points of tight contact between carbon nanotubes and neuronal membranes (Figure 6).

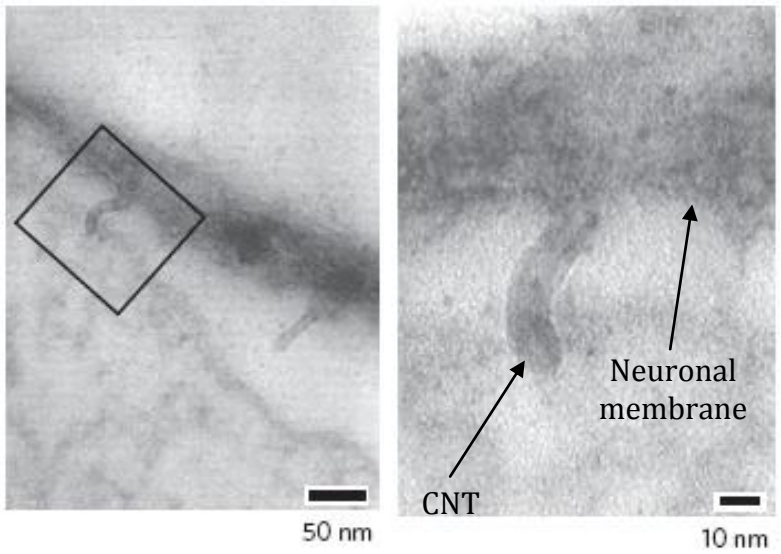

Figure 6. The interaction between MWCNTs and neurons: note how nanotubes are "pinching" neuronal membranes[3]. In the figure Neuronal membrane and the CNT are indicated.

4.2 Morphological study of neurons deposited on CNTs

On this basis, we proceeded in studying the morphological interaction between neurons and carbon nanotubes. As introduced in Appendix A, SEM is one of the best techniques that allows this kind of investigation.

In the next micrographs, it is clear that neuronal neurites interact with CNTs. We are not able to distinguish whether nanotubes penetrate the cell membrane or not, but we can correlate the "functional bridge" (highlighted in

Figure 7 E, F, G and H) with the TEM images reported by Cellot et al where it is possible to distinguish few nanotubes in contact with the cell membrane.

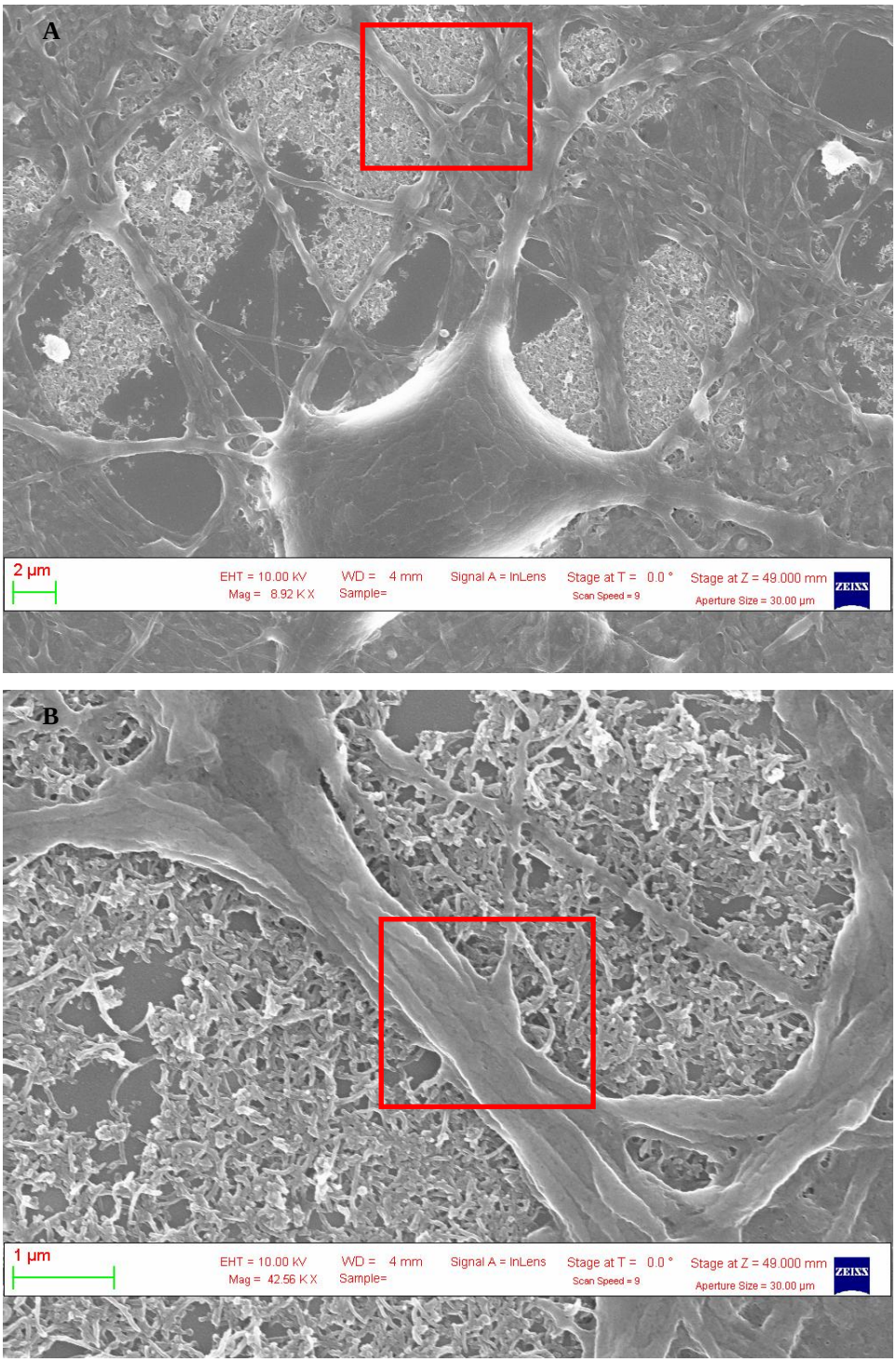

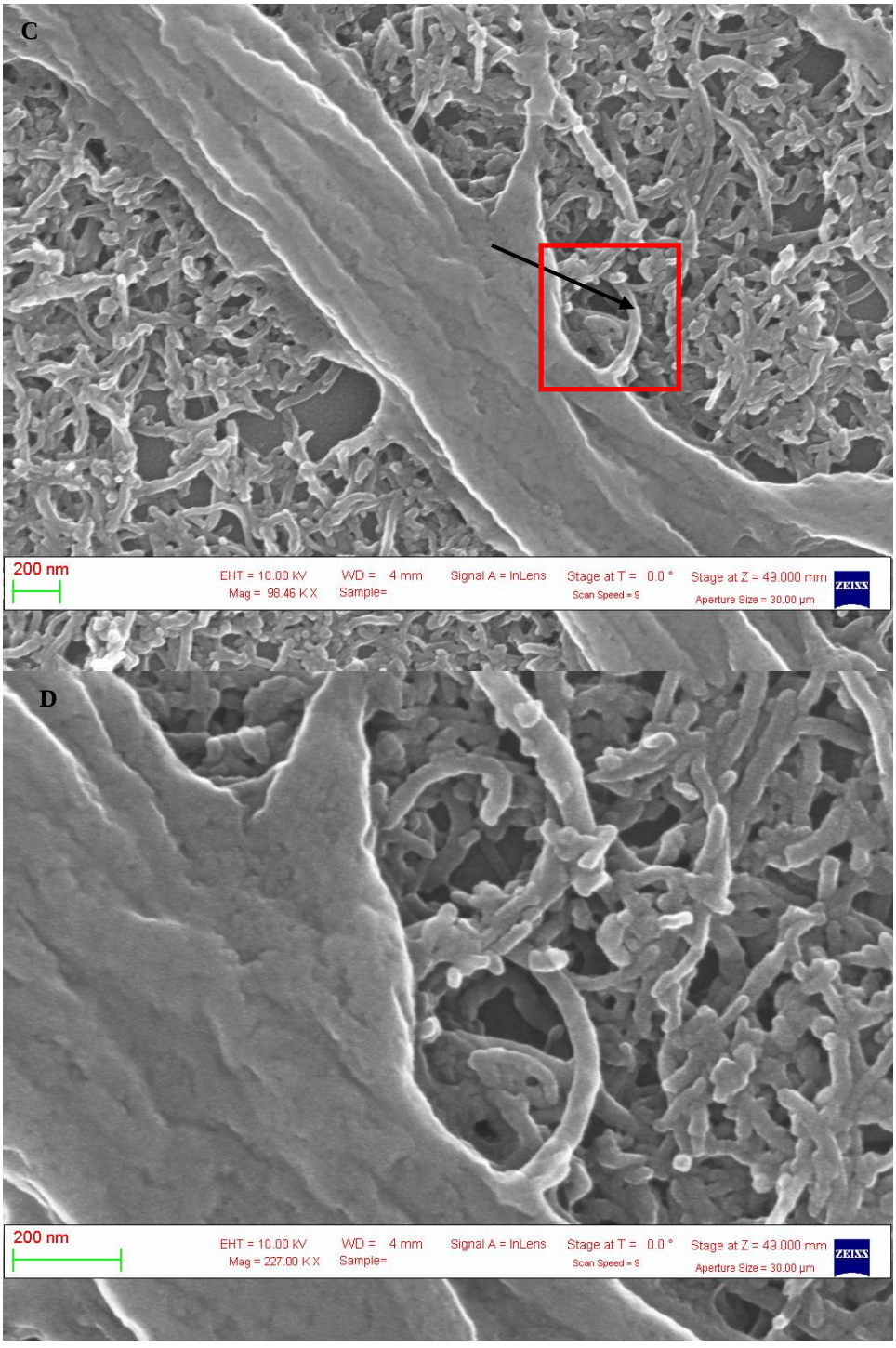
C
200 nm
EHT = 10.00 kV
Mag = 98.46 K X
WD = 4 mm
Sample=
Signal A = InLens
Stage at T = 0.0 °
Scan Speed = 9
Stage at Z = 49.000 mm
Aperture Size = 30.00 µm
ZEISS
D
200 nm
EHT = 10.00 kV
Mag = 227.00 K X
WD = 4 mm
Sample=
Signal A = InLens
Stage at T = 0.0 °
Scan Speed = 9
Stage at Z = 49.000 mm
Aperture Size = 30.00 µm
ZEISS


E
10 µm
EHT = 10.00 kV
Mag = 5.39 K X
WD = 4 mm
Sample=
Signal A = InLens
Stage at T = 0.0 °
Scan Speed = 9
Stage at Z = 49.000 mm
Aperture Size = 30.00 µm
ZEISS

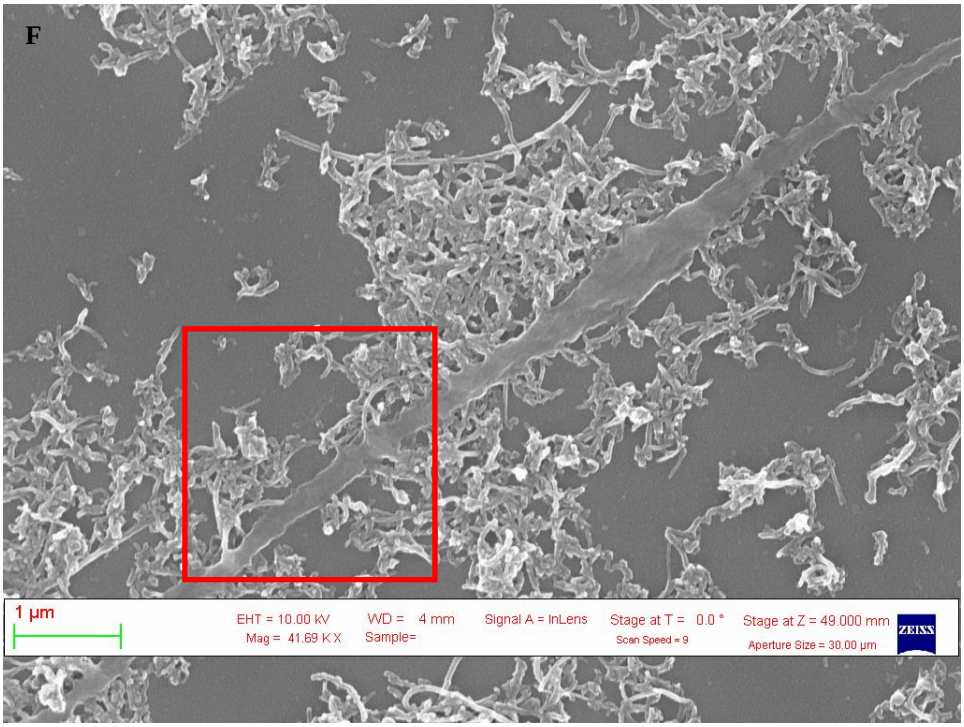
F
1 µm
EHT = 10.00 kV
Mag = 41.69 K X
WD = 4 mm
Sample=
Signal A = InLens
Stage at T = 0.0 °
Scan Speed = 9
Stage at Z = 49.000 mm
Aperture Size = 30.00 µm
ZEISS

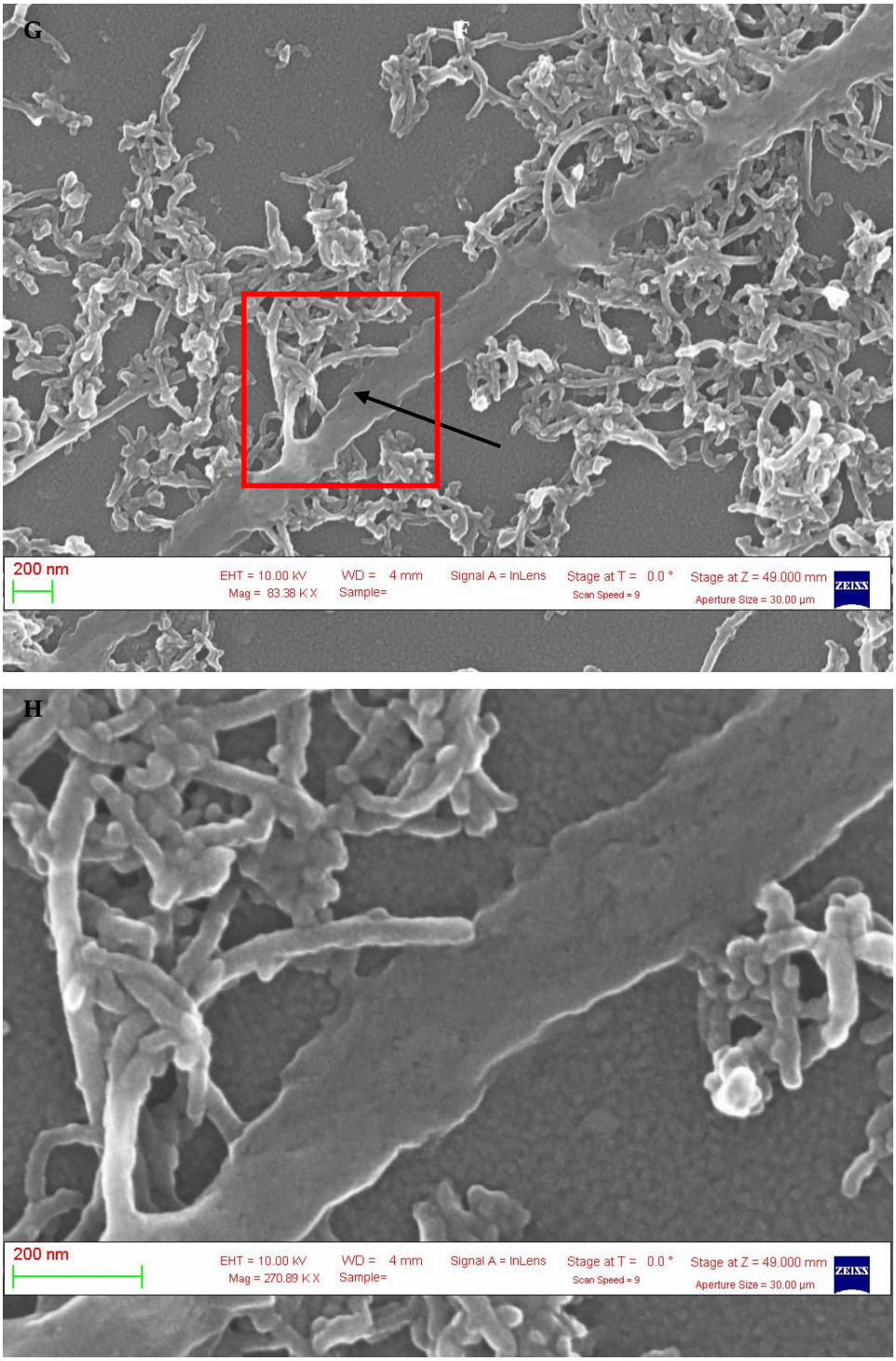

Figure 7. SEM images of hippocampal neurons grown on DMF solution of MWCNT coated substrates: A, B, C, D and E, F, G, and H are sequential magnifications referred to two different glass substrates (scale bar A = 2 µm; B, F = 1 µm; C, D, G, H = 200 nm; E = 10 µm) The red square is referred to the areas that are subsequently enlarged, the arrows indicate the CNT when it is pinching the dendrites.

The images shown in Figure 7 corroborate the hypothesis of the existence of an electrical shortcut between adjacent compartments of soma and dendrites mediated by the carbon nanotube carpet. In figure 7 the arrow indicates the possible zones in which one of these short-cuts may occur. This result could be confirmed using "non-conductive" carbon nanotubes. Actually, the functionalization breaks the carbon nanotubes electronic structure reducing the conducting properties. To this aim, our idea is to produce MWCNTs **8** (Chapter 2) coated substrates in order to study if the depolarization in neuronal membrane potential due to the integration of back-propagating action potentials is still present.

In addition, in this way we could use positively charged pre-treated substrates that, as mentioned, should also promote neuronal growth and differentiation.

4.3 Pairs of neurons electrophysiology

We pursued also in the electrophysiological side performing pairs of neuron recordings in order to characterize neuronal activity in presence of carbon nanotube substrates.

Briefly, the patch clamp technique was introduced in 1976 by Sackman and Neher: with this technique, currents of pA and potential of mV are measured. A glass micropipette (with a tip of 1-2 μm) filled with ions solution represents the recording electrode and it is sealed with the neuronal cell membrane.

Two different modes of recording can be used: current clamp configuration monitors variations in the membrane potential with the possibility of injecting currents to depolarize (positive current) o hyperpolarize (negative current) the cell; in this case spontaneous activity of neurons can be measured as a function of the number of action potentials over the time.

In voltage clamp configuration, it is possible to record currents passing through channels present in cellular membrane at determined voltage.

In this case, neuronal spontaneous activity is measured in terms of the number of post-synaptic currents over the time. Such postsynaptic currents are generated by the binding of neurotransmitters to their receptors, which are ligand-gated ion channels.

In dual electrophysiological recordings, pairs of cells, far away 150-200 μm one from the other, were chosen and one of the two cells, the presynaptic neuron, was stimulated in current clamp configuration while simultaneously the activity of the second neuron, the postsynaptic one, was monitored in voltage clamp configuration, to check the presence or the absence of a response due to the presynaptic stimulus (Figure 8).

All these recordings used an inverted microscope and this is why we need transparent substrates and transparent carbon nanotubes film to coat the glass surface.

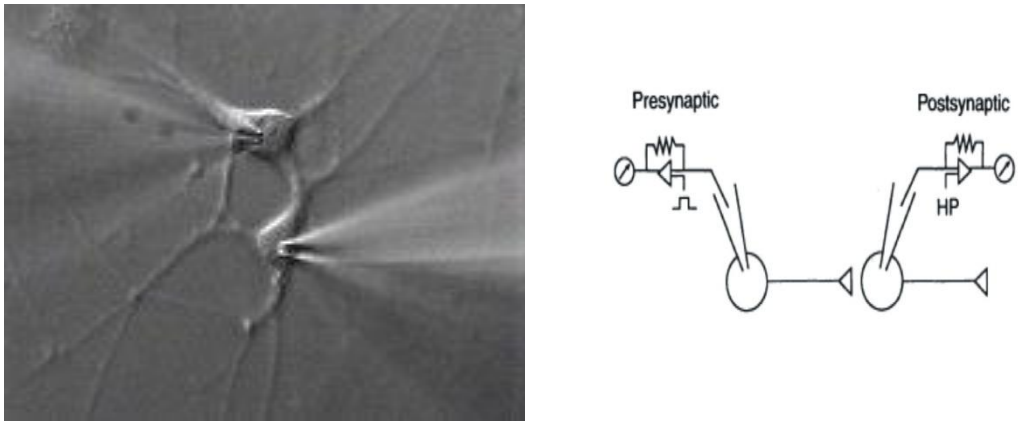

Figure 8. Dual electrophysiological recordings. Left: Image of a pair of neurons with glass pipettes for patch clamp recording. Right: Scheme of the experimental setting.

In Figure 9 (left), the example of a pair of neurons that are not monosynaptically coupled is shown. In this case, there is no response in postsynaptic trace caused by the presynaptic stimulation. Contrarily, in Figure 9 (right) the recordings relative to two neurons forming a synapse are reported: for each presynaptic action potential, it is present a deflection in the postsynaptic trace that represents an

inward current due to the activation of postsynaptic receptors via neurotrasmitters released at the presynaptic terminal

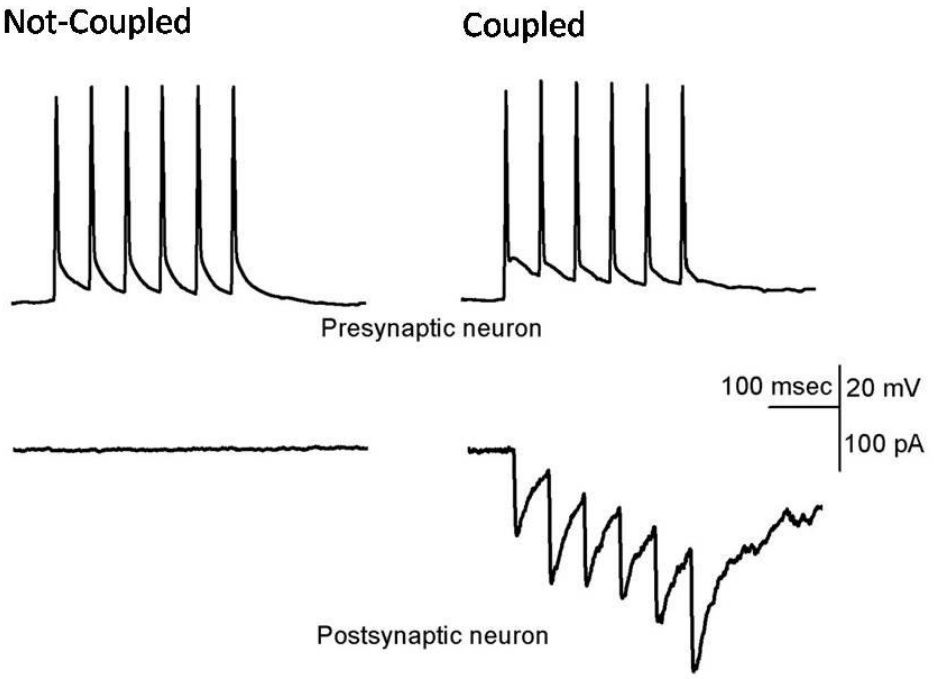

Figure 9. Examples of traces for pairs of neurons in control condition and in presence of CNT.

The probability of finding coupled pairs in control conditions and in presence of CNTs was analyzed. The experiments showed that in control (neurons grown on bare glass) the percentage of monosynaptic coupling is 39% (n=149), while when neurons are grown on CNT layers the probability is increased to 58% (n=122).

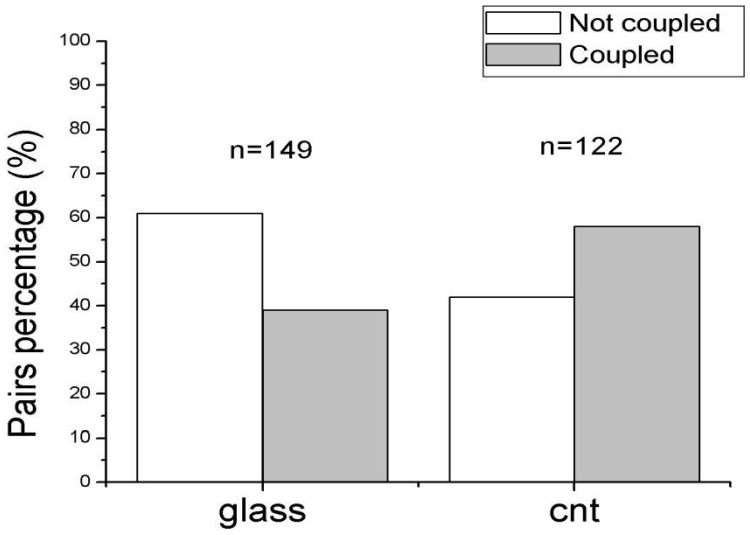

In other terms, these data indicate CNT substrates favor the formation of synaptic contacts between neurons. Such result agrees with one previously reported by Lovat et al, 2005, where an increased number of synaptic connections promotes the boosting of spontaneous activity.

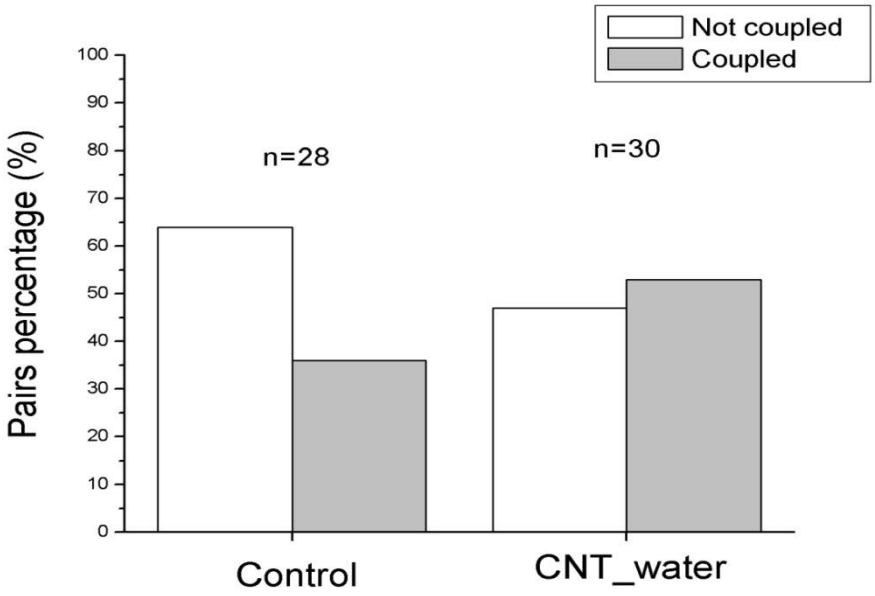

To support our previous statements, we present herein also the result obtained with water dissolved MWCNTs in which is demonstrated that the probability of finding coupled pairs is higher with respect to control, but lower

with respect to DMF dissolved MWCNTs (Coupled pairs in control: 36% n=28; in presence of water dissolved MWCNTs: 53% n=30).

This allowed us to conclude that also CNT substrate density plays a role in neuronal network activity.

Dual electrophysiological recordings demonstrate that the connectivity of neurons is improved in the presence of carbon nanotubes supporting the results obtained by Lovat et al[1] We are still investigating which is the real role played by CNTs in the modification of neuronal activity and thanks to this pairs recording we will highlight whether morphological or electrical properties of these versatile nanostructures are determining the boosted activity of neural network.

References

(1) Lovat, V.; Pantarotto, D.; Lagostena, L.; Cacciari, B.; Grandolfo, M.; Righi, M.; Spalluto, G.; Prato, M.; Ballerini, L. Carbon Nanotube Substrates Boost Neuronal Electrical Signaling. *Nano Letters* **2005**, *5*, 1107-1110.

(2) Sucapane, A.; Cellot, G.; Prato, M.; Giugliano, M.; Parpura, V.; Ballerini, L. Interactions Between Cultured Neurons and Carbon Nanotubes: A Nanoneuroscience Vignette. *Journal of Nanoneuroscience* **2009**, *1*, 10-16.

(3) Cellot, G.; Cilia, E.; Cipollone, S.; Rancic, V.; Sucapane, A.; Giordani, S.; Gambazzi, L.; Markram, H.; Grandolfo, M.; Scaini, D.; Gelain, F.; Casalis, L.; Prato, M.; Giugliano, M.; Ballerini, L. Carbon nanotubes might improve neuronal performance by favouring electrical shortcuts. *Nature Nanotechnology* **2009**, *4*, 126-133.

(4) Lodish, H.; Berk, A.; Kaiser, C. A.; Krieger, M.; Scott, M. P.; Bretscher, A.; Ploegh, H.; Matsudaira, P. *Molecular Cell Biology*; 6° ed.; W. H. Freeman, **2007**.

CONCLUSION

In this thesis we have pursued biological applications of functionalized CNTs.

As we have already stated, among the many applications of CNTs, the biological ones are the most criticized. The debate mainly concerns the toxicity and the uncertain fate of the CNTs inside the human body. Nevertheless, by dendrimer functionalization of CNTs we have obtained evidence that make us confident in a possible future exploitation of functionalized CNTs in drug delivery. We obtained successful results in gene silencing with our dedrimeric compounds and the compatibility of CNT-coated glasses with neuronal cultures was clearly proved, demonstrating the reduced toxicity of these materials. Since neuronal cells are very sensitive to contaminants and their viability is an important parameter to assess the hazard of exposure to possible toxic agent, we can consider these results rather comforting.

More in depth, for what concerns drug delivery, we can state that CNTs have crucial properties, such as the high surface area and the possibility to penetrate the cell membranes as nano-needles, that make them very promising for drug delivery application. With respect to the choice of covalent functionalization, 1,3-dipolar cycloaddition reaction of azomethine ylides is one of the most used and suitable. Together with defect functionalization, good results have been obtained, making possible to attach to the CNT dendrimeric-like structure and eventually add different molecules creating a great opportunity in this field that badly needs new types of efficient drug carriers. In our group, we are strongly pushing the direction to obtain derivatives with enhanced bioavailability and compatibility, which could be successfully adapted to different types of drugs. To address this issue, multiple functionalization of CNTs is needed and is currently under study in our laboratory.

On the other side, the main difficulty is represented by our lack of knowledge about the fate of CNTs inside the body, and we are also actively investigating this aspect. As far as we know, not surprisingly, there is no evidence about a possible "digestion" of CNTs inside the cells or at a systemic level and irrefutable evidence of exocytosis has not yet been obtained. Biodistribution studies have shown that renal excretion is the preferential way of elimination, but this has not been demonstrated for all the CNT derivatives, as mentioned in this thesis. When we combine CNTs with dendrimers or polymers, the biological tests become more and more complex. As a consequence, the fate of the compounds, their biological activity and their toxicity will be difficult to assess.

The sharp shape of CNTs leads to many worries because they are compared with asbestos fibers. Luckily this is not true, because CNTs employed in biological studies are usually short (around 500 nm) and functionalized, instead asbestos fibers are long and thick, and they easily injure the tissues provoking mesothelioma in lungs. In parallel, a still small but possibly increasing research field is represented by other carbon nanostructures like carbon nanodiamonds (spherical carbon particles ranging from few nm to 100 nm in diameter), that have been functionalized in a way that is similar to CNTs and have high surface area but with a round shape that should not cause any inflammatory response. Even in this case, though, the systemic fate remains so far unclear. With respect to other carbon nanostructures, carbon nanohorns are also under study but they bear an indented structure that may inflame tissues.

The main problem of nanotechnology, and especially of nanomedicine, is that the used materials are completely new and there has been just little time to explored their possible advantages and disadvantages in all their facets, like chronic toxicity.

In contrast to this "difficult" scenario, we are instead strongly convinced that CNT-coated substrates for neuronal cells growth represent already now great frontier for neurobiology and pathology because the boosting of the neuronal network activity is critical for people with an injured spinal cord. Further

investigations in this field are essential, and we think that a lot can be done in principle. CNTs are conductive needles that pinch the neuronal cell membrane and probably induce a short-cut that is crucial to determine the boosting of the entire neuronal network activity. The details of this interaction are not completely clear but both neurons and CNTs are able to carry charges, neurons using ions and CNTs using electrons. Although, we are currently trying to pass from bidimensional neuronal networks, to more complicated biological environments, towards the *in vivo* final tests, we already have many pieces of evidence that make us so optimistic.

In conclusion, even though a lot of studies, especially of the *in vivo* type, are still missing to draw a complete picture of the CNT use in biology and medicine, we are quite confident that in the future biological applications will be vigorously explored and many improvements will be achieved for all carbon nanostructures.

Conclusion

APPENDIX A:

REVIEW OF THE EXPERIMENTAL METHODS USED IN THIS THESIS

In this chapter we review all the methods employed to produce and characterize our derivatives.

A.1 Carbon Nanostructures Functionalization using 1,3-dipolar cycloaddition reaction

The 1,3-dipolar cycloaddition of azomethine ylides to fullerene was reported for the first time in 1993[1]. The azomethine ylide cycloaddition, yielding fulleropyrrolidines[1-3], contributed significantly to the development of new nanocarbon-based materials for strategic fields such as solar energy conversion and molecular medicine[4-6]. Therefore it represents a powerful tool to introduce covalent functionalizations to CNTs[7,8], either MWCNTs and SWCNTs (Scheme 1). Exohedral addition of organic groups helps to control solubility and morphology in the solid state and the electronic properties of the fullerene core and CNTs. In

this thesis, we extensively used 1,3-dipolar cycloaddition reaction as the starting point in every synthesis.

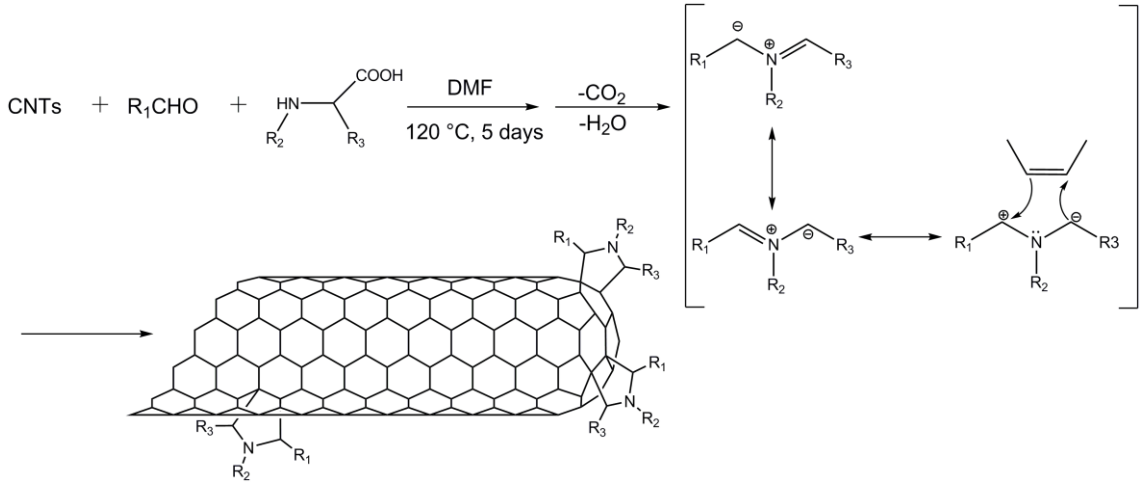

Scheme 1. CNTs addition of azomethine ylides

The reaction employs an α-aminoacid and either an aldehyde or a ketone. As seen in Scheme 1, it occurs by the condensation of the amine in the aminoacid and the carbonyl group to form a dipole intermediate, which is able to react with the numerous double bonds present in the nanotubes, both on their sidewall and on their tip. A well-established protocol consists on the addition of both reactants in excess in DMF for 5 days at 130°C; in the presence of protecting functional groups (like *tert*-butyloxycarbonyl, cleavable by means of high temperature) the reaction temperature could be decreased to 115°C. To perform this reaction, we have used {2-[2-(2-*tert*-butoxycarbonylamino-ethoxy)-ethoxy]-ethylamino}-acetic acid reported in Scheme 2. By removal of the protective groups, several different molecules can be attached to CNTs[8]. The presence of amino groups can be assessed using a quantitative test used in solid phase synthesis, known as Kaiser Test[9,10]. Side characterization techniques, as Kaiser Test, are in fact crucial to study our derivatives, since the conventional chemical characterization tools, as NMR or mass spectrometry, cannot be used with functionalized CNTs. ^{1}H NMR analyses of functionalized CNTs led to weak and broad signals that are difficult to univocally

interpret, even though new methodologies are arising in this direction, like diffusion NMR[11].

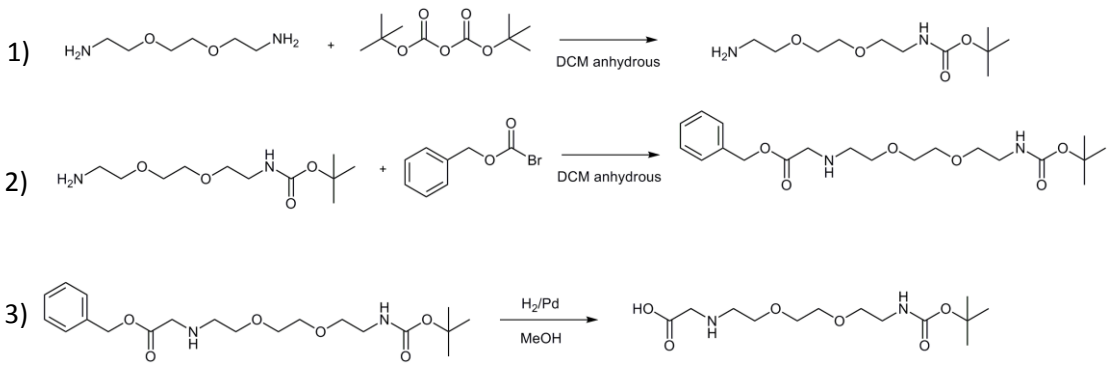

Scheme 2. 1) Synthesis of N-(*tert*-butyloxycarbonyl)-amino-diethoxy-ethyl amine. 2)Synthesis of {2-[2-(2-*tert*-butoxycarbonylamino-ethoxy)-ethoxy]-ethylamino}-benzyl ester. 3)Synthesis of {2-[2-(2- *tert*-butoxycarbonylamino-ethoxy)-ethoxy]-ethylamino}-acetic acid.

In chapter 2 we reported a well-constructed synthesis of positively charged PAMAM-modified-CNTs derivatives[12]. The use of dendrimer-like structures fulfills the main requirements of covalent carbon nanotubes chemistry. Exploiting 1,3-dipolar cycloaddition and the growing of a dendron, it is possible to provide an increased number of reactive groups at the periphery without damaging the carbon nanostructure.

In fact, dendrimers are complex polymers and own a peculiar branched-architecture with tunable nanoscale dimensions: they are made of an internal core, and interior layers, composed of repeating units named generations (indicated as G), and an exterior layer that bears the peripheral functionalities (Scheme 3).

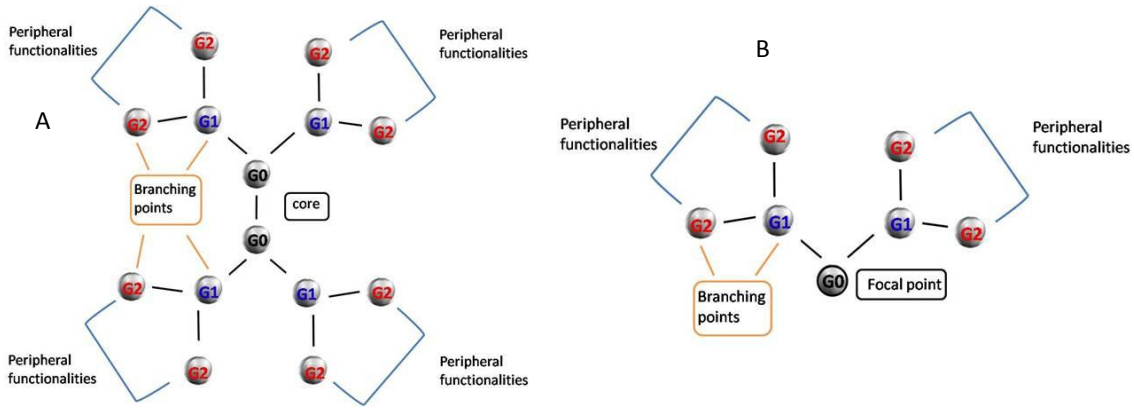

Scheme 3. (A) Dendrimer and (B) Dendron structures, generation 0 (G0) is indicated in black, generation 1 (G1) in blue, and generation 2 (G2) in red.

In Scheme 3 is indicated a derivative of dendrimer family, that is dendron. Dendron is grown developing a focal point only towards one part of the plain; by means of this branched polymeric dendron, we could functionalize CNTs introducing many amines.

A.2 Microwave

MW can be exploited to perform organic reactions. Their use as a powerful heating source in organic synthesis arose in the middle of 1980s. From the beginning, this approach has received wide attention among organic chemists because it can provide high yield, reduce side reactions, improve reproducibility and, above all, reduce chemical reaction times, of order of magnitudes[13]. In chapter 2, we proposed to use microwave for 1,3-dipolar cycloaddition with ionic liquids. This combination lead us to obtain one the highest yield reported (entry **14** Table 2 Chapter 2)[14].

Microwave frequencies range from 0.3 to 300 GHz. Domestic ovens and reactors for chemical reactions typically operate at 2.45 GHz (12.24 cm wavelength) to avoid interference with telecommunication and cellular phone frequencies. The correspondent energy is of 0.0016 eV (0.037 Kcal/mol), too small to induce chemical reactions, as it is possible to see from the comparison in Table 1[15].

Table 1. Brownian motion and bonds energies.

	Energy (eV)	Energy (Kcal/mol)
Brownian Motion	0.025 (298K)	0.56
Hydrogen Bonds	0.043 to 0.65	1 to 15
Covalent Carbon Bonds	1.73 to 5.204	40 to 120

MW induces a "dielectric heating" of the sample, based on the conversion of electromagnetic energy absorbed by the medium into heat. The MW electric field induces a polarization of the molecules at the same frequency of the light. In the infrared regime, electromagnetic field induces atomic vibrations in molecules and crystals and polarization processes resulting from the dipole moment induced by distorsion of nuclei position. In the presence of an electric field a dipole moment undergoes a torque that tends to orientate it parallel to the electric field, dissipating energy into the medium. The minimum in potential energy is when the dipole moment takes the same direction of the electric field. The electric field vector switches its orientation approximately every picosecond: the result is that the torque induces rotation of polar molecules that cannot always stand this rate. So, the delay between electromagnetic stimulation and molecular response is defined as dielectric loss (ε'') and it expresses the efficiency to convert electromagnetic energy into heat. Defining the dielectric constant (ε') as the ability of molecules to be polarized by the electric field, the quotient $\tan\delta$ is derived at (1):

$$\tan\delta = {}^{\varepsilon''}/_{\varepsilon'} \quad (1)$$

Higher $\tan\delta$, higher the efficiency of microwave absorption: this value is often used to classify microwave absorbing property of organic solvents ($\tan\delta$> 0.5 high; $\tan\delta$= 0.1-0.5 medium; $\tan\delta$< 0.1 low). An important note about CNTs is that they have a metal content because of the catalyst particle residue, made mainly of metal oxides such as iron, nickel and cobalt. These metal oxides show very high magnetic

losses that occur in MW region, and consequently they are optimal absorbers of MW. On the other hand, when the dielectric loss of solvents or reactants is too small, the addition of such metals improves dielectric heating. However, thermodynamic effects of electric field over chemical equilibrium are very well known: when the product has a large dipole moment in respect with reactants the equilibrium is shifted towards the product under the action of an applied electric field[13,16]. Besides this, the conventional thermal heating method uses an external heat source, such as in oil bath. Then transferring energy into the system is not so efficient and there is a gradient of temperature towards the reaction mixture, where the temperature is lower. On the other hand, dielectric heating implies that the reaction mixture is directly heated and the gradient of temperature is inverted and lower towards the outsides. To perform microwave reaction, vessels transparent to this wavelength are employed, such as borosilicate glass, quartz or Teflon. To this aim, quartz is particularly resistant and suitable for pristine carbon nanotubes reaction, whereas, we have found that borosilicate glass can be used with purified carbon nanotube (Chapter 2).

Brunetti et al[17] synthesized SWCNT derivatives with the combination of 1,3 dipolar cycloaddition and addition of diazonium salts, using doses of microwave higher than in our case. In general, the use of MWs with CNTs is still under development, and many different strategies can be in principle tested.

A.3 Thermogravimetric Analysis and Kaiser Test

TGA is one of the most important analytical techniques used to determine the quantity of functional groups attached on fucntionalized CNT surface. It is based on the thermal stability of materials: the change of weight of the substance is monitored as a function of the increasing temperature, with sensitivity in the nanogram range. All the derivatives described in this thesis were characterized by means of TGA.

TGA can be performed in different environments, optimized according to the experiment needs: an inert atmosphere (nitrogen or argon) is chosen for measuring the content of organic moieties bound to CNTs, which start burning at about 350°C; an oxygen atmosphere is instead chosen to evaluate the metal residue content (such as the metal catalysist used in the synthesis or the metal nanoparticles subsequently attached), which are converted into solid oxides after the burning of CNTs at about 500°C. The system sensitivity is given by the precision of the weight balance and of the power supply which provides the temperature ramp of the furnace. We usually adopt a linear temperature ramp (10°C/min) preceded by an equilibration step in which the sample is annealed at around 100°C for 20 minutes. We ramp the temperature up to 1000°C, looking for a good compromise between sensitivity and overall time. The main pieces of information regard the weight % (ash content, i.e. residual mass) and the temperature at which the organic volatile moieties burn (oxidation temperature), simply using derivative functions. To our purpose, which is the determination of the degree of functionalization of CNT substrates, we proceed in a differential manner: we evaluate the percentage loss of weight of the system for a family of different derivates grown step by step starting from the same progenitor, to correlate the number of functional groups to the number of carbon atoms (2) and/or to determine the concentration of the functional groups in the carbon matrix (3):

$$Carbon\ atoms/_{Funct\ Gr} = \frac{Weight\ \% \times Molecular\ weight\ of\ funct\ gr}{Molecular\ weight\ of\ C \times Loss\ of\ weight\ \%} \quad (2)$$

$$\frac{mmol}{g} = \frac{Loss\ of\ weight\ \% \times 10}{Molecurar\ Weight\ of\ functional\ group} \quad (3)$$

Where $funct\ gr$ means functional groups, and $Molecular\ weight\ of\ C$ is equal to 12.

The results obtained by TGA are then compared to Kaiser Test outputs. This test, introduced in 1970[9] is a quantitative measurement of free amino groups in solid state peptide synthesis. It is crucial to evaluate the success of 1,3 dipolar cycloaddition reaction occured with the aminoacid reported in Scheme 2. As already mentioned, the main goal of the synthesis is to succeed in the formation of free amino groups released after deprotection. Kaiser Test is a simple ninhydrin test, which follows the reaction shown in scheme 4:

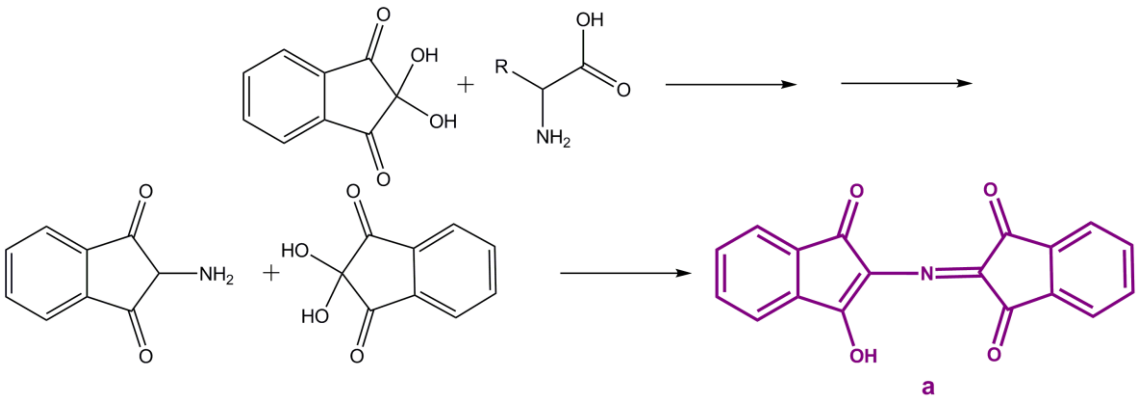

Scheme 4. Kaiser test reaction. Complex **a** is responsible for absorption at 570 nm.

This reaction, which takes place at 100°C, produces a ninhydrin complex (complex **a** in the scheme) which absorbs light at 570 nm. By means of the recorded absorbance, we are able to quantify the free amino groups: according to the Lambert-Beer law, absorbance can be in fact correlated with the concentration of amino groups as follows:

$$\frac{mmol}{g} = \frac{(Abs\ sample - Abs\ blank) \times dilution\ (mL) \times\ 10^3}{Extinction\ coefficient\ \times Sample\ weight\ (mg)} \quad (4)$$

Where the $Abs\ sample$ is the absorbance of resulting complex (Scheme 4); $Abs\ blank$ is referred to the absorbance of the blank (the mixture of ethanolic solution of phenol, KCN in pyridine and ethanolic solution of ninhydrine) at 570 nm; $dilution$ is related to the reaction process (the sample to be analyzed at the spectrophotometer is diluted of 5 mL); $Extinction\ coefficient$ is 15000 m^{-1} cm^{-1};

Sample weight is referred to the weight of CNTs used in the analysis. The sensitivity reported for this test is up to 5 μmol/g[9].

In general, a good estimation of the functional groups content in our CNTs is consistently obtained by means of these two complementary techniques.

A.4 Raman Spectroscopy

Raman scattering, based on the inelastic scattering of monochromatic light, is a valuable technique to study vibrational and rotational excitations of a molecular system. We have use Raman analyses to obtain evidence of covalent (Chapter 2) functionalization of CNTs.

When monochromatic light beam (typically a visible laser beam) hits a sample, a small fraction of it is elastically scattered (Rayleigh scattering) and a smaller fraction (one photon over 10^7) is inelastically scattered (Raman scattering). In Raman scattering the difference in energy between incident and inelastically scattered photons corresponds to the vibrational frequencies of the scattering molecules. Regarding the incident light, the scattered beamcan exibit lower or higher frequencies, known as Stokes and Anti-Stokes scattering respectively (Figure 1).

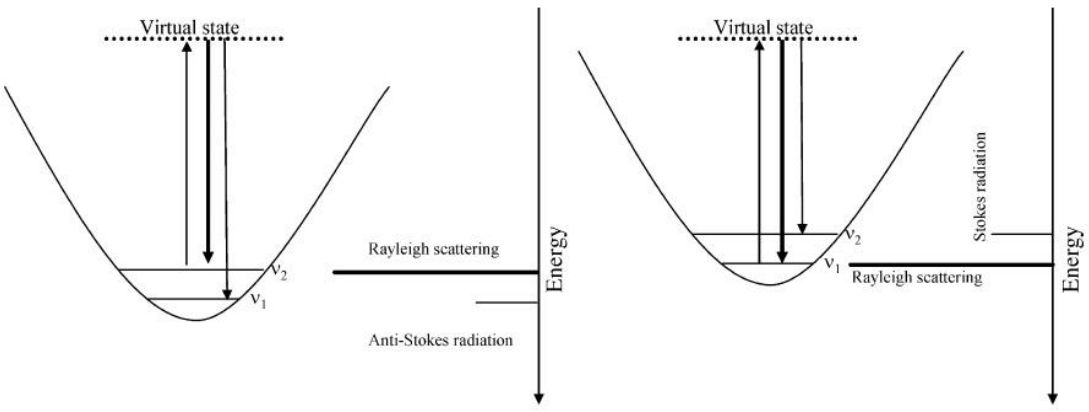

Figure 1. Schematic representation of elastic (Rayleigh) and inelastic (right: Stokes, left: anti-Stokes), adapted from reference[18].

Stokes radiation implies the energy transfer from the photon to the molecule, and the photon is consequently scattered at lower energy; the Anti-Stokes radiation is due to the energy transfer from the molecule to the photon, and the resulting radiation appears at higher energy and lower wavelength. Among the two, the Stokes process is stronger, since at room temperature the population state of a molecule is essentially in its ground vibrational state.

The quantity measured in Raman spectroscopy is the Raman shift, given by (5)

$$Raman\ shift\ =\ \tilde{\nu}\ \pm\ \tilde{\nu}_m \quad (5)$$

Where $\tilde{\nu}$ is the wavenumber (cm^{-1}) of the incident radiation and $\tilde{\nu}_m$ is the wavenumber (cm^{-1}) of the energy difference between the lowest and first excited vibrational energy levels.

The choice of the wavelength of the excitation laser is critical: it should be chosen optimizing mainly i) Raman scattering cross section (which is proportional to the inverse of the fourth power of the wavelength, therefore calling for lower wavelengths) ii) magnitude of the Raman shift in wavelength (see (5)) and iii) the potential for activating fluorescence (which is higher at lower wavelengths)[18].

A Raman set-up is made of a monochromator, adequate filters to allow the detection at very low Raman shift, and a detector that usually is a charge-coupled device detector (CCD).

Optical and spectroscopic properties of carbon nanotubes are mainly characterized by the one-dimensional confinement of the electronic and phonon structure which is more relevant for single walled CNTs. Raman phonons involve normal vibration modes, that play a key role as carrier of thermal energy in conduction processes and in determining thermodynamic properties. Raman scattering depends on specific phonon modes. To have a better understanding of CNTs Raman signals, we will use a comparison with Raman spectrum of graphene/graphite. The electronic σ bands are responsible for the strong in-plane covalent bond within the graphene sheets, whereas the π bands are responsible for

van der Waals interactions between graphene sheets in 3D graphite. Furthermore, π bands are close to Fermi level and electrons can be excited from valence band (π) to the conduction band (π*) optically. During the scattering event, it is possible to distinguish different steps: first an electron is excited from the valence to the conduction band, then this electron is scattered by emitting or absorbing phonons, finally the electron relaxes to valence band emitting a photon. The number of emitted phonons can vary and it could be one-phonon, two-phonon or multi-phonon Raman process. The number in the sequence of total scattering events, including elastic scattering by an imperfection, is called "order of a scattering event".

G (graphite) band and RBM (radial breathing mode) are first-order scattering event, involving one phonon emission. In SWCNTs, G band splits in many frequencies around 1580 cm^{-1} and it is related to the conductive properties of the tube, but in general it is the more intense band, to which the spectrum is usually normalized. The G peak corresponds to the graphite E_{2g} optic mode, that is the doubly degenerate in-plane optical vibration and that is Raman active (Figure 2).

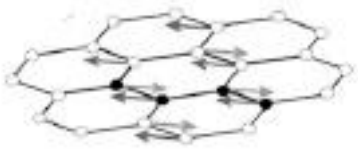

Figure 2. E_{2g} vibration mode of graphene.

On the other hand, RBM is a bond-scattering out of plane phonon mode and frequencies are about 100-500 cm^{-1}. The RBM frequency is inversely proportional to the tube diameter and the mass of all the carbon atoms along the circumferential direction is proportional to the diameter.

Second order scattering, instead, consists of two-phonon scattering events or one-phonon and one elastic scattering event: a typical example is the D-band at 1350

cm^{-1}, related to sp^3 carbon atoms in carbon nanotubes. D band is the so-called "disorder" band and it may come from a symmetry-lowering effect: it is due to defects or nanotube caps, bending of CNTs or presence of carbon nanoparticles and/or amorphous carbon. In graphite, the intensity of D band compared with the Raman-allowed E_{2g} mode depends on the size of graphite microcrystals and consequently on the order of the sample. Comparing spectra of different derivatives, it is possible to identify whether a derivative has been functionalized compared to the pristine material. This feature, indeed, is the main useful measurement for our purpose.

Another common feature in a carbon nanotube Raman spectra is the G' band, a second order scattering two-phonon mode, with a frequency of 2700 cm^{-1}. This overtone is associated with the over-bending of the longitudinal optical branches of graphite[19,20].

Generally, in the literature, there are many examples in which Raman is used to study CNT properties[21]. As already mentioned, RBM are an important feature to discriminate metallic and semiconducting CNTs[22]. Moreover, interesting studies have been recently published by Dai et al[23] about the use of SWCNTs in Raman imaging of biological system.

A.5 Visible-Near Infrared Spectroscopy

UltraViolet-Visible-Near Infrared Spectroscopy (UV-Vis-NIR) investigates SWCNTs in solution and can distinguish between metallic and semiconducting ones. We have used this technique to have a rough idea of the degree of functionalization of our SWCNT-derivative (Chapter 2).

The UV-Vis-NIR absorption is based on a peculiar characteristic of CNTs: the fact that they essentially are one-dimensional systems. As a consequence, electronic density of states consists of a series of Van Hove singularities and absorption spectra are representative of transitions between them. Simply, the density of states (DOS) are the number of one-electron levels at each energy that

can be occupied. In 1d system, like CNT, the DOS is characterized by some divergences, which are called Van Hove singularity. This measurement is performed in solution to obtained the response of individual SWCNTs of different chiral indices and/or of different diameter. Three broad bands may be observed: one is due to metallic (M1=600-700 nm), and the other two are due to semiconducting (S1=1600-1700 nm and S2=1000 nm). The outcome of the spectrum depends on different parameters, as solubility, concentration and bundle formation and it is sometimes very difficult to be reproducible; but what is more important is to demonstrate that we have introduced functional groups. In this case, the one-dimensional system becomes at least a two-dimensional system and absorption spectrum changes between not-functionalized and functionalized CNTs, because van Hove singularities band are lost. This depletion of bands permits a qualitative analysis of the degree of functionalization and it is important to notice is the decrease of intensity in absorption spectra between the starting material and the functionalized one[22,24].

As mentioned, UV-Vis-NIR spectroscopy can be exploit to distinguish between semiconducting and metallic nanotubes: Campidelli et al reported an attempt of separation via covalent functionalization exploiting NIR (and Raman) as a characterization tool[22].

A.6 Trasmission and Scanning Electron Microscopy

Electron microscopy (EM) is a powerful technique to visualize nanostructures; this is why it represents a valuable method used to characterize CNT derivatives. TEM is constantly employed in the whole thesis, while SEM (Chapter 4) is restricted to those derivatives deposited on substrates.

Appendix A: Review of the experimental methods

The introduction of EM is strictly related to the scientific revolution between the end of the XIX and the beginning of XX century, after electrons were discovered in 1897 by J.J. Thompson. E. Ruska, Nobel laureate in 1986 with G. Binnig and H. Rohrer, has significantly contributed to the description of the first electron microscope in 1934 and then to the first prototype of transmission electron microscope, realized in 1938 for "Siemens&Halske AG" company improving the Ruska's original microscope. In principle, an electron microscope is quite similar to a light microscope but with a resolution thousand times higher. According to the de Broglie principle in fact, electrons have a wavelength that is inversely proportional to their energy. In electron microscopes, electrons are extracted from a hot filament, and accelerated to energies up to few hundreds of thousands V, correspondent to wavelength down to tenths of nanometers. The main part of electron microscopes is given by the column, which host the electron gun, the acceleration field, and a series of focusing lens (condensers or magnetic fields lens) and apertures, that control the size of the beam. The microscope operate under vacuum. At the beam/specimen interface several types of signals are generated due to the complex interactions of electrons with matter, detected and processed to produce an image.

Transmission Electron Microscope[25] (TEM) is based on the detection of high electron energy transmitted through a very thin sample (<100 nm thick). In the bright-field imaging mode, the contrast is given by the different absorption of different portions of the sample. In the case of crystalline samples, electrons are diffracted and diffraction peaks positions are detected to give a contrast image. A pattern of diffraction dots is obtained in the case of perfectly crystalline materials, while a series of ring is observed for polycrystalline or amorphous materials.

HiRes TEM is an alternative working mode for TEM. In this case, differences in phase of the electrons that have interacted with the sample are detected. The HiRes mode highlights the structure of nanometer-size objects, as nanoparticles or CNTs. There is also the possibility to perform spectroscopy like Electron Energy

Loss Spectroscopy (EELS) and Energy Dispersive X-Ray (EDX) analysis, known also as micro-analysis. Samples are deposited on grids from a solution. The grids used for CNTs, and also for many other nanoparticles, are made of a metallic framework (Ni or Cu) and covered with a carbon film, continuous or with holes, thin enough to transmit electrons. When the sample cannot be solubilized, it is necessary to make an inclusion with resins and then cut thin film to deposit on the grid.

TEM is widely used for CNTs analysis, in order to investigate the dispersion and the cleanness of functionalized nanotubes, while giving essential morphological information. In our case, we have used TEM (Chapter 2, 3) to characterized reported compounds.

The SEM[26] (SEM), instead, is a fundamental technique to image the surface topography of micro and nano structured samples without any requirements for sample preparation. A focused beam is scanned over the surface and the emitted electrons derived by the interactions with the sample are detected. Three imaging signals can be interaction volume, back scattered electrons (BSE) and secondary electrons (SE). Interaction volume depends on the beam energy and the atomic number of atoms of the specimen. BSE are incident beam electrons that escape from the surface without any significant change in energy. BSE analysis is particularly interesting when information about composition is needed: it depends on chemical composition and surface morphology of samples with different atomic composition (i.e. with diverse atomic numbers), it is possible to highlight differences in contrast among the surface because the intensity of BSE depend on the second power of the atomic number.

SE, instead, depend only on surface morphology and are due to inelastic scattering. They are weakly bound outer shell electrons that receive sufficient energy to be ejected from the atoms. SE can be generated directly by the beam or by BSE and their dependence on the atomic number is negligible. While BSE return both compositional and morphological information, SE give back morphological

information because the surface sensitivity is higher. Also with SEM it is possible to perform EDX analysis.

A.7 Atomic Force Microscopy

The Atomic force microscope (AFM), invented by Binnig, Quate and Gerber in 1986[27,28], is part of the Scanning Probe Microscopy (SPM) family: it is a versatile technique that senses forces (Pauli, Van der Waals, electrostatic, etc.) between an extremely small tip and a sample. It can measure tip-sample interactions without any restriction over the conductivity of the sample (dissimilarly from STM). The specimen seen by AFM does not need then to be flat, a limitation that instead apply to STM measurements: the surface in STM must be flat because the tip-sample separation is monitored as a function of the flow of electrons and this separation is typically about 1 nm.

We used to measure the height profile of covalent functionalized MWCNTs (Chapter 2), in non-contact mode. CNTs were deposited on a flat surface of mica by spin coating deposition.

In AFM the probe is a sharp tip, placed at the end of a flexible cantilever, and a laser beam is focused on the back of it (cantilevers can be metal coated to improve the laser reflectivity). The reflected laser beam hits a four quadrants Position Sensitive Photo Diode (PSPD) that is used to track the laser spot movements induced by cantilever bending and torsion while the tip is scanning the surface. In this way, using a feedback mechanism it is possible to maintain constant the force applied by the tip on the surface (contact mode or, more properly, static mode) or the amplitude (non-contact mode or dynamic mode). Cantilevers are flexible and they are comparable to springs, those are described by Hook's law. By means of this mathematical relation, geometric calculations about the laser displacement over the PSPD return information about occurring interactions.

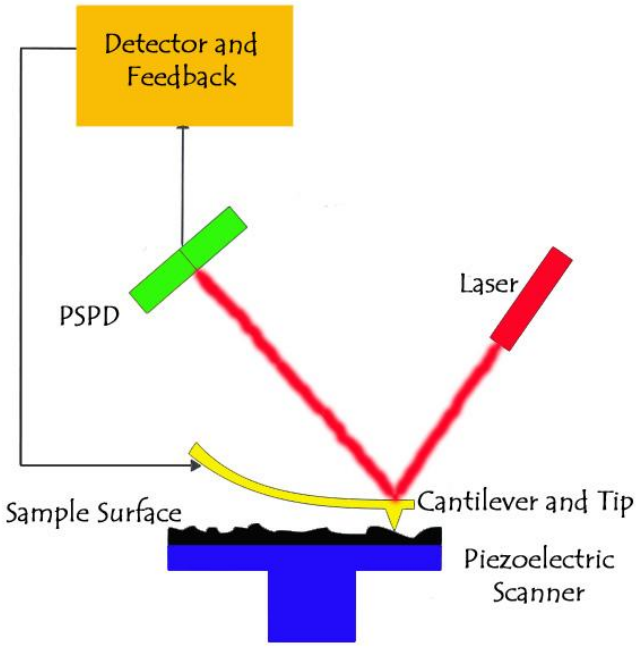

Figure 3. Schematic representation of AFM system.

The feedback system controls tip-specimen interactions, using a setpoint that is mantained while measuring. There are two ways to define a setpoint, one for contact, the other for non-contact mode: in contact mode the set-point is determined by the cantilever deflection (higher the cantilever deflection, higher the force applied and, consequently, larger tip-surface interaction; lower is the force, weaker the tip-surface interaction), while in non-contact mode it is determined by the variations in the cantilever resonance frequency (FM) or amplitude at a fixed frequency (AM). Generally, in non-contact mode, the interaction with the specimen is smaller than in contact mode, consequently dynamic mode is usually the preferred technique to image soft samples. Tip and sample movements are extremely precise and are driven by a ceramic piezo material, in a tube scanner shape: the scanner is able to perform sub-nanometric movements.

AFM-tip can also be used as a tool to immobilize DNA molecules in order to produce both DNA[29] or protein chip[30], by means of nanografting technique.

Notwithstanding, topographic AFM images of neuronal cells grown on a carpet of MWCNTs have been also reported[31].

A.7.1 Electrostatic Force Microscopy

Electrostatic Force Microscopy[32,33] (EFM) is an AFM working mode, in which a biased tip is scanned over a surface to probe surface potential and charge distribution. We employed this technique to characterize positively charged functionalized CNTs (Chapter 2), exploring the possibility to draw the CNT profile highlighting the presence of positive charges.

The working principle is based on the Coulomb interactions occurring between the sample and the tip, and it causes the subsequent changes in the oscillation amplitude and phase of the AFM cantilever vibrating at a fixed frequency. The different power law between van der Waals and Coulomb forces (van der Waals forces depend on the sixth power of the distance, while Coulomb forces depend on the second power) allows the discrimination between Coulombian interaction due to charge accumulation, and van der Waals interaction, responsible of the morphology connected forces. EFM differs from Kelvin Probe Microscope (KPM), that gives information about the surface potential of the sample, because the substrate may not be conductive, whereas the tip is a metal-coated tip, and, moreover, EFM is generally characterized by higher spatial resolution.

In EFM, to separate van der Waals and Coulomb contributes two techniques can be used: the most commonly adopted one is the second-pass technique. The second-pass technique, coherently with the van der Waals law, draws the topographic profile in the first pass, then the tip is lifted to a fixed height (usually 50 nm); in the second pass changes in amplitude and phase of the tip oscillations (mainly due to the Coulomb contribution) are measured giving information about surface charge distribution. The drawback in the tip lift is a partially loss in image resolution. The second technique is the Enhanced-EFM (E-EFM) able to perform in

one single pass both the topography and the electrostatic measurements because of the presence of an external lock-in, able to separate the two force contributions due to the different frequency dependence. In our E-EFM set-up, a conductive tip scans a surface in close proximity in non-contact mode, when a DC bias is applied to the cantilever. An external lock-in amplifier applies simultaneously an AC voltage, in addition to the DC bias applied by the AFM controller, allowing for discriminating between electrostatic and van der Waals contributions to the measured force[34]. Changing the bias of the tip, different contrast and phase and amplitude values are measured: there are several discussion about the meaning of the recorded signals but the phase shift, that exists between the driving sinusoidal signal and the cantilever response (read by the PSPD), allows to identify whether the operating regime is attractive or repulsive. Phase-shift measurements provide a practical and unambiguous method to identify the operating regime: conditions that imply positive phase shifts are characteristic of an attractive regime, while conditions that set negative phase shifts are characteristic of a repulsive regime. The phase shift is proportional to the total charge present below the tip.

We tried to use this tool to investigate the presence of positive charges on MWCNTs **8** (Chapter2), because of the results obtained by Navarro-Gomez et al[35]: in their study they compared the different conductivity of a DNA nanowire and of a SWCNT. Later on, other studied on the electrostatic response of bare nanotubes[36] were reported, but our expertise in functionalization should allow us to investigate the presence of positive charges on the nanotubes surface.

References:

(1) Maggini, M.; Scorrano, G.; Prato, M. Addition of azomethine ylides to C60: synthesis, characterization, and functionalization of fullerene pyrrolidines. *Journal of the American Chemical Society* **1993**, *115*, 9798-9799.

(2) Prato, M.; Maggini, M. Fulleropyrrolidines: A Family of Full-Fledged Fullerene Derivatives. *Accounts of Chemical Research* **1998**, *31*, 519-526.

(3) Tagmatarchis, N.; Prato, M. The addition of azomethine ylides to [60]fullerene leading to fulleropyrrolidines. *Synlett* **2003**, 768-779.

(4) Prato, M. [60]Fullerene chemistry for materials science applications. *J. Mater. Chem.* **1997**, *7*, 1097-1109.

(5) Mateo-Alonso, A.; Guldi, D.; Paolucci, F.; Prato, M. Fullerenes: Multitask Components in Molecular Machinery. *Angewandte Chemie International Edition* **2007**, *46*, 8120-8126.

(6) Mateo-Alonso, A.; Sooambar, C.; Prato, M. Synthesis and applications of amphiphilic fulleropyrrolidine derivatives. *Org. Biomol. Chem.* **2006**, *4*, 1629-1637.

(7) Tasis, D.; Tagmatarchis, N.; Bianco, A.; Prato, M. Chemistry of carbon nanotubes. *Chemical Reviews* **2006**, *106*, 1105-1136.

(8) Singh, P.; Campidelli, S.; Giordani, S.; Bonifazi, D.; Bianco, A.; Prato, M. Organic functionalisation and characterisation of single-walled carbon nanotubes. *Chemical Society Reviews* **2009**, *38*, 2214-2230.

(9) Kaiser, E.; Colescott, R. L.; Bossinger, C. D.; Cook, P. I. Color test for detection of free terminal amino groups in the solid-phase synthesis of peptides. *Analytical Biochemistry* **1970**, *34*, 595-598.

(10) Sarin, V.; Kent, S.; Tam, J.; Merrifield, R. Quantitative monitoring of solid-phase peptide synthesis by the ninhydrin reaction. *Analytical Biochemistry* **1981**, *117*, 147-157.

(11) Marega, R.; Aroulmoji, V.; Dinon, F.; Vaccari, L.; Giordani, S.; Bianco, A.; Murano, E.; Prato, M. Diffusion-Ordered NMR Spectroscopy in the Structural Characterization of Functionalized Carbon Nanotubes. *Journal of the American Chemical Society* **2009**, *131*, 9086-9093.

(12) Herrero, M. A.; Toma, F. M.; Al-Jamal, K. T.; Kostarelos, K.; Bianco, A.; Da Ros, T.; Bano, F.; Casalis, L.; Scoles, G.; Prato, M. Synthesis and Characterization of a Carbon Nanotube−Dendron Series for Efficient siRNA Delivery. *Journal of the American Chemical Society* **2009**, *131*, 9843-9848.

(13) Loupy, A. *Microwaves in Organic Synthesis*; 2° ed.; Wiley-VCH, 2006.

(14) Guryanov I.; Toma F. M.; Montellano López A.; M., C.; Da Ros T.; Angelini G.; D'Aurizio E.; Fontana A.; Prato M.; Bonchio M. Microwave-Assisted Functionalization of Carbon Nanostructures in Ionic Liquids. *Chemistry - A European Journal*.

(15) Goshe, A. J.; Steele, I. M.; Ceccarelli, C.; Rheingold, A. L.; Bosnich, B. Supramolecular recognition: On the kinetic lability of thermodynamically stable host–guest association complexes. *Proceedings of the National Academy of Sciences of the United States of America* **2002**, *99*, 4823-4829.

(16) Kappe, C. O. Controlled Microwave Heating in Modern Organic Synthesis. *Angewandte Chemie International Edition* **2004**, *43*, 6250-6284.

(17) Brunetti, F. G.; Herrero, M. A.; Muñoz, J. D. M.; Díaz-Ortiz, A.; Alfonsi, J.; Meneghetti, M.; Prato, M.; Vázquez, E. Microwave-Induced Multiple Functionalization of Carbon Nanotubes. *Journal of the American Chemical Society* **2008**, *130*, 8094-8100.

(18) Browne, W. R.; McGarvey, J. J. The Raman effect and its application to electronic spectroscopies in metal-centered species: Techniques and investigations in ground and excited states. *Coordination Chemistry Reviews* **2007**, *251*, 454-473.

(19) Dresselhaus, M.; Dresselhaus, G.; Saito, R.; Jorio, A. Raman spectroscopy of carbon nanotubes. *Physics Reports* **2005**, *409*, 47-99.

(20) Saito, R.; Dresselhaus, G.; Dresselhaus, M. S. *Physical Properties of Carbon Nanotubes; 1°* ed.; World Scientific Publishing Company, **1998**.

(21) Jorio, A.; Dresselhaus, Gene; Dresselhaus, Mildred S. *Carbon Nanotubes: Advanced Topics in the Synthesis, Structure, Properties and Applications; 1°* ed.; Springer, **2008**.

(22) Campidelli, S.; Meneghetti, M.; Prato, M. Separation of Metallic and Semiconducting Single-Walled Carbon Nanotubes via Covalent Functionalization. *Small* ***20*****07**, *3*, 1672-1676.

(23) Liu, Z.; Li, X.; Tabakman, S. M.; Jiang, K.; Fan, S.; Dai, H. Multiplexed Multicolor Raman Imaging of Live Cells with Isotopically Modified Single Walled Carbon Nanotubes. *Journal of the American Chemical Society* **2008**, *130*, 13540-13541.

(24) Krupke, R.; Hennrich, F.; Hampe, O.; Kappes, M. M. Near-Infrared Absorbance of Single-Walled Carbon Nanotubes Dispersed in Dimethylformamide. *The Journal of Physical Chemistry B* **2003**, *107*, 5667-5669.

(25) Williams, D. B.; Carter, C. B. *Transmission Electron Microscopy: A Textbook for Materials Science; 2°* ed.; Springer, **2009**.

(26) Goldstein, J.; Newbury, D. E.; Joy, D. C.; Lyman, C. E.; Echlin, P.; Lifshin, E.; Sawyer, L.; Michael, *J. Scanning Electron Microscopy and X-ray Microanalysis; 3°* ed.; Springer, **2003**.

(27) Smith, D.; Binnig, G.; Quate, C. Atomic point-contact imaging. *Applied Physics Letters* **1986**, 49, 1166-1168.

(28) Ohnesorge, F.; Binnig, G. True atomic resolution by atomic force microscopy through repulsive and attractive forces. *Science* **1993**, **260**, 1451-1455.

(29) Castronovo, M.; Radovic, S.; Grunwald, C.; Casalis, L.; Morgante, M.; Scoles, G. Control of Steric Hindrance on Restriction Enzyme Reactions with Surface-Bound DNA Nanostructures. *Nano Letters* **2008**, *8*, 4140-4145.

(30) Bano, F.; Fruk, L.; Sanavio, B.; Glettenberg, M.; Casalis, L.; Niemeyer, C. M.; Scoles, G. Toward Multiprotein Nanoarrays Using Nanografting and DNA Directed Immobilization of Proteins. *Nano Letters* **2009**, *9*, 2614-2618.

(31) Cellot, G.; Cilia, E.; Cipollone, S.; Rancic, V.; Sucapane, A.; Giordani, S.; Gambazzi, L.; Markram, H.; Grandolfo, M.; Scaini, D.; Gelain, F.; Casalis, L.; Prato, M.; Giugliano, M.; Ballerini, L. Carbon nanotubes might improve neuronal performance by favouring electrical shortcuts. *Nature Nanotechnology* **2009**, *4*, 126-133.

(32) Martin, Y.; Williams, C. C.; Wickramasinghe, H. K. Atomic force microscope--force mapping and profiling on a sub 100-[A-ring] scale. *Journal of Applied Physics* **1987**, *61*, 4723-4729.

(33) Girard, P. Electrostatic force microscopy: principles and some applications to semiconductors. *Nanotechnology* **2001**, *12*, 485-490.

(34) Park Systems Atomic Force Microscope, AFM/SPM.

(35) Gómez-Navarro, C.; Moreno-Herrero, F.; de Pablo, P. J.; Colchero, J.; Gómez-Herrero, J.; Baró, A. M. Contactless experiments on individual DNA molecules show no evidence for molecular wire behavior. *Proceedings of the National Academy of Sciences of the United States of America* ***20*02**, *99*, 8484-8487.

(36) Wang, Z.; Zdrojek, M.; Melin, T.; Devel, M. Electric charge enhancements in carbon nanotubes: Theory and experiments. *Physical Review Letter B* **2008**, *78*, 85425-85430.

Appendix A: Review of the experimental methods

APPENDIX B:

EXPERIMENTAL SECTION

B.1 Materials

MWCNTs were purchased from Nanostructured & Amorphous Materials Inc., Huston, TX; Stock #: 1240XH, 95%, OD 20-30 nm). HiPCO purified SWCNTs CNI® were received from Carbon Nanotechnologies Incorporated. Chemicals and solvents for synthesis were obtained from Sigma-Aldrich and they were used without further purification. The radioactive tracer $[^{111}In]Cl_3$ was obtained from Amersham Pharmacia Biosciences as an aqueous solution and used without further purification.

Non-coding siRNA was obtained from Eurogentec. The proprietary sequence siCONTROL TOX (referred to throughout this manuscript as siTOX) was purchased from Dharmacon (Lafayette, CO, USA). Dulbecco's modified eagle medium (DMEM), minimum essential medium (MEM), fetal bovine serum (FBS), penicillin/streptomycin, and phosphate buffered saline (PBS) from Gibco, Invitrogen (UK). Cervical cancer cell line HeLa (CCL-2.2) and human lung carcinoma A549 (CCL-185) from ATCC (UK). DeadEnd™ Fluorometric TUNEL System was from Promega (UK). Annexin-V-Fluos staining kit from Roche Diagnostics GmbH (Germany). Six- to eight-week-old BALB/c mice were obtained

from Harlan (Oxfordshire, UK), allowed to acclimatise for 1 week and were kept in groups of 5 for the duration of the experiments and given food and water. All experiments were conducted with prior approval from the UK Home Office.

Standard dissociated hippocampal cultures were prepared according to Malgaroli[1]. Hippocampi were dissected from 0- to 3-day-old animals killed by decapition in accordance with the regulations of the Italian Animal Welfare Act and approved but the local Authority Veterinary Service.

B.2 Syntheses

Synthesis of G_0 dendron-MWCNT 1. 300 mg of MWCNTs were suspended in 250 mL of DMF. The mixture was first sonicated in sonic bath for 5 minutes, and then paraformaldehyde (450 mg) and {2-[2-(2-tert-butoxycarbonylamino-ethoxy)-ethoxy]-ethylamino}-acetic acid (450 mg) were added and the addition was repeated every 24h for three times, sonicating 15 minutes each time. The reaction was heated at 115°C for 120h. The product was filtered with a Millipore system (JH 0.45 μm filter) dried with diethyl ether and recovered, sonicated for 30 minutes in DMF, then filtered and recovered again and finally sonicated for 30 minutes in MeOH. Following a final filtration, the product, obtained as a fine black powder (339 mg), was dried at the vacuum pump. TEM charcterization of Boc-protected MWCNT **1** is reported at pag. 32, AFM characterization is reported at pag. 33 and the average diameter ranges from 20 to 25 nm. The Kaiser test of this derivative was 0 μmol/g, the loss of weight at 450°C measured by TGA was 3.7% in the batch reported in Chapter 1 and 1.2% for the batch reported in Chapter 2.

Boc-protected G_0 dendron-MWCNT **1** (240 mg) underwent deprotection via HCl_g in 200 mL of DMF, stirring at RT overnight. Again, the product was filtered with a Millipore system (JH 0.45 μm filter), washed with ether and recovered, sonicated for 30 minutes in DMF, then filtered and sonicated again for 30 minutes in MeOH. Afterwards, 230 mg of G_0 dendron-MWCNT **1** were recovered. The Kaiser test for the first batch reported in Chapter 2 was 481 μmol/g, and 72 μmol/g for

the batch reported in Chapter 3. TEM characterization for MWCNT **1** is reported at pag. 30.

Synthesis of alkylated G_0 dendron-MWCNT 2. 10 mg of MWCNT **1** were added to 5 mg of glycidyl trimethylammonium chloride in 15 mL of MeOH, and the resulting mixture was kept at 40 °C for 48h. Dendron-MWCNT **2** was filtered with a Millipore system (JH 0.45 μm filter), washed with diethyl ether and recovered. Then the suspension was sonicated for 30 minutes in MeOH and washed with diethyl ether and recovered, then filtered and sonicated again. Following a final filtration, dendron-MWCNT **2** was obtained as a fine black powder (10 mg). Kaiser test of MWCNT **2** was 0 μmol/g, the loss of weight measured by means of TGA at 450°C was 1.4%. TEM charcterization is reported at pag. 30.

Synthesis of $G_{0.5}$ dendron-MWCNT 3. 210 mg of MWCNT **1** were mixed with 105 mL of methyl acrylate and 21 mL of N-ethyldiisopropyl amine in 100 mL of MeOH, and the resulting mixture was kept at 80 °C for 72h. Dendron-MWCNT **3** was filtered with a Millipore system (JH 0.45 μm filter), and then sonicated with MeOH and washed with diethyl ether as previously described. 190 mg were recovered. The Kaiser test of MWCNT **3** was 0 μmol/g.

Synthesis of G_1 dendron-MWCNT 4. 180 mg of MWCNT **3** were added to 90 mL of diethylamine and 90 mL of MeOH, the reaction was stirred at 80°C for 72h. Dendron-MWCNT **4** was filtered with a Millipore system (JH 0.45 μm filter), and then sonicated with MeOH and washed with diethyl ether as previously described. After a final filtration, dendron-MWCNT **4** was recovered as a fine black powder (190 mg). The Kaiser test of MWCNT **4** was 0 μmol/g and the relative loss of weight calculated by means of TGA was 12.5% for the bactch studied in Chapter 1. The Kaiser test for the bactch studied in Chapter 2 was 111 μmol/g.

Synthesis of alkylated (G_1) dendron-MWCNT 5. 10 mg of MWCNT **3** were added to 7.6 mg of glycidyl trimethylammonium chloride in 15 mL of MeOH, and the resulting mixture was kept at 40 °C for two days. Dendron-MWCNT **5** was filtered

with a Millipore system (JH 0.45 μm filter), and then sonicated with MeOH and washed with diethyl ether as previously described. After a final filtration, dendron-MWCNT **5** was obtained as a fine black powder (10 mg). The Kaiser test of derivative MWCNT **5** was 0 μmol/g, the loss of weight calculated by TGA 3.8%. TEM characterization is reported at pag. 30.

Synthesis of $G_{1.5}$ dendron-MWCNT 6. 178 mg of MWCNT **5** were mixed with 60 mL of methyl acrylate and 18 mL of N-ethyldiisopropyl amine in 60 mL of MeOH, and the resulting mixture was kept at 80 °C for 72h. The product was filtered with a Millipore system (JH 0.45 μm filter), and then sonicated with MeOH and washed with diethyl ether as previously described. 173 mg were recovered. Kaiser test for MWCNT **6** was 0 μmol/g. TEM characterization is reported at pag. 32.

Synthesis of (G_2) dendron-MWCNT 7. 130 mg of MWCNT **6** were added to 65 mL of diethylamine and 65 mL of MeOH, the reaction was stirred at 80°C for 72h. Dendron-MWCNT **7** was filtered with a Millipore system (JH 0.45 μm filter), and then sonicated with MeOH and washed with diethyl ether as previously described. After a final filtration, dendron-MWCNT **7** was obtained as a fine black powder (134 mg). Kaiser test for MWCNT **7** was 1097 μmol/g and loss of weight was 18% for the batch reported in Chapter 1. TEM characterization is reported at pag. 31. For the batch reported in Chapter 2, Kaiser test was 212 μmol/g.

Synthesis of alkylated G_2 dendron-MWCNT 8. 70 mg of MWCNT **7** were added to 755 mg of glycidyl trimethylammonium chloride in 70 mL of MeOH, and the resulting mixture was kept at 40 °C for two days. Dendron-MWCNT **8** was filtered with a Millipore system (JH 0.45 μm filter), and then sonicated with MeOH and washed with diethyl ether as previously described. After a final filtration, dendron-MWCNT **8** was obtained as a fine black powder (72 mg). Kaiser test for MWCNT **8** was 0 μmol/g, the loss of weight was 28% in the batch described in Chapter 1 and 5.6% for the second batch reported in Chapter 2. TEM characterization was reported at pag. 30, 31 and 61. AFM characterization is reported at pag. 33 and the

average diameter ranges from 35 to 40 nm. E-EFM characterization is reported at pag. 37.

Synthesis of SWCNT 9. 8 mg of HiPCO purified SWCNTs, used as received from NRI®, were dispersed in 8 mL of DMF and mixed with sarcosine (12 mg) and heptaldehyde (12 mg), which were added other three times every 24h and sonicated for 15 minutes each, for 120h at 120°C. Afterwards it was filtrated through a Millipore filter (JH 0,45 mm). The resulting material was washed on the filter with DMF and diethylether, recovered, and re-suspended in DMF upon sonication for 20 minutes. It was re-filtered, re-washed on the filter with DMF and diethylether and finally 6 mg were recovered. TGA loss of weight calculated at 500°C was 7%. TEM charcterization is reported at pag. 46, UV-Vis-NIR spectrum is reported at pag. 47.

Synthesis of SWCNT 10. 5 mg of HiPCO purified SWCNTs, used as received from NRI®, were dispersed in 0.5 mL of [bmim]BF_4) and mixed with sarcosine (7.5 mg) and aldehyde (7.5 mg), added othe three times every 24h, sonicated for 15 minutes each, and heated for 120h at 120°C. Afterwards they were filtrated through a Millipore filter (JH 0,45 mm). The resulting material was washed on the filter with DMF and diethylether and recovered, then it was re-suspended in DMF upon sonication for 20 minutes. It was re-filtered, re-washed on the filter with DMF and diethylether and at this point the collected black material was suspended in acetone and sonicated for 20 minutes in order to remove all the ILs. Finally, it was filtered again, washed on the filter with acetone and diethylether. 6 mg of product were recovered. TGA loss of weight calculated at 500°C was 7%. TEM charcterization is reported at pag. 48, UV-Vis-NIR spectrum is reported at pag. 46.

Synthesis of SWCNT 11. 5 mg of HiPCO purified SWCNTs, used as received from NRI®, were dispersed in the IL ([bmim]BF_4) and mixed with sarcosine (1 mmol) and aldehyde (2 mmol). The reactions were carried out in closed glass test tubes with stirring, under microwaves irradiation (20 W at 120°C). The reaction

mixtures were cooled down at room temperature and then suspended in DMF. Afterwards they were filtrated through a Millipore filter (JH 0,45 mm). The resulting material was washed on the filter with DMF and diethylether and recovered, then it was re-suspended in DMF upon sonication for 20 minutes. It was re-filtered, re-washed on the filter with DMF and diethylether and at this point the collected black material was suspended in acetone and sonicated for 20 minutes in order to remove all the ILs. Finally, it was filtered again, washed on the filter with acetone and diethylether. About 5 mg were recovered. Thermal reactions, with and without ILs, were carried out for comparison purposes, by heating analogue mixtures in closed vials using an oil bath. TGA loss of weight calculated at 500°C was 9%. Raman spectrum was reported at pag. 47. TEM charcterization is reported at pag. 48, UV-Vis-NIR spectrum is reported at pag. 47.

Synthesis of SWCNT 12. 5 mg of SWCNTs were dispersed in 0.5 mL of [omim]BF_4, afterwards 1 mmol of sarcosine and 2 mmol of heptaldehyde were added to the mixture. The reaction was carried out under MW irradiation at 20 W, for 1 hour (Tbulk= 120°C), with stirring. After the work-up procedure as described abovefor compund **11**, 5 mg of product were recovered. TGA loss of weight calculated at 500°C was 6%. TEM charcterization is reported at pag. 46, UV-Vis-NIR spectrum is reported at pag. 46.

Synthesis of SWCNT 13. 5 mg of SWCNTs were dispersed in 0.5 mL of [hvmim][$(CF_3SO_2)_2N$], afterwards 1 mmol of sarcosine and 2 mmol of heptaldehyde were added to the mixture. The reaction was carried out under MW irradiation at 20 W, for 1 hour (Tbulk= 120°C), with stirring. After the work-up as described above for compound **11**, 6 mg of product were recovered. TGA loss of weight calculated at 500°C was 0%. TEM charcterization is reported at pag. 46, UV-Vis-NIR spectrum is reported at pag. 46.

Synthesis of SWCNT 14. 5 mg of SWCNTs where dispersed in 0.5 mL of [omim]BF_4 and 170 μL of o-DCB, afterwards 1 mmol of sarcosine and 2 mmol of

heptaldehyde were added to the mixture. The reaction was carried out under MW irradiation at 20 W, for 1 hour (Tbulk= 120°C), with stirring. After the work-up as described above for compound **11**, 6 mg of product were recovered. TGA loss of weight calculated at 500°C was 16%. Raman spectrum was reported at pag. 47. TEM charcterization is reported at pag. 48, UV-Vis-NIR spectrum is reported at pag. 47.

Synthesis of SWCNT 15. 5 mg of SWCNTs were dispersed in 0.5 mL of [bmim]BF_4, yielding a gel, afterwards equimolar amounts (0.5 mmol) of sarcosine and $C_8F_{17}(CH_2)_2CHO$ were added to the mixture. The reactions were carried out under MW irradiation at 20 W for 1 hour (Tbulk= 120°C), with stirring. After the work-up as described above for compound **11**, 6 mg of product were recovered. TGA loss of weight calculated at 500°C was 14%. TEM charcterization is reported at pag. 49 and 50, UV-Vis-NIR spectrum is reported at pag. 50.

Synthesis of SWCNT 16. 5 mg of SWCNTs were dispersed in 0.5 mL of [bmim]BF_4, yielding a gel, afterwards equimolar amounts (0.2 mmol) of sarcosine and $C_8F_{17}(CH_2)_2CHO$ were added to the mixture. The reactions were carried out under MW irradiation at 20 W for 1 hour (Tbulk= 120°C), with stirring. After the work-up as described above for compound **11**, 6 mg of product were recovered. TGA loss of weight calculated at 500°C was 16%. TEM charcterization is reported at pag. 49 and 50, UV-Vis-NIR spectrum is reported at pag. 50.

Synthesis of SWCNT 17. 5 mg of SWCNTs were dispersed in 0.5 mL of [bmim]BF_4, yielding a gel, afterwards equimolar amounts (0.15 mmol) of sarcosine and $C_8F_{17}(CH_2)_2CHO$ were added to the mixture. The reactions were carried out under MW irradiation at 50 W for 1 hour (Tbulk= 140°C), with stirring. After the work-up as described above for compound **11**, 6 mg of product were recovered. TGA loss of weight calculated at 500°C was 27%. TEM charcterization is reported at pag. 49 and 50, UV-Vis-NIR spectrum is reported at pag. 50.

Synthesis of DTPA-G_2 dendron-MWCNT 7. MWCNT **7** (5 mg) were dispersed in dry DMSO/DMF (0.4:2.5 mL) and neutralized with DIEA (diisopropylethylamine) (50 μl) to (MWCNT **7**). Diethylentriaminepentaacetic (DTPA) dianhydride (28.5 mg) was added and the mixture was stirred for 48 h at room temperature. The DMSO solution was partly evaporated and diluted with water. The MWCNTs were recovered by centrifugation, re-dispersed in water and lyophilized. 5 mg were recovered. The Kaiser test was 0 μmol/g and TEM characterization was reported at pag. 70.

Preparation of [^{111}In]DTPA-MWCNT 7. As a standard procedure, dispersions of DTPA-MWCNT or DTPA alone (80-400 μL of 250 μg/mL) were diluted with an equal volume of 0.2 M ammonium acetate buffer pH 5.5, to which 2-20 MBq as indium chloride ($^{111}InCl_3$) was added. The indium was left to react with the DTPA-MWCNT and DTPA alone for 30 min at room temperature, after which the reaction was quenched by the addition of 0.1 M EDTA chelating solution (1/20 the reaction volume is added). $^{111}InCl_3$ alone, used as a control, was also subjected to the same conditions of the labeling reaction. Aliquots of each final product were diluted five folds in PBS and then 1 μL spotted on silica gel impregnated glass fiber sheets (PALL Life Sciences, UK). The strips were developed with a mobile phase of 50 mM EDTA in 0.1 M ammonium acetate and allowed to dry before analysis. This was then developed and the autoradioactivity quantitatively counted using a Cyclone phosphor detector (Packard Biosciences, UK). The immobile spot on the TLC strips indicated the percentage of radiolabeled [^{111}In]DTPA-MWCNT conjugate, while the free ^{111}In or [^{111}In]DTPA were shown by the mobile spot. The mobile spot on the TLC strips indicated the percentage of free DTPA present in the DTPA-MWCNT mixture while precipitated ^{111}In or radiolabeled [^{111}In]DTPA-MWCNT conjugate remain at the application point.

Synthesis of MWCNT 9. 50 mg of MWCNTs, used as received, were dispersed in 8 mL of DMF and mixed with sarcosine (75 mg) and heptaldehyde (75 mg), added other three times every 24h, sonicated for 15 minutes each, and then heated for 120h at 120°C. Afterwards it was filtrated through a Millipore filter (JH 0,45 mm).

The resulting material was washed on the filter with DMF and diethylether and recovered, then it was re-suspended in DMF upon sonication for 20 minutes. It was re-filtered, re-washed on the filter with DMF and diethylether and finally 22 mg were recovered. The metallic residue of MWCNT **9** was 3.9%. TEM characterization is reported at pag. 78.

B.3 Characterization techniques and sample preparation

Thermogravimetric analysis. TGA Q500 (TA Instruments) was used to record TGA analysis under N_2 or under air, by equilibrating at 100°C, and following a ramp of 10 °C/min up to 1000°C. About 0.5 mg per each analysis were required.

Transmission Electron Microscopy (Trieste). TEM analyses were performed on a TEM Philips EM208, using an accelerating voltage of 100 kV. About 1 mg of each compound was solubilized or dispersed in 1 mL of solvent. Then, one drop of this solution was deposited on a TEM grid (200 mesh, Nichel, carbon only; carbon lacey).

Transmission Electron Microscopy (London). Dendron-MWCNT **8** (15 µL of 1.0 mg/mL in 10% dextrose) was complexed with an equal volume of siRNA at 1:16 siRNA:dendron-MWCNT mass ratio. The complex was left to equilibrate for 30 min. A drop of the suspension was placed on a grid with a support film of Formvar/carbon, excess material was blotted off with a filter paper and the complexes were examined under a FEI CM120 BioTwin Transmission Electron Microscope (Einhoven, Netherlands) using a Lab6 emitter. Images were captured using an AMT Digital Camera.

Atomic force microscopy. AFM samples were prepared by the deposition of one drop of a highly diluted nanotubes solution on mica substrate and spin coating in a row. Pristine MWCNTs and MWCNTs after cycloaddition were dispersed in DMF, MWCNT **8** was dispersed in MeOH. The samples were examined with a XE-100 microscope (Park Scientific Instruments Advanced Corp.–PSIA) at room

temperature. In all AFM measurements, the images were taken in non-contact (NC) mode with scan speed of 0.3 Hz using standard silicon rectangular cantilevers (Park, 950M-ACTA) with nominal spring constants of 40 N/m and radius of curvature < 10 nm. In all NC-AFM measurements, the tip scanned the sample with the drive frequency of 330 kHz to acquire the topographic image of various sizes (range from 1.2 μm to 5 μm). The distributions of average diameters were obtained by estimating diameter of single MWCNTs (with and without functionalizations) from NC-AFM topographic images and their corresponding average line profiles. A number of 36, 24 and 37 nanotubes were observed for evaluating the distribution of average diameters of pristine MWCNTs, conjugates boc-protected **1** and **8**, respectively.

Electrostatic Force Microscopy. The EFM analysis was performed using a PSIA XE-100 AFM endowed with an external lock-in amplifier (SR830, Stanford Research Systems) in order to carry out single pass EFM characterization of surfaces. A solution of pristine MWCNTs in DMF (1 mg/mL) or of functionalized CNT in MeOH (1 mg/mL) were put for 3 times (50 μL each time, total volume 150 μL) on a silicon wafer (2 cm x 1 cm) by spin coating (6000 rpm for 15 sec each). The spin coater was a Laurell Technologies Corporation 10:04 AM Model WS-400B_6NPP/LITE model.

Bucky gel preparation (Chieti). The proper amount of purified and unpurified HiPCO SWCNTs was poured in an agate mortar and grinded for 30 min with 1 mL (or 1g in the case of solid IL) of the ionic liquid. The obtained suspension was poured in a vessel and sonicated with a ultrasonic bath sonicator (Bandelin Sonorex, 35 KHz) for 1 h. The sonication increases the apparent viscosity of originally liquid samples. [Hvim][$(CF_3SO_2)_2N$] is solid at room temperature, therefore, the grey powder obtained by 30 min grinding in the mortar was poured in a vessel and heated at 50°C before sonication. The obtained samples were either used for synthetic purposes or poured in the rheometer for the rheological measurements. No centrifugation step was performed in order to remove excess

IL. The samples appear to be quite stable and do not tend to display separation into a black gel phase and a transparent liquid phase within a few weeks.

Rheology (Chieti). Static and dynamic measurements were performed on a Thermo Scientific modular rheometer Haake M.A.R.S. II equipped with Electron Corporation thermo-controller system Haake Phoenix (data evaluation: RheoWin software 3.61) using the cone plate geometry (cone diameter 6 mm, angle 0.5°). All samples, subjected to vacuum pumping before measurements, were directly loaded onto the plate of the rheometer and were allowed to equilibrate for 6 minutes. As a matter of fact we did not prestress the samples or allow a longer equilibration time because prestressing the samples or allow equilibration would have required to leave the samples undisturbed between the plates for ca. 24 h and this delay would have favoured the undesired hydration of the ionic liquids. The shear stress sweep tests showed that 1.0 Pa satisfies the linear viscoelasticity for all samples. The dynamic storage and loss moduli were examined in the linear viscoelastic regime at 25°C unless otherwise stated.

Microwave. Continuous microwave irradiation was carried out in a CEM-Discover monomode microwave apparatus, with simultaneous monitoring of irradiation power, pressure and temperature. Compressed air was applied to improve the temperature control of the reaction mixtures.

Raman spectroscopy. Micro-Raman spectra were recorded with a Via Renishaw spectrometer equipped with a He-Ne (632.8 nm) laser. The analyses were conducted on solid samples.

UV-Vis-NIR spectroscopy. UV-Vis-NIR spectra were recorded in 1-cm quartz cuvettes on a Varian Cary 5000 spectrophotometer. The spectra were recorded in DMF solution

Electrophoretic motility shift assay. 0.5 μg of siRNA in 30μL of water complexed to dendron-MWCNT **8** at different mass ratios, or 0.5 μg of free siRNA as a control,

were added to 1% agarose gel containing ethidium bromide. The gel was run for 45 min at 70 V and then photographed under UV light using GeneGenius system, PerkinElmer Life and Analytical Sciences (USA).

Evaluation of fluorescent siRNA complex uptake in HeLa Cells. ATTO 655-labeled siRNA (λ_{ex}= 655 nm, λ_{em}= 690 nm) was used to prepare fluorescent siRNA complexes. siRNA was complexed with the different generations of dendron-MWCNTs at a 1:16 mass ratio. HeLa cells were grown to confluency in glass coverslips in 24-well tissue culture dishes at a density of 50000 cells per well in MEM supplemented with 10% FBS and 1% penicillin/streptomycin. After 24h, the cells were trasfected with non-coding siRNA conjugated to ATTO 655. Briefly, 50 μL of the preformed siRNA complex was diluted 10 times with complete medium, and 500 μL of the complex-containing medium was added to each well yielding a final siRNA concentration of 80 nM (1μg/mL). The cells were incubated with the siRNA:MWCNT complexes for 4h in serum-free medium, after which serum was added to achieve a final serum concentration of 10%. After 24h, the cells were washed with PBS solution, fixed with 4% paraformaldehyde in PBS for 15 minutes at RT, and then rinsed with PBS. For nuclear staining, cells were permeabilized with 0.1% Triton X-100 in PBS for 10 minutes at RT, treated with RNAase (100 μg/mL) for 20 minutes at 37°C, incubated with 1 mg/mL propidium iodide (Molecular Probes) in PBS for 5 minutes, and then rinsed three times with PBS. Coverslips were mounted with aqueous poly(vinyl alcohol) Citifluor reagent mixed with AF100 antifade reagent (10:1) (Citifluor) prior to use. Slides were examined under the CLSM using a 63X oil immersion lens.

Assessment of cell viability. A549 cells (50,000 cells/well) maintained in DMEM media supplemented with 10 % fetal bovine serum (FBS), 50 U/mL penicillin, 50 μg/mL streptomycin, 1% L-glutamine and 1% non-essential amino acids at 37 °C in 5% CO_2, were sub-cultured into 24-well plates for 24h before incubation with the *f*-CNT. Cells were incubated with dendron-MWCNT **8** in serum-free media for

4h after which serum-containing media was added to make the final concentration of serum to 10%. Cell death was assessed after 24h of incubation (immediate) or allowed to recover (delayed) for additional 48h. Final concentrations reached were 10 μg/mL. The live-death cell assay was performed with a PI/annexin-V-FITC staining kit according to the instructions of the manufacturer. A CyAn ADP flow cytometer (DakoCytomation) was used to analyze 20000 cells per sample. All conditions were tested in triplicate.

Transfection of HeLa cells with siRNA. HeLa cells were maintained in MEM media, supplemented with 10% fetal bovine serum (FBS), 50 U/mL penicillin, 50 μg/mL streptomycin, 1% L-glutamine and 1% non-essential amino acids at 37°C in 5 % CO_2. Cells (5000 cells/well) were subcultured into 16-well chamber slides. 24hs later, cells were transfected with siTOX, an apoptosis inducing siRNA. Briefly, 30 μL of the pre-formed dendron-MWCNT:siRNA complex was diluted 5 times with serum free media and 150 μL of the complex containing media were added to each well yielding a final siRNA concentration of 80 nM. Four hours later, 150 μL of fresh media containing 20% FBS was added to each well. After 48 h incubation at 37°C and 5 % CO_2, the DeadEnd™ Fluorometric TUNEL System was used to label nicked DNA through incorporation of fluorescein-12-dUTP. Samples were incubated with recombinant terminal deoxynucleotidyl transferase (rTdT) indicated by manufacturer instructions and fluorescein labelling was visualized using confocal laser scanning microscopy (CLSM) (Zeiss LSM 510 Meta; Carl Zeiss, Oberkochen, Germany) using 30 mW 488 nm Argon laser excitation source, LP 505 nm output filter, and a Plan-Neofluar 10X lens. Propidium iodide was used to counterstain nuclei.

Whole body imaging of [^{111}In]DTPA-MWCNT using Nano-SPECT/CT. Balb/C mice were anaesthetised by isofluorane inhalation. Each animal was injected via tail vein injection with 250 μL containing 50 μg of [^{111}In]DTPA-MWCNT containing approximately 5-6MBq. [^{111}In]EDTA was injected for comparison. Immediately after injection (t=0.5hrs) and at 3.5hs and 24hs, mice were imaged using the Nano-

SPECT/CT scanner (Bioscan, USA). SPECT images were obtained in 16 projections over 40-60 min using a 4-head scanner with 1.4 mm pinhole collimators. CT scans were taken at the end of each SPECT acquisition and all images were reconstructed with MEDISO software (Medical Imaging Systems). Fusion of SPECT and CT images was carried out using the PMOD software.

Tissue biodistribution of [^{111}In]DTPA-MWCNT. Animals (n=3-4) were injected with 250μL containing 50 μg of [^{111}In]DTPA-MWCNT or [^{111}In]EDTA in 5% dextrose via tail vein injection. Twenty four hours after injection, mice were killed, and blood was collected. Heart, lungs, liver, spleen, kidneys, muscle and bone were sampled, each sample being weighed and counted on a Gamma Counter (Perkin Elmer, USA), together with a dilution of the injected dose with dead-time limit below 60%. The percentage injected dose per gram tissue or the percentage injected dose per organ was calculated for each tissue.

Preparation of CNT coverslips from a water solution. 5 mL of a water solution (0.04 mg/mL) of MWCNTs **9** were evaporated over 3 glass substrates, those were deposited in a crystallizer (crystallizer surface area = 1809 mm^2). The solution was slowly dried out. The substrates were then placed in oven at 350 °C under nitrogen atmosphere in order to remove the organic functionalization.

Preparation of CNT coverslips from a DMF solution. The coverslips were heated at 80°C and 2 mL (200 μL x 10 times) of a 0.01 mg/mL solution of MWCNTs **9** were deposited onto their surface. Then, we treated the substrates for 20 minutes at 350°C under N_2 atmosphere. SEM characterization of these substrates is reported at pag. 80 and 81.

Preparation of neuronal cultures[1]. Hippocampi were isolated from newborn rats, digested and recovered, cells were plated on bare glass coverslips and on CNTs treated glass coverslips. Coverslips were placed in Petri dishes and cultured in serum containing medium in a 5% CO_2-humified incubator for 7-9 days.

Scanning Electron Microscopy. SEM measurements were carried out with a Zeiss Supra™ microscope. Substrates with cells were metalized with about 10 nm of Ni (6 seconds, 300 W, throttle valve 25%, Argon 25 sccm).

Electrophysiological recordings. Cultures were superfused with a solution containing (mM): NaCl 150, KCl 4, $MgCl_2$ 1, $CaCl_2$ 2, HEPES 10, glucose 10. Recordings were obtained from neurons with patch pipettes (4-7 MΩ) using an Axoclamp 2 unit (Axon Instrument) in current clamp mode. Pipettes were filled with a solution containing (mM): K gluconate 120, KCl 20, HEPES 10, EGTA 10, $MgCl_2$ 2, Na_2ATP 2 (pH 7.35 adding KOH). In voltage clamp an EPC-7 Amplifier (List Germany) was used, and all recordings were taken at the same holding potential of -58 mV. Membrane potentials were corrected for liquid junction potentials.

References:

(1) Malgaroli, A.; Tsien, R. Glutamate-induced long-term potentiation of the frequency of miniature synaptic currents in cultured hippocampal neurons. *Nature* **1992**, *357*, 134-139.